DYNAMIC CONVEX OPTIMAL POWER FLOW APPROACHES FOR MODERN POWER GRID

by

Seyedmahdi Moghadasi

A dissertation submitted to the faculty of
The University of North Carolina at Charlotte
in partial fulfillment of the requirements
for the degree of Doctor of Philosophy in
Electrical Engineering

Charlotte

2017

Approved by:

_____
Dr. Sukumar Kamalasadan

_____
Dr. Yogendra Kakad

_____
Dr. Badrul Chowdhury

_____
Dr. Artie Zillante

ABSTRACT

SEYEDMAHDI MOGHADASI. Dynamic convex optimal power flow approaches for modern power grid. (Under the direction of DR. SUKUMAR KAMALASADAN)

Non-convexity of Optimal Power Flow (OPF) problem in power systems poses difficulties in reaching optimal solutions which can adversely affect the overall solution efficiency, convergence and appropriate scheduling of generators. Dynamic convex OPF approaches aims to provide optimal generation scheduling and determine appropriate control action across operational time frames for different components of active power systems. In this work, an approach based on convex Optimal Power Flow (OPF) formulation integrated within Receding Horizon Control (RHC) method using second order conic programming (SOCP) suitable for active power distribution system is proposed. The main advantages of the RHC-Convex OPF approach are that, it can; a) integrate dynamic models and uncertain energy resources and, b) reach global optimal scheduling with faster computation time. An architecture for real-time implementation is also presented.

Also, a new voltage stability constrained convex optimal power flow (VSC-OPF) approach is proposed using semi-definite programming (SDP). Methods within this approach provides optimal dispatch solution considering a) maximum stability margin, b) minimum operating cost constrained by stability margin and c) an intermediate function that can define a trade-off between cost and enhancing stability. Further, these methodologies are extended for optimal scheduling of integrated AC-DC system. The proposed methods address some limitations of AC-DC OPF methods due to non-convexity, separate scheduling of AC and DC networks or using equivalent of DC network. The advantages of the proposed approach are that it can; a) find the optimal operating point, b) find the maximum loadablility point and c) assess voltage security cost.

ACKNOWLEDGEMENTS

I was fortunate to get support from many people during my doctoral studies, some of whom are acknowledged here.

I would like to thank my adviser Professor Sukumar Kamalasadan for his support and providing feedback to my work, which helped me to complete this dissertation.

Thanks are also due to other members of my dissertation committee: Professors Yogendra Kakad, Professor Badrul Chowdhury and Professor Artie Zillante, who were inspiring in teaching and my research.

This work was supported in part by the U.S. National Science Foundation. I would also like to thank UNC-Charlotte for the Graduate Assistant Support Plan (GASP) award.

Many thanks to my fellow students and friends at UNC-Charlotte who have directly or indirectly supported my work.

DEDICATION

To my parents and my wife Ensieh,

for their love and support

TABLE OF CONTENTS

LIST OF FIGURES

LIST OF TABLES

CHAPTER 1: INTRODUCTION

Dynamic optimal power flow (OPF) aims to provide generation schedule and determine control action across operational time frames for different components of active power systems. Receding horizon control (RHC) is an effective dynamic optimization approach over a defined horizon, taking into account parameter uncertainties through re-estimating future values based on real-time data [1]. Non-convexity of OPF problem, however, creates major difficulties to reach the optimal solution and the efficiency of solution algorithm deteriorates significantly. In this chapter, we discuss the challenges associated with conventional OPF models and summarize the recent advances in convex relaxation of OPF problem classified into second order conic programming (SOCP), semi definite programming (SDP) and chordal relaxation. Also, RHC and its capability in dynamic optimization and handling uncertainties is discussed. Further, the outline of the dissertation and the framework of the problems in each chapter are explained.

1.1 Optimal Scheduling of Power Grid: Conventional OPF Methods and The Need for Convex OPF

Fast optimal scheduling of power grid is now a major obstacle for economically operating electric grid with increasingly incorporating inherent stochastic generations such as renewable sources, plug-in electric vehicles (PEV), price responding demands, and electricity markets [2]. Optimal power flow (OPF), evolved in 1962 [3], formulated the basic problem of finding a local optimum operating point for a power system given that both the demand and supply are deterministic. During the past decades,

considerable effort has been devoted to developing the OPF formulation and proposing solution algorithms in three major and apparently independent directions: a) addressing the OPF difficulties in scalability and efficiency, b) handling uncertainty in input variables and parameters, and c) finding the global optimum solution instead of a local optimum.

In this section, a literature review on conventional OPF and the challenges with optimality and dynamic solution while integrating resource uncertainties are explained. 1.1.1 introduces the evolution of optimal power flow (OPF) problem and a survey of reported works on OPF and Economic Dispatch. 1.1.2 discusses conventional OPF methods including heuristic based approaches. Section 1.1.3 summarizes recent advances in convex relaxation of OPF problem classified based on bus injection and branch flow models.

1.1.1 Economic Dispatch and Optimal Power Flow

Economic dispatch (ED) problem is usually referred to as a special case of OPF problem whereby the transmission's active and reactive power flow equations are relaxed. ED problem is first formulated in 1920's [4, 5] much earlier than introducing OPF problem.

The goal of ED is economical allocation of the specific load to available generation units. First the idea of incremental method was developed for ED problem in early 1930 [6]. Kron's work on loss treatment [7] then provided a reference for two decades. Classic coordination equations known as B matrix was formulated by Kirchmayer and Stagg [8]. This efforts in this direction were continued by evolving the correct transmission loss penalty factor reported in [9]. During these years a lot of parallel studies also investigated the ED problem on the multi-area power systems, which was also started by Kron studies [10, 11]. The following set of equations (1.1) captures

the main progress in the ED problem demonstrated in this era.

$$P_L = \sum_{i=1}^{n_g} \sum_{j=1}^{n_g} P_i B_{ij} P_j + \sum_{i=1}^{n_g} B_{0_i} P_i + B_{00} \tag{1.1}$$

$$\left(\frac{1}{1 - \frac{\partial P_L}{\partial P_i}} \right) \frac{\partial C_i}{\partial P_i} = \lambda$$

Where Pi, B_{ij} and λ are injected power, loss coefficient and Lagrange multiplier respectively. A significant turning point happened in early 1960's whereby the first OPF formulation was developed by Squires and Carpentier [3]. The most important contribution was the mathematical formulation of including AC power flow equations inside the optimization problem. The solution of this OPF yields the optimum operation point of the power system. Objective of OPF problem is to minimize power system operation cost constrained by power flow equations and other physical limitations. During the past decades, large volume of published studies on OPF are based on Carpentier formulation. In fact, this milestone provided a mathematical foundation for implementation of various optimization techniques such as nonlinear programming (NLP) to be examined on OPF problem. This progress continued and opened windows to other innovative algorithms. The general NLP-OPF formulation is shown in (1.2).

A significant turning point happened in early 1960's whereby the first OPF formulation was developed by Squires and Carpentier [3]. The most important contribution was the mathematical formulation of including AC power flow equations inside the optimization problem. The solution of this OPF yields the optimum operation point of the power system. The objective of OPF problem is to minimize power system operation cost constrained by power flow equations and other physical limitations. During the past decades, large volume of published studies on OPF are based on Carpentier formulation. In fact, this milestone provided a mathematical foundation for implementation of various optimization techniques such as nonlinear programming

(NLP) to be examined on OPF problem. This progress continued and opened windows to other innovative algorithms. The general NLP-OPF formulation is shown in (1.2).

$$Min \sum_{i \in N_G} c_i \left(P_i, v_i\right) \tag{1.2}$$
$$s.t. \begin{cases} g\left(Pi, v_i\right) \leq b_i \\ h(Pi, v_i) = d_i \end{cases}$$

where Pi and v_i are injected power and voltage respectively. OPF problem contains three types of variables/parameters;

- control variables $\rightarrow$ ex. voltage and power at PV buses
- state variables $\rightarrow$ ex. transmission's flow
- parameters $\rightarrow$ ex. coefficient of cost functions

A large body of researches have investigated the solution to OPF problem. These efforts are captured and summarized by surveys on this problem [12–18]. In 1977, first comprehensive survey on ED and OPF was presented by Happ [12]. In 1999, Momoh presented a review on OPF methods classified into six categories. The most recent survey on OPF published in 2008 whereby Pandya [17] reviewed OPF techniques presented after 1993. Several survey+ on specific applications of OPF were also presented during recent years. Qiu [19] presented a survey on application of OPF in electricity markets. OPF is a nonconvex optimization problem and classified as an NP-hard problem. Beside non-linearity, large scale of variables and uncertainty in control variable/parameters makes OPF a challenging problem to be solved in shorter time steps.

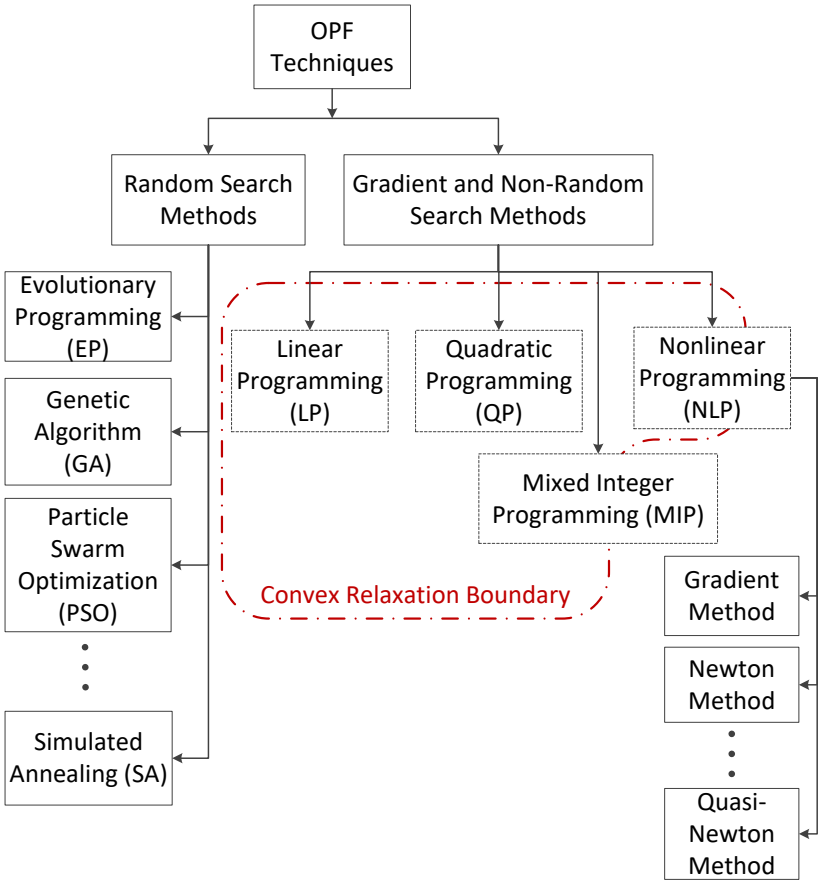

Figure 1.1: OPF Techniques and Methods

1.1.2 Conventional OPF Methods

The conventional optimization techniques contributed to OPF problem can be classified to following methods.

1.1.2.1 Linear Programming

Linear programming (LP) is one of the most applied methods. The method consists of a linear objective function and constraints and also involves non-negative variables. The objective and constraint functions of OPF problem are, therefore, linearized to be solved by LP methods. To minimize line losses and find the optimal capacitor placement, [20] deployed a recursive LP method and approximated the OPF problem during each iteration. Ref. [21] proposes methods relied on DC OPF in lower level and

used LP for solution. The most common algorithms to solve LP-OPF are the revised simplex and interior point methods originally developed by Dantzig and Karmarkar. LP method has the advantages of handling large number of variables in a time efficient manner and yet yielding optimal solution. However, the significant drawback of using LP is its over simplification of OPF problem in modeling stage. The error generated in sequential approximation, therefore, casts doubt on LP solution optimality.

1.1.2.2 Quadratic Programming

Quadratic programming OPF (QP-OPF) is a specific optimization which differs from LP-OPF in objective function. Quadratic programming is a useful technique to model loss and conservative voltage regulation (CVR) in OPF problems. This technique is widely used in various optimization problems of power grid. Ref. [22] introduced a QP based programming method for phasor measurement units (PMUs) placement to provide a complete grid observability. Although there are efficient algorithms to solve this problem, QP-OPF carries the disadvantage of approximation of OPF problem. Modified simplex method is an efficient algorithm to solve the resulting QP problem.

1.1.2.3 Mixed Integer Programming

Integer variables impose immerse difficulties to OPF problem, and converts a LP-OPF problem to a non-convex OPF problem. Mixed integer linear programming (MILP) was developed to solve specific type of LP-OPF problems which contain integer variables such as position of tap-changer and switched reactive compensator. "Branch and Bound" algorithm is an effective tool dealing with discrete feasible areas. Ref. [23] suggested an iterative mixed integer linear programming for short term scheduling of active distribution systems. The computational burden is the major drawback of MILP and its non-linear variance mixed integer nonlinear programming (MINLP) methods.

1.1.2.4 Nonlinear programming

The constraints of OPF shown in (1.2) include power flow equations. In the case of using AC power flow equations, the problem turns into the type of nonlinear programming. This optimization problem will be a non-convex NP-hard problem, and thus the methods of LP, QP and MILP are no longer applicable to such problems. Sequential unconstrained minimization technique (SUMT) is a technique for solving nonconvex NLP-OPF problems through barrier functions. The Karush-Kuhn Tucker (KKT) conditions provides the necessary condition for the optimal solution of NLP [24]. The KKT conditions also provide a filtering stage for the possible optimal candidates. Other NLP techniques include gradient, Newton, and Quasi-Newton. These methods are explained in the following parts.

1.1.2.5 Gradient Search Method

The gradient search (GS) method uses gradient function information to find the optimal solution. The method suggests moving in opposite direction of gradient function which is the path of the steepest descent direction. Gradient is re-evaluated at each step until reaching the local optimum solution. To find the step size, a one-variable optimization problem is required to be solved at each iteration. Ref. [25] proposed a hybrid model consisting of two stage optimization to clear the optimal multi-lateral transaction and determine the associated load curtailment. GS methods have the disadvantage of slow convergence where the size of problem is increased. Differentiated objective function and constraints are also the necessary conditions of using GS. These methods may results in a local optimum point, and can not differentiate a local solution from global optima. The trap of local optimum is, therefore, another challenge for GS method. Convexity is the sufficient condition for a local solution to be considered as the optima.

1.1.2.6 Newton Method

The Newton's optimization technique stems from Newton's method for nonlinear equations. This method is based on quadratic approximation obtained from Taylor expansion. The second derivative of Lagrangian function called Hessian matrix is included to provide a more precise move from previous point and choose a better candidate for the next iteration. The method has the advantages of fast convergence. Nevertheless, formation and inversion of Hessian matrix are challenging and imposes heavy computational burden. The method also cannot provide information about global optima. In [26], a new model for incorporating voltage source converter (VSC) based HVDC systems in OPF based on Newton's method are developed, and multiplier method is used to deal with the constraints.

1.1.2.7 Quasi-Newton Method

Similar to Newton method, Quasi-Newton relies on the local 2nd order approximation of objective function. However, Hessian matrix is not explicitly computed at each iteration. Instead of direct computation, Hessian is updated based on the gradient vectors successively. Several algorithms were developed based on Quasi-Newton such as variable metric method. Ref. [27] proposed a hybrid OPF which involves the sequential quadratic programming (SQP) and differential evolution (DE) methods. This method has the advantages of lower computational burden and can handle ill-conditioned matrix.

1.1.2.8 Heuristic and Evolutionary Methods

Evolutionary algorithms are not the focus of this chapter; however, they have some advantages in comparison with conventional methods of OPF problem. Evolutionary methods encompasses a wide variety of random search approaches such as genetic algorithms (GA), Particle Swarm Optimization (PSO), and Evolutionary Programming (EP). These methods find the optimal solution based on a initial population

and yield multiple solution in one single simulation. Unlike direct methods and other conventional OPF, these methods are simple and are not dependent to the function's gradient or continuity [28]. The methods, are very sensitive to initial feasible value and parameter tuning. Fig. 1.1 depicts the classification of OPF techniques based on the search methods. Other random search methods are simulated annealing, tabu search and ant colony. These methods are also failed to provide information about global optima.

1.1.3 Convex OPF: Optimal Solution

A large body of researchers have investigated the solution to OPF problem [12–18] as discussed in section 1.1.2, and numerous studies have proposed optimization algorithms to solve OPF problem including linear programming, nonlinear programming, and evolutionary programming. The main disadvantage of these methods is various well known limitations referred to as the non-exact relaxation of nonlinear OPF, heavy computational burden and locally optimum solution. These limitations are mainly resulting from non-convexity of OPF equations [29].

Power flow equations placed as constraints in OPF problems are nonlinear quadratic functions. Given a quadratic cost function, OPF problem is defined as quadratically constrained quadratic programming (QCQP) problem [30]. This problem is a non-convex NP-hard optimization problem. In recent years, considerable contributions are being reported in convexification and relaxation of OPF. DC optimal power flow is considered the simplest relaxation to OPF problem [31, 32]. However, there are certain drawbacks associated to the use of DC OPF. Unlike convex relaxation methods, DC OPF may results in infeasible solution, and casts doubt on its optimality. DC modeling has certain deficiency in modeling specific OPF problems because of dropping some power flow variables such as reactive powers.

Based on power flow models, convex relaxation of OPF is generally classified into two types: Relaxation of bus injection model (BIM) OPF, and Relaxation of branch

flow model (BFM) OPF. These models use different equations and set of variables, but they are mathematically equivalent [33]. The proposed relaxations based on these models are discussed in the following sections.

1.1.4 Relaxation of BIM-OPF

Three major relaxation methods are proposed for BIM-OPF. Semidefinite programming (SDP) relaxation, chordal relaxation and second order conic programming (SOCP) relaxation. BIM are developed based on net complex power injection and voltages at buses (1.3). The relaxation is derived by imposing convex supersets over the non-convex feasible set of OPF problem and minimizing cost function over these sets.

$$\begin{aligned} &Min\ C\left(.\right) \\ &s.t.\begin{cases} s_j = \sum_{k:j\sim k} y_{jk}^H V_j \left(V_j - V_k\right)^H \end{cases} \end{aligned} \tag{1.3}$$

The first SDP relaxation was proposed in 2008 by [34]. An equivalent rank-1 matrix is introduced to transform the constraints into linear space. SDP relaxation of BIM-OPF is then obtained by dropping the rank-1 constraint. This yields a quadratic convex optimization problem. Ref. [35] developed practical conditions using angle difference and showed unchanged pareto-optimal points by taking the convex hull. The analysis on SDP relaxation is presented in [29] where SDP relaxation as the dual of OPF problem is proposed and necessary and sufficient condition for zero duality gap are derived.

Chordal relaxation is first proposed in [36] and [37]. In this relaxation, a chordal extension to the graph matrix is introduced, and OPF problem is solved over new chordal space. Like SDP, chordal relaxation eliminates the rank-1 condition over the feasible area.

Table 1.1: Notations

i, j, h	system buses
V	bus voltage
y_{jk}	line admittance between j and k
s_j	net power injection at bus j
$T(N, E)$	radial network
k, T	time step and horizon time
S_{ij}, P_{ij}, Q_{ij}	power from bus i to j
R_{ij}, X_{ij}	line resistance and reactance
B_i, G_i	shunt admittance
I_{ij}	current from bus i to j
λ_{ij}	relaxed current from bus i to j
v_{ij}	voltage from bus i to j
ω_{ij}	relaxed voltage from bus i to j
$B_\perp$	reduced incidence matrix
$\beta_\perp$	phase angle difference over edges
θ_*	voltage recovered angle

First SOCP relaxation of BIM-OPF problem is presented in [38]; This method formulates BIM-OPF by introducing new set of real variables. These real variables bring the problem from a complex domain to a real space. Transforming quadratic equality constraint into inequality then yields the SOCP relaxation of BIM-OPF.

Optimal solution to the original OPF can be recovered from the solution of relaxed problems. The necessary condition of exact relaxation are based on cycle condition which imposes zero sum of the angle difference over cycles. Fig. 1.2 illustrates the relaxation stages and solution recovery of BIM-OPF problem. Ref. [33] demonstrated that the feasible region of original OPF is an effective subset of these relaxations which guaranties optimal solution. It is also identified that similarity between feasible sets is where the power system holds the radial structure.

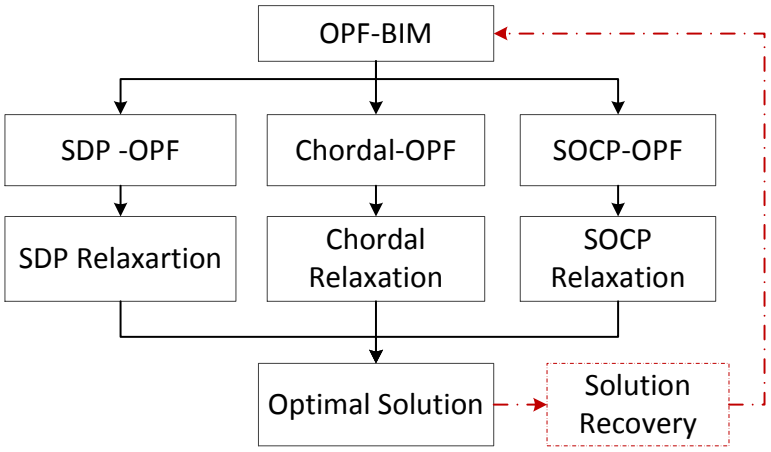

Figure 1.2: Relaxation Methods of BIM-OPF

SOCP provides tight and simple relaxation to BIM-OPF. This relaxation transforms the feasible area to a tighter space compared with SDP and chordal relaxations. In radial system, SOCP therefore, is an effective solution for convexification. In mesh networks, however, cycle condition causes difficulties for SOCP method. SDP and chordal are the replacing candidate for mesh networks whereby chordal provides the advantage of tight boundaries while the computation burden is a major drawback in SDP. Fast computation especially in large sparse network is the superiority of chordal method [36] despite the fact that its feasible area is an effective subset of SDP relaxation.

1.1.5 Relaxation of BFM-OPF

The relaxation of BFM-OPF problem can be classified into two successive stages of a) angle relaxation and b) conic relaxations. This results into SOCP relaxation. The branch flow OPF [39]- [40] first introduced by Baran-Wu for optimal capacitor placement in distribution systems, exploited the voltage and current angle relaxation; however, this model was non-convex as a result of quadratic equality constraints. BFM includes line current as OPF variable alongside the magnitude of bus voltage (1.4).

$$Min\ C\left(.\right) \tag{1.4}$$

$$s.t. \begin{cases} S_{ij} = V_i I_{ij}^* \\ V_i - V_j = z_{ij} I_{ij} \\ s_j = \sum_h S_{jh} - \sum_i \left(S_{ij} - z_{ij} \left|I_{ij}\right|^2\right) + y_j^* \left|V_j\right|^2 \\ \forall\ \left\{i, j, h, \left(i, j\right), \left(j, h\right)\right\} \in\ T\left(N, E\right) \end{cases}$$

In 2006, [38] proposed the convexification of branch flow OPF for radial system using second order conic programming (SOCP) relaxation. Several continuous convex relaxation of this model were then propounded by using second order cone approximation [41]- [42]. In important studies, [43]- [45] observed and proved the exactness of angle and conic relaxation, providing an exact optimal solution for OPF problem in radial networks. Notations are given in Table 2.1.

The relaxation method consisting of two consecutive stages transform OPF problem to a convex optimization problem. The angle relaxation step consists of eliminating angle of all bus voltages and line currents yielding the angle relaxed OPF. In the second step referred as the conic relaxation, the conic equality constraints are relaxed to conic inequality constraints. These relaxations yield SOCP-OPF problem, which is a convex optimization problem. These relaxations are exact; which means the solution to SOCP-OPF provides the optimal solution to the BFM-OPF problem.

OPF convexification flowchart are shown in Fig. 1.3. The angle recovery algorithm is used to recover voltages and currents of the BIM-OPF. The reduced incidence matrix B and the phase angle difference over transmission lines β_{ij} are calculated; The necessary condition of angle recovery (1.5) always holds for radial networks [45]; the voltage angle are then recovered through (1.6).

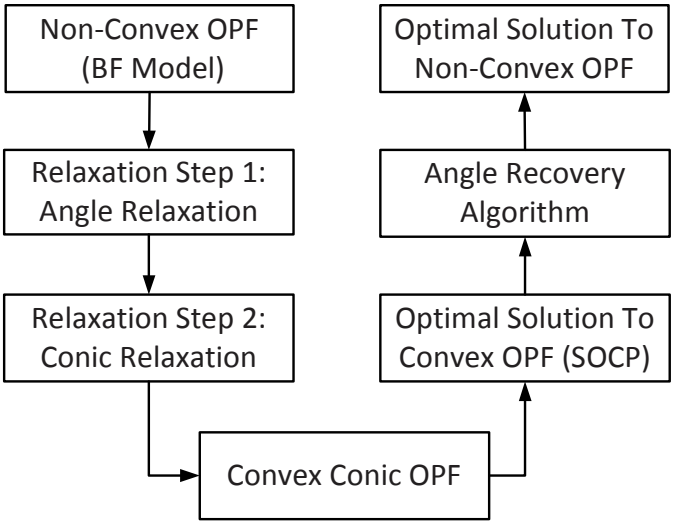

Figure 1.3: SOCP Relaxation of BFM-OPF: Two Step Relaxation

$$B_{\perp} B_T^{-1} \beta_{\perp} - \beta_{\perp} = 0 \tag{1.5}$$

$$\theta_* = Res.\big(B_T^{-1} \beta_T\big) \in (-\pi, \pi) \tag{1.6}$$

The other variables such as current phase are then recovered using Ohm's law and power injection equation. SOCP relaxation to BFM-OPF have several advantages. First it facilitates the placement of lower and upper bound constraints on voltage and line flows. Second it can simplify computing procedure through recursive structure.

The exactness of proposed BIM and BFM relaxations are classified based on the required conditions. Ref. [46, 47] proved the polynomial time performance for quadratically constrained OPF over radial power systems. Sufficient conditions of exact relaxation are derived in [48] for acyclic systems with no upper limit on voltage magnitudes.

These sufficient conditions can be applied for special cases of mesh networks, but they are not applicable to general mesh networks. Significant amount of relaxations tend to be exact in mesh networks using SDP and chordal relaxation [30]. Several

global optimization methods are also introduced in recent years and can be used where the relaxation conditions fail. Branch and bound method [49] and moment-sos are important global optimization methods extended to OPF problem.

1.2 Receding horizon control (RHC): Dynamic Solution

Distribution systems gradually transform from a passive network to an active system [2] as a result of evolving rapid distributed energy resources (DER), storage facilities alongside with renewable supplies and electricity markets [50–53]. This increases the degree of freedom on OPF problem and necessitates dealing with uncertainties through a dynamic optimization [54]. Receding horizon control (RHC) is a promising method to schedule the control variables over a time horizon divided by small time steps [1]. RHC output is a set of consecutive control actions, created by minimizing the objective function over a horizon window. The process has the capability of dealing with the constrained dynamic optimization problems which includes consideration of uncertain inputs or parameters. In dynamic systems, state update is captured by (1.7) whereby the dynamic matrix $\hat{A}_{(k|t)}$ and input matrix $\hat{B}_{(k|t)}$ are determined based on the input updates available at the current step. The control actions $\hat{u}_{(k|t)}$ are the solution of the optimization problem (1.8).

$$\hat{A}_{(k+1|t)} = \hat{A}_{(k|t)}\hat{x}_{(k|t)} + \hat{B}_{(k|t)}\hat{u}_{(k|t)} \tag{1.7}$$

$$Min \quad \sum_{k=t}^{t+T} \hat{J}_{(k|t)}\left(\hat{x}_{(k|t)}, \hat{u}_{(k|t)}\right) \tag{1.8}$$

$$Sub. \quad \hat{A}_{(k+1|t)} = \hat{A}_{(k|t)}\hat{x}_{(k|t)} + \hat{B}_{(k|t)}\hat{u}_{(k|t)}$$

$$\left(\hat{x}_{(k|t)}, \hat{u}_{(k|t)}\right) \in \hat{C}_{(k|t)} \quad k = t, ..., T$$

The RHC consists of the following steps:

1. The objective function $\hat{J}_{(k|t)}$ is defined over the time horizon $[t : t + T - 1]$. In

OPF problem , this objective represents the operational cost. The system parameters and constraints $\hat{C}_{(k|t)}$ are included based on the data update available until time step t.

2. The optimization problem (1.8) is solved, and the system control variables are determined over the horizon window $[t : t + T - 1]$. The first control actions, $\hat{x}_{(k|t)}$ and $\hat{u}_{(k|t)}$, are sent to the system.

3. Feedback of system variables and external signals are sent back to the optimization routine to update the system states and re-forecast these inputs over the next horizon window $[t + 1 : t + T]$.

4. The system moves into the next time step $t + 1$, and $[t + 1 : t + T]$ becomes the new horizon window. The preceding steps are repeated over the new window.

The RHC method continues until the time step reach to the horizon T. Handling the time horizon is a significant feature which brings in the ability to include uncertain parameters and system feedback. This method also creates a platform to handle dynamic components within the optimization problem.

1.3 Dynamic Convex OPF

The convex OPF methods are efficient techniques to obtain the optimal solution for OPF problem. However, the new challenges in modern power system which are explained through introduction and are summarized below, necessitate the extension of convex OPF approaches, SOCP-OPF for radial distribution system and SDP-OPF for transmission systems, to formulate the incorporation of the new players and DC network in convex OPF problems.

As a result of integrating distributed energy resources (DER), storage facilities alongside renewable supplies and electricity markets, distribution systems are gradually being transformed into an active system. These changes increase the degree

of freedom on OPF problem and require dealing with uncertainties through fast optimization techniques such as convex conic programming. Receding horizon control (RHC) is a promising method to schedule the control variables over a time horizon divided by small time steps. However, The studies presented so far focus on either the OPF convexification or RHC method independently.

In transmission system, incorporating voltage stability limits inside optimal power flow (OPF) is becoming an essential part for economic power dispatch in new energy management systems. Intensified congestion on power transmission system besides demand growth and rise of stochastic players push the system closer to its stability limits. Voltage source converter (VSC) based DC transmission systems can alleviate this burden by providing DC corridors for active power and managing reactive power at converter terminals. The new method incorporating voltage stability margin into convex OPF is required to model this margin either in the objective or constraints of OPF problem, which forms convex voltage stability constrained OPF (Convex VSC-OPF). In AC-DC system, the convex OPF is required to reach the minimum cost or maximum stability margin of both systems together, which is also suitable for meshed DC networks.

1.4 Dissertation Framework

This dissertation focuses on the dynamic convex optimal power flow approaches in modern power grid, which mitigate some limitations of existing methods in radial and mesh networks. The dissertation framework consists of following sections:

-In chapter 2, a dynamic optimal scheduling of active power distribution systems is proposed using receding horizon convex OPF. The main advantages of the proposed method are a) optimum scheduling b) including the dynamic of storage c) integration of uncertain resources. The effectiveness of this method is evaluated on active distribution systems connected to upstream network and neighboring distribution system. The proposed method includes physical constraints, market price variation, energy

storage dynamics and source uncertainties.

-An architecture for the real-time implementation of dynamic convex OPF is proposed in chapter 3, and the scalability of proposed method is examined on a larger system. This real-time framework is useful especially for implementation on the grids with small scheduling time steps.

- In chapter 4, a new convex VSC-OPF architecture taking into account different types of VSC-OPF methods including maximum stability margin, minimum margin constrained, and multi-objective VSC-OPF is proposed. This method is also implemented to derive system PV curve and the results are compared with CPF.

In chapter 5, convex VSC-OPF and OPF formulations are presented to find maximum loading point margin and minimum operating cost of integrated AC-DC system, which is suitable for active DC meshed networks. The proposed methods address some limitations of AC-DC OPF methods due to non-convexity, separate scheduling of AC and DC networks or using equivalent of DC network.

The conclusion and future work are explained in 6.

CHAPTER 2: DYNAMIC OPTIMAL SCHEDULING OF POWER DISTRIBUTION SYSTEMS USING RECEDING HORIZON CONVEX OPF

2.1 Introduction

Distribution systems are gradually being transformed from a passive network into an active system [2] as a result of integrating distributed energy resources (DER), storage facilities alongside renewable supplies demand response and electricity markets. These changes increase the degree of freedom on OPF problem and necessitate dealing with uncertainties through fast optimization techniques [55, 56]. Receding horizon control (RHC) [1] is a promising method to schedule the control variables over a time horizon divided by small time steps. In our earlier work, we proposed and examined the framework of an online ACOPF integrated in RHC [57] to re-forecast the future market price. Ref. [58] proposed the iterative method of prox-average message passing to decentralize the optimization over devices. It also suggests RHC as an extension to that approach. Recently [59] examined RHC-ACOPF to find better DG set-points. A parallel multi-stage dispatch using RHC propounded by [60] evaluated the control feasibility of network layers in bulk power system. Other studies have investigated the RHC in scheduling of deferrable electric loads without power constraints [61], and for scenario-based optimal power dispatch [62]. There are two potential drawbacks of using RHC with nonlinear ACOPF: a) computational burden at each time step and b) issues related to local optimum solution.

The studies presented so far focus on either the OPF convexification or RHC method independently [57]. In this chapter, a dynamic convex OPF is proposed by incorporating a convex conic OPF within the RHC (RHC-SOCP-OPF) [63, 64]. This method results in finding the optimal schedule, and at the same time brings

saving in computation time due to efficient convex optimization algorithms compared with a non-convex optimization in ACOPF. The proposed method could also include dynamic device models in the minimization problem such as energy storage and at the same time allows for including measurements and other stochastic variables. To the best of our knowledge, it is the first time that a method introduces the convex OPF integrated in RHC. The proposed method is tested on IEEE distribution systems, equipped with various constraints and components associated with a micro grid.

Rest of the chapter is organized in the following order. 2.2.1 presents the RHC formulation dealing with OPF problem, and 2.2.2 discusses the convexification of OPF problem using SOCP. Section 2.3 formulate the dynamic convex OPF. Implementation of the developed method on the 32-bus and the study results are presented in section 2.4. The case study contains market interactions including neighboring distribution companies (DISCOs) and upstream network, uncertain wind generation, storage, distributed energy resources, and contracted loads. Study results evaluate the effectiveness of convex RHC-SOCP-OPF compared with RHC-ACOPF. Finally, conclusion is presented in section 2.5.

2.2 System Architecture and Modeling

The proposed dynamic convex OPF architecture consists of two major sections: a) RHC based dynamic modeling and wind forecast and b) convex conic OPF formulation within RHC.

2.2.1 RHC For Dynamic Device Modeling and Forecasting

RHC output is a set of consecutive control actions, created by minimizing the objective function over a horizon window. The process has the capability of dealing with the constrained dynamic optimization problems which includes consideration of uncertain inputs or parameters.

2.2.1.1 RHC: Dynamic Device Modeling

The RHC equation which models the dynamic behavior of components are presented in (2.1).

$$\hat{A}_{(k+1|t)} = \hat{A}_{(k|t)}\hat{x}_{(k|t)} + \hat{B}_{(k|t)}\hat{u}_{(k|t)} \tag{2.1}$$

The state of the charge (SOC) of storage is then obtained and presented in (2.2). Notations are shown in Table 2.1.

$$E_{s,i}^{k+1} = E_{s,i}^{k} + P_{ch,i}^{k}\eta_{ch,i} - P_{disch,i}^{k}/\eta_{dich,i} \tag{2.2}$$
$$k \in [t : t + T - 1]$$

The RHC method continues until the time step reach the horizon T. Handling the time horizon is a significant feature in the proposed approach which brings in the ability to include uncertain parameters and data-update through system feedback. Thus this method creates the platform to handle the optimization incorporating dynamic components such as storage in power distribution system.

2.2.1.2 RHC: Forecasting Wind Generation

Uncertainty is generally modeled using stochastic models based on random variables. To this end, a multi-variable normal distribution $f(z_1, z_2, \cdots, z_T)$ is assigned to model over horizon steps; The density function is shown in (2.3). This function is parametrized with $T \times T$ covariance matrix, Σ, and $1 \times T$ mean vector μ.

Fig. 2.1 depicts the forecasting section inside the RHC structure dealing with SOCP-OPF problem. We developed (2.3)-(2.5) to forecast the random variable $\hat{z}$ over the horizon window $[k : k + T - 1]$ using online data $z_t, z_{t-1}, \cdots, z_{t-N+1}$ with the conditional expectation expression. The model works as follows: First the linear

regression method is deployed to generate the forecast values. i.e. the conditional expectation of random variable at time step k $\left(\hat{z}_{k|t}\right)$ is estimated as linear function of the last N actual feedback values, $Z = [z_t, z_{t-1}, \cdots, z_{t-N+1}]$, density function expectation $E\{z\}$ and variance $E\{z_t - E\{z_t\}\}^2$. This recursive formulation deals with random variables in which the variables have a normal joint distribution.

$$f(z_1, z_2, \cdots, z_T) = \frac{1}{\sqrt{(2\pi)^T |\Sigma|}} \left(-\frac{1}{2}(z-\mu)^\intercal \Sigma^{-1}(z-\mu)\right) \tag{2.3}$$

$$\hat{z}_{(k|t)} = E(z_k | z_t, z_{t-1}, \cdots, z_{t-N+1}) = \alpha + \beta^T Z$$

$$\alpha = E\{z_k\} - \beta^T \begin{bmatrix} E\{z_t\} \\ E\{z_{t-1}\} \\ E\{z_{t-2}\} \\ \vdots \\ E\{z_{t-N+1}\} \end{bmatrix} \tag{2.4}$$

$$\beta = \begin{bmatrix} \frac{E\{(z_t - E\{z_t\})(z_k - E\{z_k\})\}}{E\{z_t - E\{z_t\}\}^2} \\ \frac{E\{(z_{t-1} - E\{z_{t-1}\})(z_k - E\{z_k\})\}}{E\{z_{t-1} - E\{z_{t-1}\}\}^2} \\ \frac{E\{(z_{t-2} - E\{z_{t-2}\})(z_k - E\{z_k\})\}}{E\{z_{t-2} - E\{z_{t-2}\}\}^2} \\ \vdots \\ \frac{E\{(z_{t-N+1} - E\{z_{t-N+1}\})(z_k - E\{z_k\})\}}{E\{z_{t-N+1} - E\{z_{t-N+1}\}\}^2} \end{bmatrix} \tag{2.5}$$

The forecasted values $\hat{z}_{(k|t)}$ resulting from (2.3)-(2.5) is then used in RHC optimization (2.2) to obtain the optimal control variables $\hat{x}_{(k|t)}, \hat{u}_{(k|t)}, k \in [t, t+T-1]$ which minimizes the cost function over the next time horizon T. The process is repeated at

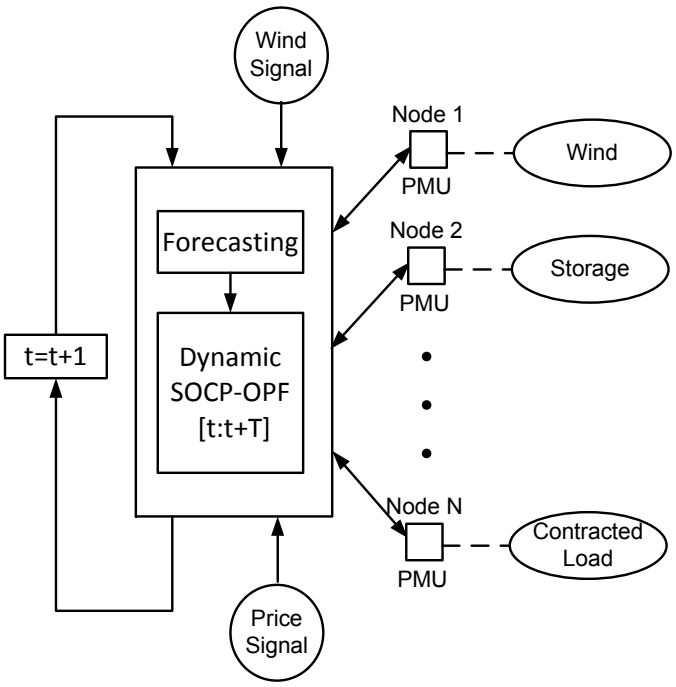

Figure 2.1: RHC Dealing With OPF in Modern Power Grid

the next time step.

RHC scheduling differs from day-ahead scheduling in terms of consecutive control actions and moving horizon. If horizon window is 24-hours, and time step is 1-hour, day-ahead scheduling determines the control variables over the next 24-hours $[k, k+1, \cdots, k+24]$. In day-ahead scheduling, unlike RHC, the optimization is not repeated until the end of current horizon $(k+24)$. The next optimization is, therefore, carried out for the day after current horizon, which is $[k+25, k+26, \cdots, k+48]$. In RHC, the cost function is minimized at each time step over the moving horizon. It means the optimization is repeated at the beginning of next time step $(k+1)$ over receding horizon of $[k+1, k+2, \cdots, k+25]$ using updated forecast and input. Then the control actions are derived and utilized as the new system schedule. These steps are repeated for all following time steps $(k+2), (k+3), \cdots, (k+24)$.

2.2.2 Convex Conic OPF

The convex OPF is a requirement to reach an optimal solution with less computation time. The proposed SOCP-OPF is formulated based on branch flow model (BFM). The branch flow model is the method of modeling power flow problem using branch variables such as line current and line power unlike the nodal variables in the bus injection method (BIM). The branch flow model is described based on a directed tree graph denoted as $T(N, E)$. The directed tree graph starts with node 0 which is connected to the upstream network; the tree covers all network nodes. The direction of edges is chosen arbitrarily. BFM equations are demonstrated in (2.6)-(2.8). Notations are given in the Table 2.1.

$$S_{ij} = V_i I_{ij}^* \tag{2.6}$$

$$V_i - V_j = Z_{ij} I_{ij} \tag{2.7}$$

$$S_j = \sum_h S_{jh} - \sum_i \left(S_{ij} - Z_{ij} \left|I_{ij}\right|^2\right) + y_j^* \left|V_j\right|^2 \tag{2.8}$$

$$\forall \ \{i, j, h, (i, j), (j, h)\} \in \ T(N, E)$$

The OPF model based on BFM, is a non-convex optimization problem due to nonlinear equality constraints. The relaxation method to bring the optimization as a convex function consist of two consecutive stages [45], [30]. The idea is to derive the convex OPF by imposing convex supersets and minimizing the same cost function over these supersets. The first step, angle relaxation, consists of eliminating the angles of bus voltage and line current from (2.6)-(2.8). This procedure can be explained as follows.

A_1 : Substitute $Z_{ij} = R_{ij} + jX_{ij}$, $y_j = G_j + jB_j$, $S_{ij} = P_{ij} + jQ_{ij}$, and $S_j = P_j + jQ_j$ into (2.8), yielding in (2.9) and (2.10) by equating real and imaginary parts.

Table 2.1: Notations

i, j, h	nodes of radial system
$T(N, E)$	radial network
k, T	time step and horizon time
S_{ij}, P_{ij}, Q_{ij}	Power from bus i to j
R_{ij}, X_{ij}	line resistance and reactance
B_i, G_i	shunt admittance
I_{ij}	current from bus i to j
λ_{ij}	relaxed current from bus i to j
v_{ij}	voltage from bus i to j
ω_{ij}	relaxed voltage from bus i to j
$B_\perp$	reduced incidence matrix
$\beta_\perp$	phase angle difference over edges
θ_*	voltage recovered angle
$P^k_{wg,i}, P^k_{dg,i}$	wind and DG generation
$P^k_{cl,i}$	contacted load curtailment
$P^k_{m,i}, P^k_{nd,i}$	wholesale and neighboring power exchange
$c^k_{WG,i}, c^k_{DG,i}$	wind and DG operation cost
$c^k_{CL,i}$	contacted load cost
$c^k_{M,i}, c^k_{ND,i}$	wholesale and neighboring price
$E^k_{s,i}$	energy storage at time step k
$P^k_{ch,i}, P^k_{dich,i}$	storage charging and discharging rate
$\eta_{ch,i}, \eta_{dich,i}$	storage charging and discharging efficiency
ACOPF	Non-convex OPF
SOCP-OPF	Convex Conic OPF
RHC-ACOPF	ACOPF integrated in RHC
RHC-SOCP-OPF	Convex conic OPF integrated in RHC

A_2 : Substitute I_{ij} from (2.7) into (2.6) giving $V_j = V_i - Z_{ij}S^*_{ij}/V^*_i$. Take the magnitude squared of both sides resulting in $|V_j|^2 = |V_i|^2 + |Z_{ij}|^2 |I_{ij}|^2 - Z_{ij}S^*_{ij} - Z^*_{ij}S_{ij}$.

A_3 : Take magnitude squared of (2.6) yielding $|I_{ij}|^2 = S^2_{ij}/|V_i|^2$.

A_4 : Substitute $Z_{ij} = R_{ij} + jX_{ij}$ and $S_{ij} = P_{ij} + jQ_{ij}$ into A_2 and A_3 yielding (2.11) and (2.12) respectively.

These substitutions result in obtaining the set of equations which contains the angle

relaxed variables $|V_j|^2$ and $|I_{ij}|^2$ instead of complex variables of V_j and I_{ij} as it can be seen in (2.9)-(2.12).

$$P_j = \sum_h P_{jh} - \sum_i \left(P_{ij} - R_{ij} |I_{ij}|^2\right) + G_j |V_j|^2 \tag{2.9}$$

$$Q_j = \sum_h Q_{jh} - \sum_i \left(Q_{ij} - X_{ij} |I_{ij}|^2\right) + B_j |V_j|^2 \tag{2.10}$$

The $|V_j|^2$ and $|I_{ij}|^2$ are then respectively replaced with new variables ω_j and λ_{ij}, as shown in (2.14)-(2.17). In the second step, referred as the conic relaxation, the conic equality constraints are relaxed to conic inequality constraints $\left(\lambda_{ij} \leq \frac{P_{ij}^2+Q_{ij}^2}{\omega_i}\right)$. These relaxations convert the ACOPF problem to the convex SOCP-OPF problem (see (2.14)-(2.17)). The objective function (2.13) is the generation cost, and it is the same for both ACOPF and SOCP-OPF.

$$Min \sum_{i \in N_G} c_i \left(P_g^i\right) \tag{2.13}$$

$$P_j = \sum_h P_{jh} - \sum_i \left(P_{ij} - R_{ij}\lambda_{ij}\right) + G_j\omega_j \tag{2.14}$$

$$Q_j = \sum_h Q_{jh} - \sum_i \left(Q_{ij} - X_{ij}\lambda_{ij}\right) + B_j\omega_j \tag{2.15}$$

$$\omega_j = \omega_i - 2\left(R_{ij}P_{ij} + X_{ij}Q_{ij}\right) + \left(R_{ij}^2 + X_{ij}^2\right)\lambda_{ij} \tag{2.16}$$

$$\lambda_{ij} \leq \frac{P_{ij}^2 + Q_{ij}^2}{\omega_i} \tag{2.17}$$

These relaxations are exact; i.e. SOCP-OPF in (2.13)-(2.17) gives the optimal solution to the ACOPF problem. Then a "centralized angle recovery" algorithm based on (2.18), (2.19) recovers the voltage and current angles. This step includes calculating the reduced incidence matrix B and the phase angle difference β_{ij} . The other

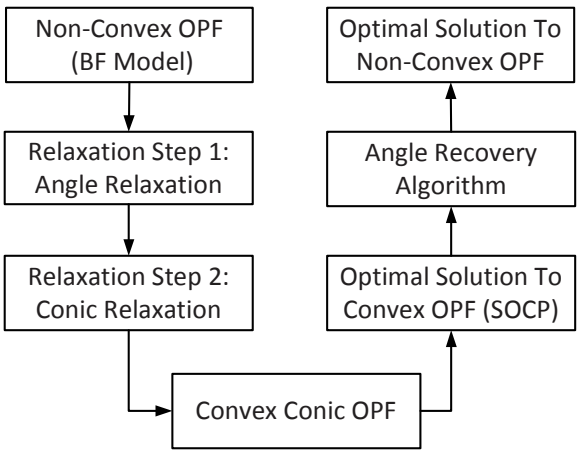

Figure 2.2: OPF Convexification: Two Step Relaxation

variables can then be recovered using Ohm's law and power injection equations.

$$B_{\perp}B_T^{-1}\beta_{\perp} - \beta_{\perp} = 0 \tag{2.18}$$

$$\theta_* = Res.\big(B_T^{-1}\beta_T\big) \in (-\pi, \pi) \tag{2.19}$$

There are two main methods for voltage angle recovery a) "centralized angle recovery" and b) "distributed angle recovery". In the centralized angle recovery all the angles are computed in one step as opposed to distributed angle recovery where the angles are computed in each step. It has been proven that the necessary condition of angle recovery (2.18) always holds for radial networks [45]. The overall algorithmic flowchart for OPF convexification is shown in Fig. 2.2.

2.3 Proposed Integrated RHC-SOCP-OPF Formulation

The overall structure of proposed method is depicted in Fig. 2.3. In order to implement an RHC optimization structure, the first step is to formulate the RHC-ACOPF problem for the system including the storage, wholesale market, neighboring DISCO, and wind generation. It is worth noting that any stochastic generation models can be included in the proposed formulation. For OPF algorithm, previously discussed BF model formulated over a time horizon is derived.

In order to reach optimal solution two relaxation steps are implemented: angle

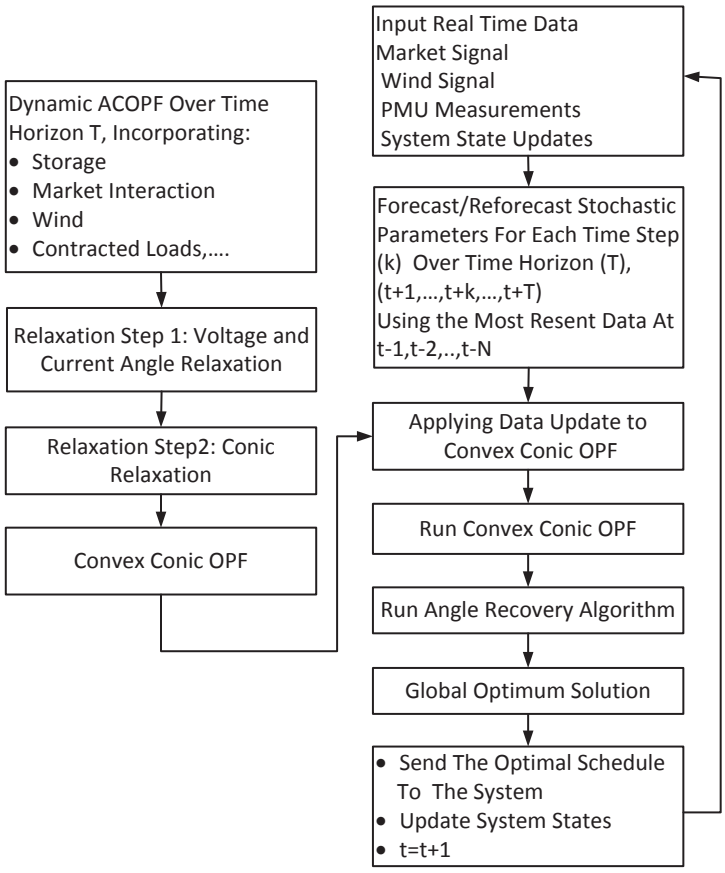

Figure 2.3: Optimal Scheduling using Convex RHC

relaxation and conic relaxation. A rotated quadratic cone technique with "change of variable concept" is used to obtain the SOCP form of the formulation (2.20) as,

$$2x_i x_j \geq \sum_{k=3}^{n} y_k^2 \quad k \in [R^{n^t}] \tag{2.20}$$

$$x_i = I^2, \quad x_j = V^2, \quad y_k = P^2 + Q^2$$

where R^{n^t} defines the space for the decision variables.

As the result, the quadratic equality constraints are converted to conic constraints inside the convex OPF formulation.

2.3.1 Objective Function

The proposed objective function takes into account the generation cost, contracted load cost and the cost for energy exchanged with upstream network and neighboring DISCO. The cost function at the time step t is represented in (2.21).

$$\sum_{k=t}^{t+T-1} \sum_{i \in N} \left(c^k_{WG,i}\left(P^k_{wg,i}\right) + c^k_{DG,i}\left(P^k_{dg,i}\right) + c^k_{CL,i}\left(P^k_{cl,i}\right) \right. \\ \left. + c^k_{M,i}\left(P^k_{m,i}\right) + c^k_{ND,i}\left(P^k_{nd,i}\right) \right) \\ k \in [t : t+T-1] \tag{2.21}$$

The distribution system here is considered to have the capability for exchanging power with the rest of grid, and the objective function is the total operation cost of the system.

The generation cost is considered as linear function of generated power. However, the quadratic objective functions can also be included inside the SOCP problem by using the "change of variable concept"as discussed earlier. The cost function may also include other objectives, such as conservation voltage reduction (CVR) and line losses.

2.3.2 Constraints

The RHC structure creates the capability to update the constraints (as shown in (2.22) at time step k). These time steps are associated with distribution lines, generation, expected wind generation, spot market price, demand and storage at each time step over the next horizon window as depicted in Fig. 2.3. Despite the conventional day-ahead scheduling which provides a constant limit for these values at each time step, the constraints are updated at each time step over the horizon.

$$
\begin{aligned}
&P^k_{wg.min,i} \le P^k_{wg,i} \le P^k_{wg.max,i} \\
&P^k_{dg.min,i} \le P^k_{dg,i} \le P^k_{dg.max,i} \\
&Q^k_{dg.min,i} \le Q^k_{dg,i} \le Q^k_{dg.max,i} \\
&P^k_{nd.min,i} \le P^k_{nd,i} \le P^k_{nd.max,i} \\
&Q^k_{nd.min,i} \le Q^k_{nd,i} \le Q^k_{nd.max,i} \\
&P^k_{m.min,i} \le P^k_{m,i} \le P^k_{m.max,i} \\
&Q^k_{m.min,i} \le Q^k_{m,i} \le Q^k_{m.max,i} \\
&P^k_{cl.min,i} \le P^k_{cl,i} \le P^k_{cl.max,i} \\
&Q^k_{cl.min,i} \le Q^k_{cl,i} \le Q^k_{cl.max,i} \\
&P^k_{ch.min,i} \le P^k_{ch,i} \le P^k_{ch.max,i} \\
&P^k_{disch.min,i} \le P^k_{disch,i} \le P^k_{disch.max,i} \\
&E^k_{s,min,i} \le E^k_{s,i} \le E^k_{s.max,i} \\
&\lambda^k_{ij} \le \lambda^k_{ij.max} \\
&\omega^k_{i.min} \le \omega^k_i \le \omega^k_{i.max} \\
&S^k_{ij} \le S^k_{ij.max}
\end{aligned} \tag{2.22}
$$

Corresponding power flow equations represented in (2.23) are the relaxed power balance constraints over the horizon window.

$$
\begin{aligned}
&P^k_{wg,i} + P^k_{dg,i} + P^k_{cl,i} + P^k_{ch,i} - P^k_{disch,i} - P^k_{d,i} \\
&\qquad = \sum_h P^k_{ih} - \sum_j \left(P^k_{ji} - R^k_{ji}\lambda^k_{ji}\right) + G^k_i \omega^k_i \\
&Q^k_{wg,i} + Q^k_{dg,i} + Q^k_{cl,i} - Q^k_{d,i} \\
&\qquad = \sum_h Q^k_{ih} - \sum_j \left(Q^k_{ji} - X^k_{ji}\lambda^k_{ji}\right) + B^k_i \omega^k_i \\
&k \in [t : t + T - 1]
\end{aligned} \tag{2.23}
$$

The voltage drop constraint is shown in (2.24).

$$\omega_i^k = \omega_j^k - 2\left(R_{ji}^k P_{ji}^k + X_{ji}^k Q_{ji}^k\right) + \left(R_{ji}^{k\,2} + X_{ji}^{k\,2}\right)\lambda_{ji}^k \tag{2.24}$$

The relaxed line current flow constraint is (2.25).

$$\lambda_{ij}^k \leq \frac{P_{ij}^{k^2} + Q_{ij}^{k^2}}{\omega_i^k} \qquad\qquad k \in [t : t+T-1] \tag{2.25}$$

The state of energy stored in the storage at each time step is dictated by the preceding energy, charging, and discharging rate. The coefficients representing the charging and discharging efficiency can be represented as in (2.26).

$$E_{s,i}^{k+1} = E_{s,i}^k + P_{ch,i}^k \eta_{ch,i} - P_{disch,i}^k / \eta_{disch,i} \tag{2.26}$$

2.4 Case Studies and Simulation Results

The first case study is conducted on the 32-bus distribution system to examine the proposed architecture of integrated RHC and convex optimization examined the 8-bus test system. In these studies, the wind generation is considered as a stochastic variable; i.e. the expectation of wind generation at time step k of horizon window $[t, \ldots, k, \ldots, t+T-1]$ is forecasted by moving one step forward, t to t+1. The actual and forecasted wind data from the electric reliability council of Texas (ERCOT) is used for the real-time wind estimation at each time step.

The time horizon T is considered $24h$, and each time step is considered $1h$. However, if the optimization problem is solved in the order of seconds or minutes depending on the system size, it is feasible to reduce the time step to less than few minutes. Four methods are compared to test the effectiveness of developed RHC-SOCP-OPF method.

Method A: Day-ahead scheduling using ACOPF.

This method uses day-ahead scheduling using the non-convex OPF (ACOPF) equations, in which the objective function is minimized (one-time) over the horizon window and the system schedule is determined for each time step $[1 : 24]$ as explained in 2.2.1.

Method B: Day-ahead scheduling using SOCP-OPF.

This method, like method A, is a day-ahead scheduling but, it incorporates convexified power flow formulation (SOCP-OPF) as shown in (2.13)-(2.17).

Method C: Online scheduling using RHC-ACOPF.

This method incorporates RHC (explained in III-A) inside the non-convex OPF equations (ACOPF) in which the cost function is consecutively minimized at each time step over the moving horizon using updated forecast and input.

Method D: Online scheduling using RHC-SOCP-OPF.

The proposed method consists of integrated RHC with convexifed OPF equations (SOCP-OPF), viz., RHC-SOCP-OPF as discussed in 2.3.

Note: The system physical constraints (2.22), and storage dynamic constraint (2.26) are included in all four methods.

The simulation results are reported based on Intel 2.4 GHz Core i5 CPU. The optimization package GAMS with MOSEK solver, is used to implement the SOCP-OPF. For non-convex OPF, NLP CONOPT solver is used to examine the ACOPF formulation.

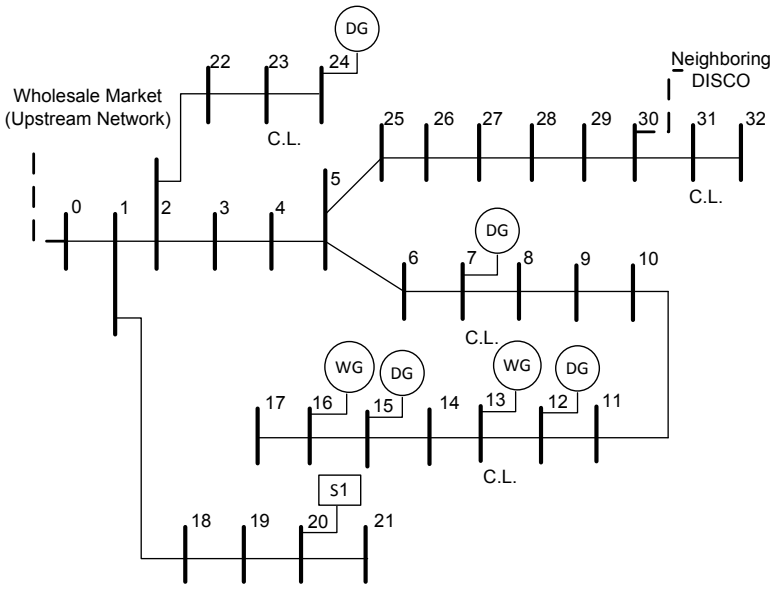

Figure 2.4: Modified 32-bus Distribution Test System

Case I: 32-bus Test System

The 32-bus radial distribution system [65] is considered to examine the convex RHC method. The system is 12.66 kV and contains 33 buses (bus 0 is the contact point to upstream network) and 32 lines. Test system is modified to incorporate the market transaction, wind generation, and storage (see Fig. A.1). This radial network is connected to the upstream network and neighboring DISCO through tie lines from bus 0 and bus 30 respectively. Two wind farms are located at bus 13 and 16. One storage station is connected to bus 20. Contracted loads are considered at bus 7, 13, 24, and 31.

The market price at each time step is the multiplication of market price variation coefficient and the base price. The load demand variation at different nodes are calculated with the same procedure. DISCO optimize its operation schedule based on the energy market price in upstream, neighboring DISCO, wind variation, etc. Neighboring DISCO and upstream networks are capable to exchange power with the test system based on the hourly energy price. The base market price, and neighboring price are considered \$0.09/kWh and \$0.0825/kWh respectively. The cost of contracted

loads is \$0.1/kWh. The least operational cost is associated with wind generators \$0.05/kWh. The variation coefficient of energy price with respect to base price are presented in Table A.1. The detailed data of DGs and storage capacity for modified 32-bus test system are given in Appendix (See Table A.2 and A.3). Power base for two systems is 100 kW. The DG's generation cost for the test systems are shown in Table A.4 and A.5.

Table 2.2: Price Variation Coefficient At Different Time Steps

Step (k)	Price Coe.	Load	Step (k)	Price Coe.	Load
1	0.7	0.88	13	1.31	1.38
2	0.64	0.83	14	1.46	1.41
3	0.62	0.80	15	1.66	1.44
4	0.59	0.78	16	1.43	1.45
5	0.62	0.80	17	1.80	1.43
6	0.63	0.85	18	1.43	1.39
7	0.65	0.92	19	1.18	1.39
8	0.65	1.02	20	1.14	1.34
9	0.77	1.11	21	1.07	1.28
10	0.84	1.20	22	0.92	1.15
11	0.95	1.28	23	0.85	1.02
12	1.09	1.34	24	0.80	0.94

Other system data are given in [65]- [66]. Fig. 2.5 depicts the active power generation at bus 16 using convex methods A to D. It can be notified that the day-ahead scheduling (method A and B) over estimated and under estimated wind generation up to 1 p.u. compared with RHC methods (method C and D). It is noticeable that the both method C and D presented same optimal scheduling at bus 16. The reason is the low wind price which dictates higher priority to dispatch the wind generators. This also allows the wind to operate at its maximum. The disadvantage of day-ahead scheduling is shown in Fig. 2.6, in which optimization methods A and B under estimated the power exchange with upstream network during hours 13 to 19. According to real-time data, wind availability is less during these hours. This reduction causes the increase in power exchange with upstream network represented in RHC methods

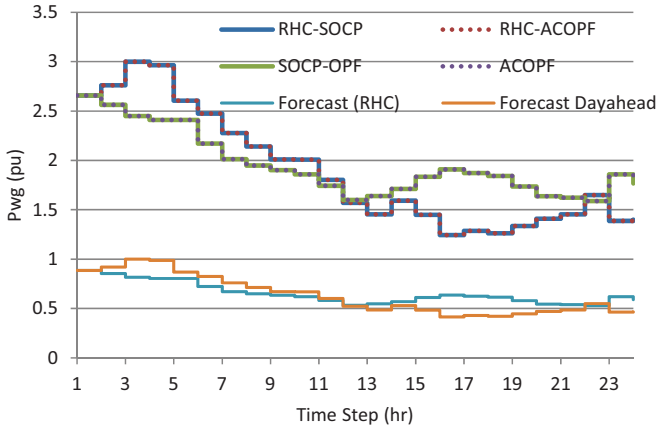

Figure 2.5: Optimal Wind Schedule at Bus 16; Normalized Wind Forecast Using Day-ahead and RHC method

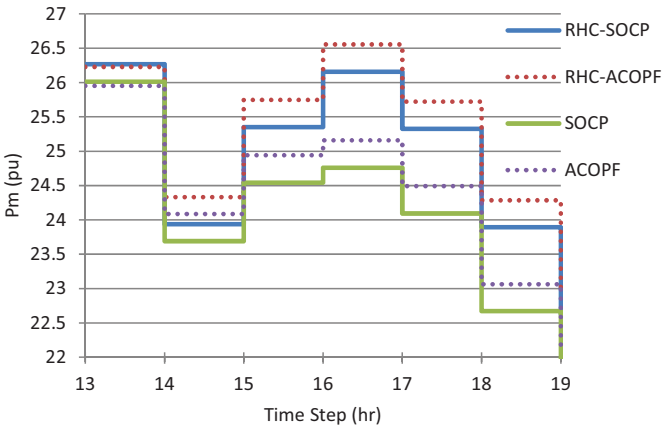

Figure 2.6: Power Exchange with Upstream Network

C and D.

Fig. 2.7 explains the charging and discharging schedules of storage S_1 at bus 20 with market price variation. The E_s shows the amount of energy stored in storage S_1. These optimized values are obtained by using RHC convex OPF (method D). The charging and discharging pattern are explained with the price of upstream market. During the hours 1 to 9 the price at the upstream network are low. The storage is, therefore, scheduled to be charged. It stores the energy during this period for lesser price. As the price during hours 13 to 21 increases, it is more economical to use the storage as the energy source rather than buying energy from other sources. The

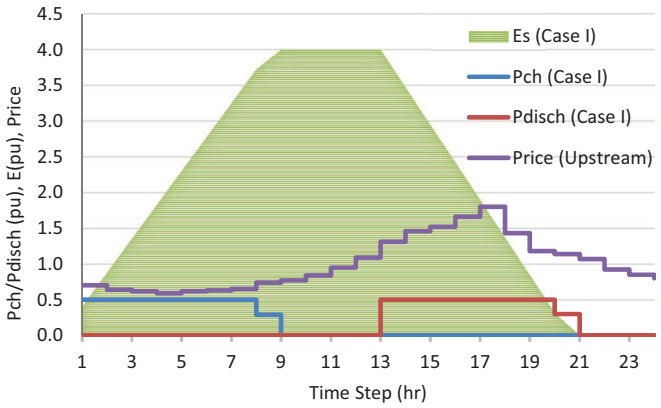

Figure 2.7: Optimal P_{ch} and P_{Dich} Schedules For Storage S_1 at Bus 20 Using RHC Convex OPF

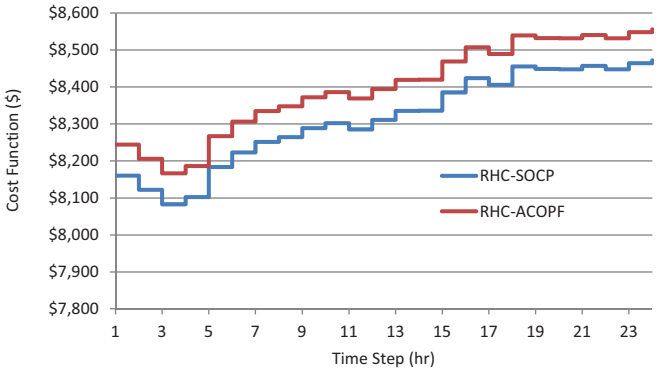

Figure 2.8: Total Cost Over The Time Horizon; RHC Convex OPF versus RHC-ACOPF

performance of convex method D is compared with non-convex OPF (method C) in Fig. 2.8. The proposed convex method D results in reduction of the cost function at all steps of RHC implementation. This improvement is the result of convex nature of proposed method D, which guarantees the global optimum solution. Table 2.3 provides the total cost at time steps 1,8,16,24. It can be seen that method D yields to 1% reduction in cost by finding the optimal schedule of the active distribution system. Table 2.4 illustrates the performance of RHC methods C and D. The proposed method D shows the reduction in simulation time, and at the same time ensure convergence to the optimal solution in comparison with non-convex method C which yields a local optimum with a simulation time around twice that of method D.

Table 2.3: Total Cost Function [$] At Different Time Step

Step (k)	1	8	16	24
RHC-SOCP	8160	8264	8423	8472
RHC-ACOPF	8244	8347	8507	8556

Table 2.4: simulation time comparison

RHC-SOCP Average Simulation Time (Sec)	6.8333
RHC-ACOPF Average Simulation Time (Sec)	14.2751

2.5 Conclusion

A dynamic optimal power scheduling method for radial distribution system is proposed including dynamic components, market transactions, contracted loads and renewable generation. The convex OPF is formulated within the RHC using two step relaxation in second order conic programming (SOCP). This convex RHC method takes into account the input uncertainties such as wind through re-estimating the future inputs based on the online input data, which is repeated at each time step over the horizon window. The proposed method addresses the possible disadvantages of dynamic methods based on non-convex ACOPF, referred as the local optimum solution and time inefficiency. The method effectiveness examined on the 32-bus; The results shows the improvements in comparison with non-convex ACOPF method.

CHAPTER 3: SCALABILITY AND REAL-TIME IMPLEMENTATION OF RECEDING HORIZON CONVEX OPF

3.1 Scalability of Receding Horizon Convex OPF

The scalability of the proposed receding horizon convex OPF is examined in this chapter. In chapter 2, the convex RHC OPF formulation is developed to find the optimal schedule of active radial systems. The test system for RHC-ACOPF problem includes the storage, wholesale market, neighboring DISCO, wind generations, DER, and contracted loads. On the other hand, the horizon window for each step of optimization is 24 hours. All these variables increase the size of optimization problem rapidly as the size of test system increases. To test the effectiveness of RHC convex OPF on larger active distribution systems, three case studies are considered. The Case I is the modified 32 bus test system. Case Studies II and III are implemented on modified 119-bus radial system. Four methods are compared to test the effectiveness of developed RHC-SOCP-OPF method.

Method A: Day-ahead scheduling using ACOPF.

This method uses day-ahead scheduling using the non-convex OPF (ACOPF) equations, in which the objective function is minimized (one-time) over the horizon window and the system schedule is determined for each time step [1 : 24] as explained in 2.2.1.

Method B: Day-ahead scheduling using SOCP-OPF.

This method, like method A, is a day-ahead scheduling but, it incorporates convexified power flow formulation (SOCP-OPF) as shown in (2.13)-(2.17).

Method C: Online scheduling using RHC-ACOPF.

This method incorporates RHC (explained in III-A) inside the non-convex OPF equations (ACOPF) in which the cost function is consecutively minimized at each time step over the moving horizon using updated forecast and input.

Method D: Online scheduling using RHC-SOCP-OPF.

The proposed method consists of integrated RHC with convexifed OPF equations (SOCP-OPF), viz., RHC-SOCP-OPF as discussed in 2.3.

The system physical constraints (2.22), and storage dynamic constraint (2.26) are included in all four methods.

3.1.1 Case Study 119-bus Test System

A modified 119-bus distribution system is examined to test the effectiveness of proposed method as shown in Fig. A.2 . The system operates at 11 kV and contains 22709.7kW and 17041.1 kVar of demand. The system is modified to incorporate the market and neighboring DISCOs transaction, wind generation, contracted loads and storage. This radial network is connected to the upstream network from bus 1 and exchanges power with neighboring DISCOs through tie lines from the buses 48 and 80. The DGs are connected to the feeders at the buses $35, 44, 52, 56, 60, 64, 69, 84, 85$ $, 89, 96, 109, 116, 121$. Seven wind generators are integrated to the system through buses $14, 20, 50, 74, 76, 101, 113$. The contracted loads are connected to buses $24, 25, 42$ $, 43, 55, 59, 79, 82, 97, 112, 117$ and up to 20% of these loads are contracted to be curtailed. We report the simulation time based on Intel 2.4 GHz Core i5 CPU. The optimization package GAMS along with SOCP solver is used to implement the formulation. Two test cases are studied.

- Case II: Modified 119-bus with one storage at bus 21.
- Case III: Modified 119-bus with four storages at buses 21,36,51,75.

The base Market price, neighboring price and the variation coefficient of energy price with respect to base price are considered same as the 32-bus test system and presented in Table A.1. The detailed data for DGs and storage sizes associated with modified 119 bus test system are given in Table A.3. Other system data such as demand

Table 3.1: DG, Wind and Energy Storage Capacities

	pgmax [p.u.]	smax [p.u.]		pgmax [p.u.]	smax [p.u.]
bus14	2	-	bus74	10	-
bus20	7	-	bus75	0	6
bus21	0	8	bus76	10	-
bus35	5	-	bus80	10	-
bus36	0	8	bus84	3	-
bus44	7	-	bus85	3	-
bus48	10	-	bus89	2	-
bus50	10	-	bus96	2	-
bus51	0	6	bus101	7	-
bus52	10	-	bus109	7	-
bus56	5	-	bus113	10	-
bus60	2	-	bus116	10	-
bus64	2	-	bus121	3	-
bus69	5	-	-	-	-

level and line impedance are considered same 119-bus and provided in [67]. Fig. 3.2 demonstrates the power received from upstream network using methods A to D. Day-ahead scheduling either overestimates or underestimates the amount of power required to be imported from grid. The pattern of difference between method B and D is close to the pattern of deviation between day-ahead forecast wind and RHC forecast. The effect of proposed RHC method D on charging and discharging pattern of storage (S3) in comparison to the day-ahead scheduling B is shown in Fig. 3.3. The charging and discharging schedule shifts one step by using the RHC method, which

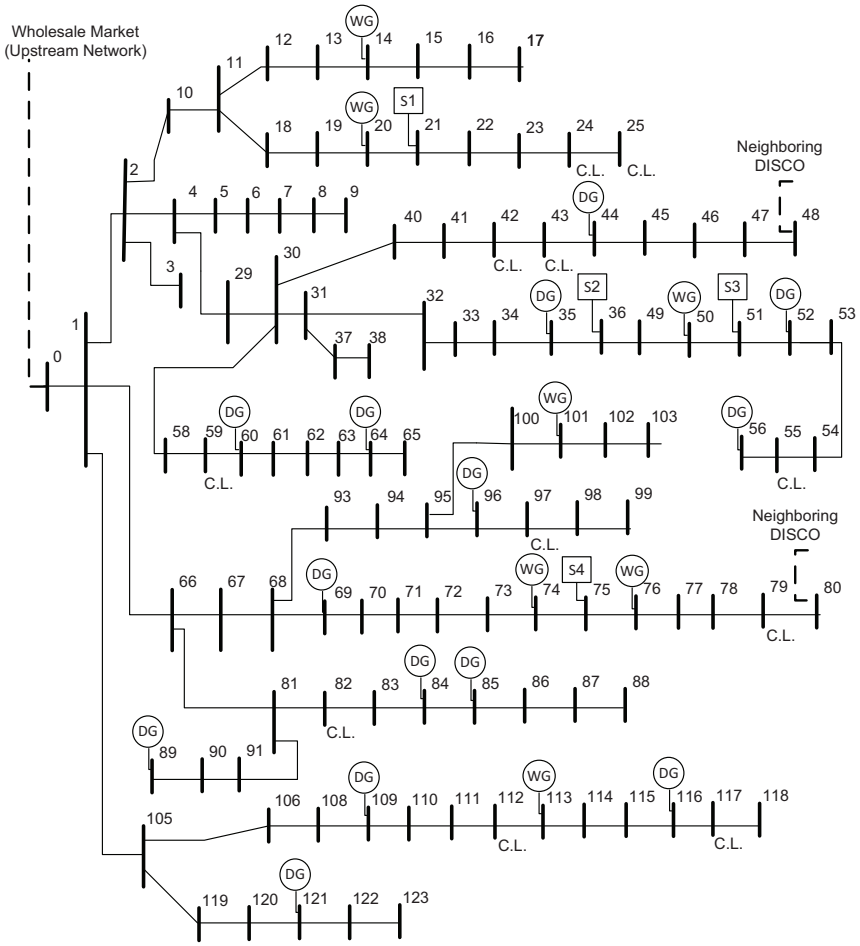

Figure 3.1: Modified 119-bus Distribution Test System

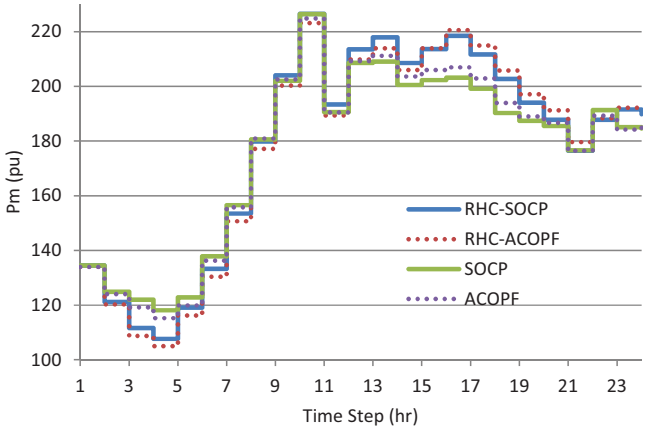

Figure 3.2: Power Exchange with Upstream Network; 119-bus Incorporating One Storage (Case II)

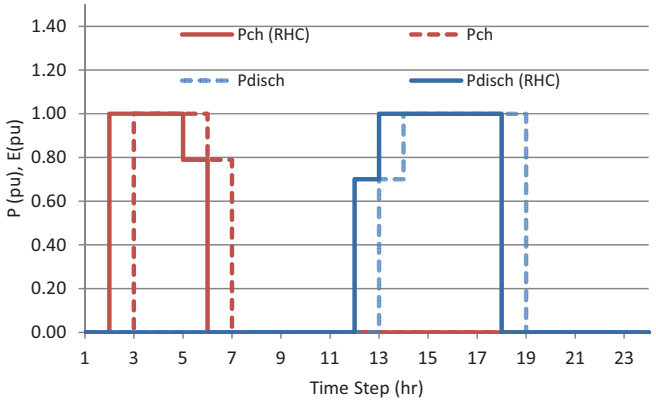

Figure 3.3: Optimal P_{ch} and P_{Disch} Schedule For Storage S3 Using Proposed Method D Compared to Method B; Case III

Table 3.2: Simulation Time Comparison: Modified 119-bus

RHC-SOCP Average Simulation Time (Sec)	151.8
RHC-ACOPF Average Simulation Time (Sec)	333.0

demonstrates the disadvantage of day-ahead scheduling dealing with uncertainty in the system.

The charging and discharging schedule of storage S1 is shown in Fig. 3.4 using the RHC convex OPF. The schedules are same for Cases II and III, and the location of storage S1 at both systems are identical. However, additional storages are located at other branches of the system in Case III. The pattern shows that as during hours 1 to 9 the price at the upstream network are low, the storage is, therefore, scheduled to be charged. As the price during hours 13 to 21 increases, the storage is scheduled to be discharged instead of buying energy from upstream or dispatching costly generators. The comparison between Fig. 3.3 and 3.4 shows that the size and location of storage can also affect the storage schedule in addition to the price variation.

Table 3.2 compares the computational time performance of proposed optimization method RHC-SOCP with non-convex RHC-ACOPF at each time step. The convex method D outperforms conventional method C and provides considerable time reduction. In 32-bus system, the computation time ratio of convex RHC-SOCP to

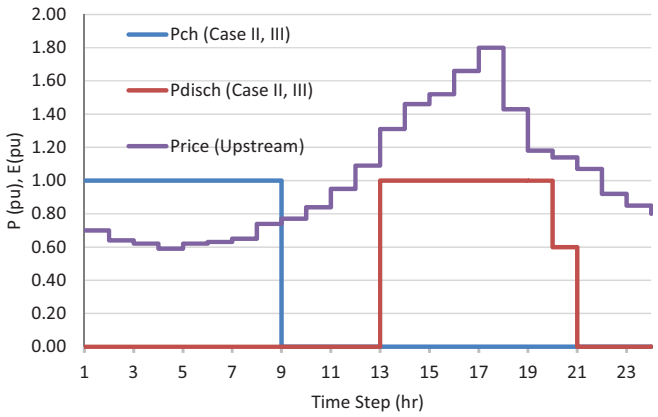

Figure 3.4: Optimal P_{ch} and P_{Disch} Schedule for Storage S1 Using Proposed Method D; 119-bus (Case II) and (Case III)

Table 3.3: Total Saving [$] Over The Horizon Window Comparing RHC-SOCP and RHC- ACOPF ; modified 119-bus Incorporating One Storage (Case II)

Step	Case II	Case III	Step	Case II	Case III
1	101	101	16	113	111
8	106	105	24	114	111

non-convex RHC-ACOPF is 47% (6.83/14.27). In a larger system (119-bus), this ratio is even better 45% (151.8/333). This shows that the comparative performance of RHC-SOCP method is not declined when system size is increased. The other important advantage is reaching the global optimal solution.

Table 3.3 provides the total savings in operational cost at different time steps. The proposed method D yields reduction in total cost by finding the optimal schedule of the active distribution system (see Fig. 3.5).

3.1.2 Case Study IV: Real-Time Implementation

The proposed architecture for real-time implementation of RHC convex OPF is presented in Fig.3.6. The architecture contains three main sections: energy management system (EMS), control interface, real-time digital simulator (RTDS). The first section (EMS) acts as the master control for the whole structure and integrates RHC forecasting and dynamic optimization (SOCP-OPF) formulated in section 2.3.

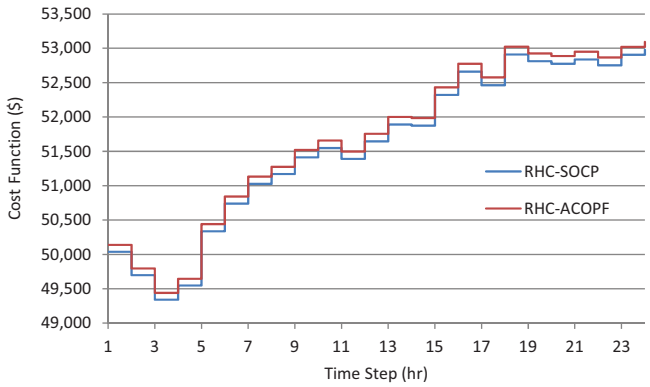

Figure 3.5: Total Saving [$] Over The Horizon Window Comparing RHC-SOCP and RHC- ACOPF (Case II)

Master program receives the update for actual load, price, and wind. Based on the new updates, it reforecasts the wind generation over the horizon window. These informations alongside with price, load, and other system updates are sent to the optimization program. The optimization determines the control variables at each time step over the horizon window $[t : t + T - 1]$. This control actions are sent to the real-time simulator.

The second section provides the control interface for the exchange of the signals between the EMS and real-time simulator. A TCP protocol is used to connect the master (EMS) and real-time simulator. The third part is the model of the test system in RSCAD implemented in RTDS real-time simulator [68]. The input control actions provided by EMS is applied to the test system at the beginning of each time step. The required feedback such as storage's energy is sent back to EMS through control interface. This feedback as well as the other external signals serves as the updated input for master program to re-forecast and re-optimize the control variables over the next horizon window $[t+1 : t+T]$. The 8-bus radial distribution system (Fig. 3.7) is considered to examine the proposed real-time architecture for RHC convex OPF. The system is operated at 15 kV, and contains 8 buses and 7 lines. Each load is 5+j2.5 p.u.. The line impedances are 0.05+j0.1 Ω, and power base is 1 MW. The variation

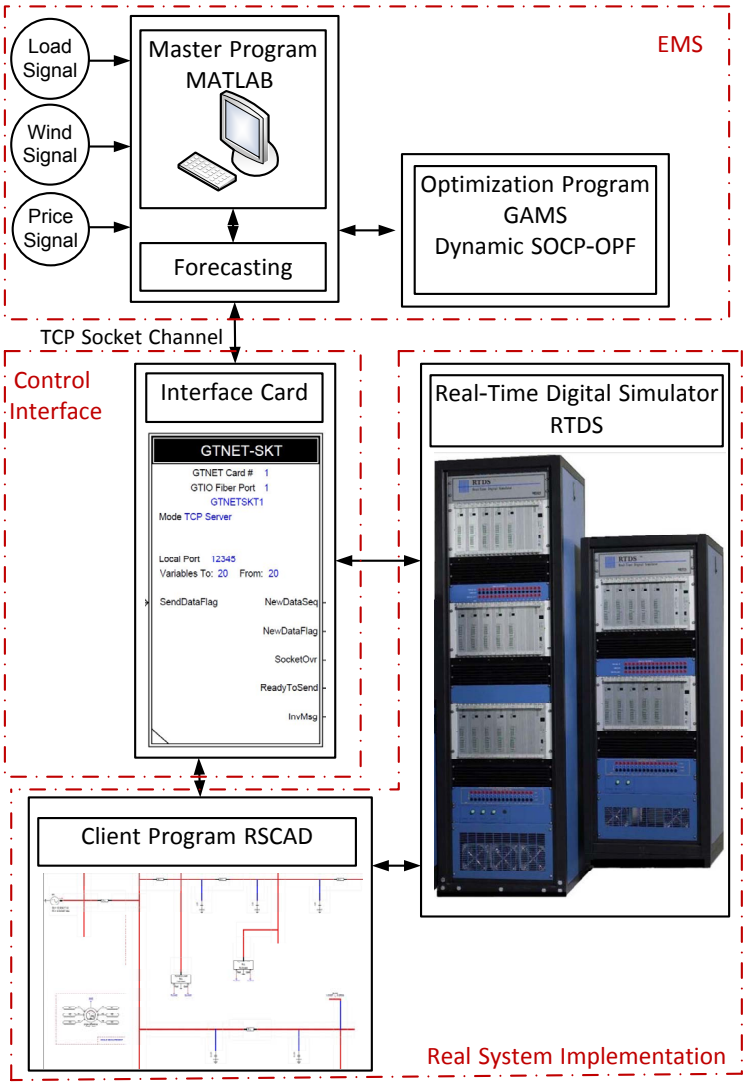

Figure 3.6: Real-Time Implementation Architecture of proposed method

coefficient of energy price with respect to base price are presented in Table A.1. This distribution network is connected to the upstream from bus 0. One wind farm and a storage station are located at bus 6 and bus 7 respectively.

For the real-time simulation, two subsystems for the "control" and "power distribution system" are modeled in RSCAD. The subsystem #1 manages the various control signals which are either imported to or exported from the power system. It also establishes the channel to the EMS through the interface card. The subsystem #2 contains the real-time model of power distribution system and exchanges the required

signals with subsystem #1. The EMS receives the feedback from the real-time simulator. It performs the new forecast over the horizon using RHC, and sends this data as well as the new price and load data to the optimization routine. It runs the proposed SOCP-OPF method and obtains the optimal schedules for DG, storage and contracted loads (if any) over the next horizon $[t+1 : t+T]$. This control signal will be sent to the real-time simulator at the beginning of the each step.

Fig. 3.8 shows the SOC for the storage along with the charging and discharging rates. The state of charge (SOC) is equivalent to the energy (E) stored inside the storage. The storage initial charging is 50%. During the hours 2 to 6, the price at the upstream network are low. The storage is, therefore, scheduled to be charged. When the price during hours 13 to 18 increases, the storage is discharged to avoid energy import from upstream. The real-time active power flow on storage line P_{sl} is shown in Fig. 3.8. The small high frequency fluctuations are related to the converter switching.

Fig. 3.9 depicts the comparison between real-time and scheduled values of power imported from upstream (modeled as a power source) and the wind generation at each time step. The amount of power imported from upstream at each time step and over the horizon window is determined by the wholesale market price, load level, and the amount of wind generation. For instance, it can be seen that the imported power decreases by 0.96 p.u. at the beginning of time step 2. The reason is that the storage starts to be charged at time step 2 with the rate of 1 p.u./hr. At the same time the loading level decreases by factor of 0.05 (0.88-0.83) which is equal to 1.25 p.u.. On the other hand, there is an increase in wind generation from step 1 to step 2 by 0.71 p.u.. The imported power, therefore, decreases by 0.96 p.u. (=1.25+0.71-1). The small oscillations on the power variation are caused by rapid changes in the generator settings.

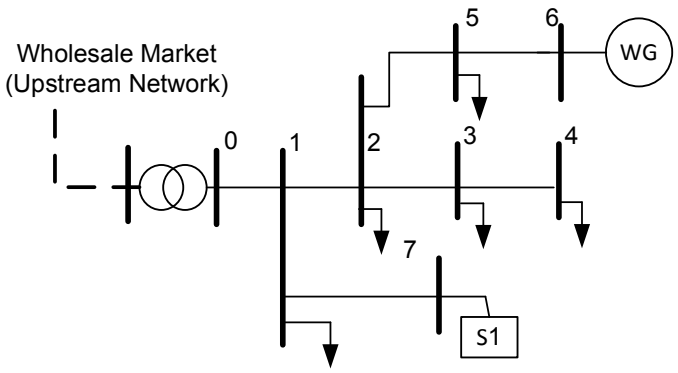

Figure 3.7: 8-bus Distribution System for the Real-time Test Implementation

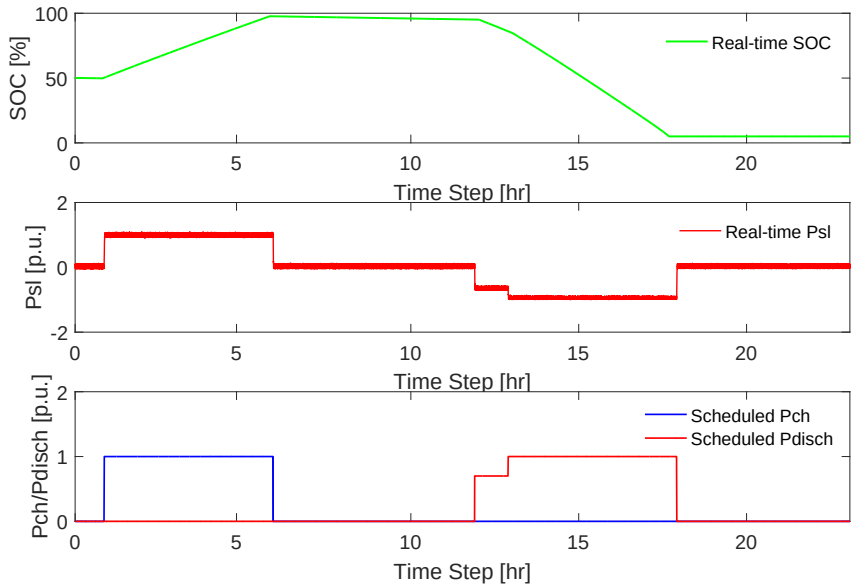

Figure 3.8: Real-time SOC; Real-time Power Flow on Storage Line Psl; Scheduled Charging Pch and Discharging Power Pdisch

3.2 Conclusion

In this chapter, a dynamic convex optimal power flow method for active distribution systems, which includes dynamic components, market transactions, contracted loads and renewable generation is proposed. The RHC convex OPF takes into account the system uncertainties such as wind through re-estimating the future inputs based on the online data over the horizon window. The proposed method also addresses some disadvantages of ACOPF methods, referred as the local optimum solution and time inefficiency. The effectiveness of RHC convex OPF is examined on the modified 32-

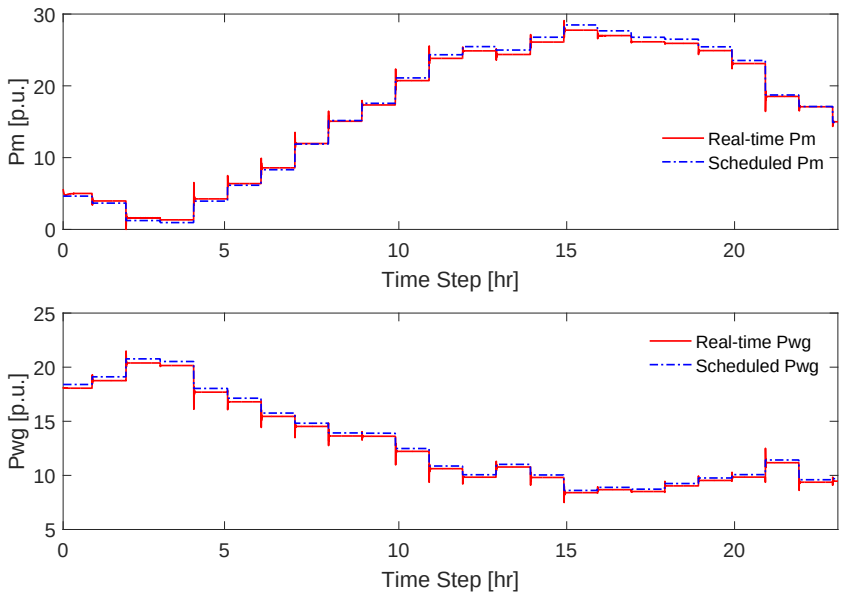

Figure 3.9: Real-time and Scheduled Power Exchange With Upstream Network; Real-time and Scheduled Wind Generation Power

bus test system. An architecture for real-time implementation of proposed method is also presented. The scalability of proposed method is tested on modified 119-bus test system. The results show the improvements in operation cost and computational time in comparison with the current methods.

CHAPTER 4: AN ARCHITECTURE FOR VOLTAGE STABILITY CONSTRAINED CONVEX OPTIMAL POWER FLOW FOR TRANSMISSION SYSTEM

Moving towards the competitive environment in power grid intensifies congestion on power transmission systems. This trend besides demand growth and rise of stochastic players such as renewable sources push the system closer to its stability limits [2]. Such a stressed system challenges independent system operators (ISOs) for providing fair access for market participants [69], [70] and ensuring a stable system. Recently voltage instability scenarios have caused several blackouts. Incorporating voltage stability limits inside optimal power flow (OPF) is, therefore, becoming an essential part for economic power dispatch in new energy management systems. In general, the steady-state voltage stability limits are modeled as the margin that defines the distance to maximum or critical loading points [71]. This margin can be included either in the objective or constraints of OPF problem, which forms voltage stability constrained OPF (VSC-OPF) [72].

Several studies have proposed optimization algorithms to solve OPF problems more efficiently. These algorithms generally have limitations referred to as providing non-exact relaxation and locally optimum solutions [73]. These limitations are mainly resulting from non-convexity of OPF equations [29]. Power flow equations acting as constraints in the OPF problem are nonlinear quadratic functions, and thus OPF is a non-convex and NP-hard optimization problem. In recent years, contributions are made to convexify OPF [30] to efficiently solve the problem and find the optimal solution. Convex relaxation of OPF is generally classified into two types: Relaxation of bus injection model (BIM) OPF, and branch flow model (BFM) OPF. Power

transmission systems are mostly modeled using BIM-OPF, and SDP relaxation is used to convexify the optimization problem. The first semidefinite programming (SDP) relaxation for meshed networks was proposed in 2008 [34]. The detailed analysis on SDP relaxation is then presented in [29], and a sufficient condition for OPF problem is derived.

Considerable number of studies have investigated the voltage stability constrained OPF (VSC-OPF) using non-convex methods. Ref. [74] formulated the voltage stability margin as an optimization problem, and [75] examined the maximum loadability point. An OPF algorithm using evolutionary programming was illustrated in [76] based on gradient information. Ref. [77] introduced a stability constrained OPF method by converting the dynamic equations to their numerical equivalents. Ref. [78] suggested an optimization technique to identify the voltage collapse point based on saddle-point and limit-induced bifurcations. Ref. [79] presented a review on OPF methods including voltage security constraints. New OPF techniques are then proposed based on interior point methods [72] to evaluate voltage security cost.

Developing convex OPF with voltage stability constraints viz., VSC-OPF is an open problem, with only few studies investigating the convexfication of VSC-OPF. Recently [80] presented a dispatch method for enhancing voltage stability by solving a quasi-SDP OPF problem with a stability index. In this chapter, a convex relaxation for voltage stability constrained OPF (VSC-OPF) using semidefinite programming (SDP) is proposed [81], which formulates three types of convex VSC-OPF algorithms.

These methods find the optimum dispatch with the goals of a) maximum stability margin, b) minimum operating cost constrained by a stability margin and c) an intermediate multi-objective function that can define a trade-off between cost and enhancing stability. The proposed convex method is also implemented to derive the voltage versus power curve (PV curve) and are examined on IEEE 14-bus, 57-bus, and 118-bus test systems.

Rest of the chapter is organized as follows. Section 4.1 presents the formulation dealing with steady state VSC-OPF. Section 4.2 proposes a general convex VSC-OPF formulation and details the convexification of VSC-OPF by defining the corresponding substitute variables in convex space. Further convex formulations for three types of convex VSC-OPF algorithms using SDP are derived. Implementation of these methods on the IEEE test systems and result analysis are presented in section 4.5.1-4.5.3, and section 4.6 summarizes the contribution.

4.1 Voltage Stability Constrained OPF

Stability constrained OPF problem aims to provide the optimal dispatch and at the same time ensures that solution remains within the boundary of proper distance to the maximum loading point. In this chapter, the definition of VSC-OPF is based on steady state voltage stability model. A conventional VSC-OPF formulation based on [79] is represented in (4.1).

$$\underset{(P_i,P_i^m,v_i,v_i^m,\lambda^m)}{Min} \sum_i c_i\left(x,P_i,P_i^m,v_i,v_i^m,\lambda,\lambda^m\right) \tag{4.1}$$

$$s.t. \begin{cases} h(x,Pi,v_i,\lambda)=0 \\ h(x^m,P_i^m,v_i^m,\lambda^m)=0 \\ \underline{b}_i \le g\left(x,Pi,v_i,\lambda\right) \le \overline{b}_i \\ \underline{b}_i^m \le g\left(x^m,P_i^m,v_i^m,\lambda^m\right) \le \overline{b}_i^m \\ \underline{d}_i \le f(\lambda,\lambda^m) \le \overline{d}_i \end{cases}$$

In this formulation the loading factor λ determines the current loading level of power grid, and the critical and maximum loading points are represented by λ^c and λ^m respectively. The functions $g(.)$ and $h(.)$ define the equality constraints and inequality constraints associated with current and maximum loading points respectively. Also, in the last constraint, $f(.)$ provides the connection between λ and λ^m. The generators

are assumed to have same terminal voltage at λ and λ^m. The optimization approaches contributed to VSC-OPF problem can be classified into three major categories [72].

4.1.0.1 Maximum Stability Margin

In this method the output is an operating point that creates the maximum distance to the maximum loading point. Equation (4.2) shows the objective function while the constraints remains the same as in (4.1).

$$Min \ -(\lambda^m - \lambda) \tag{4.2}$$

4.1.0.2 Minimum Margin Constrained

In this method a minimum acceptable distance to the maximum loading point is incorporated in the constraints, and the system operating cost is considered as the objective function (4.3). The rest of constraints are the same as (4.1).

$$\begin{aligned} &Min \sum_{i \in N_G} c_i(P_i) \\ &s.t. \begin{cases} \lambda^m - \lambda \geq \triangle\lambda_{min} \end{cases} \end{aligned} \tag{4.3}$$

4.1.0.3 Multi Objective

In this method, a linear combination of stability margin and operating cost is considered as the objective function as shown in (4.4). The rest of constraints are the same as (4.1).

$$Min \ \ \omega_1 \sum_{i \in N_G} c_i(P_i) - \omega_2(\lambda^m - \lambda) \tag{4.4}$$

It can be seen that these VSC-OPF methods are non-convex due to the nonlinear equality and inequality constraints.

Table 4.1: Indexes and Short Usages

i, j, k	Bus indexes.
lm	Line index from bus l to bus m.
N	Set of buses.
N_G	Set of generation buses $N_G \subseteq N$.
N_L	Set of line flows $N_L \subseteq N \times N$.
S^n $n \times n$	positive semidefinite (PSD) space.
$Re\{.\}, Im\{.\}$	Real and imaginary part.
$Tr\{.\}, rank\{.\}$	Trace and rank of given matrix.
SDP	Semidefinite programming
VSC-OPF	Voltage stability constrained OPF

4.2 Proposed Convex Voltage Stability Constrained OPF

The OPF problem in transmission systems is commonly formulated using bus injection model (BIM) and aims to minimize the operation cost. In convex OPF, the convex relaxation is derived by imposing convex supersets over the non-convex feasible set of OPF problem and minimizing the cost function over these sets. The non-convex and convex models use different equations and set of variables [33]. Non-convex OPF may results in a local solution while the convex OPF finds the global optimum solution, although there are cases in which the relaxation is not tight [82]. In convexification process an equivalent rank-1 matrix is introduced to transform the constraints to a linear space. SDP relaxation of BIM-OPF is then obtained by dropping this rank-1 constraint which yields a quadratic convex optimization problem [29]. Notations are given in Table 4.1 and Table 4.2.

In this section, we design an SDP based convex stability constrained OPF. In VSC-OPF two vector variables are required to model the operating and critical points since the maximum loading point is also needed to be determined from the solution of VSC-OPF. Therefore, unlike the convex OPF, in convexification of VSC-OPF problem, two voltage vector variables are defined. The first one is associated with the optimal operating point $V = \left[Re\{v\}^T Im\{v\}^T\right]$ and the other one $V^m =$

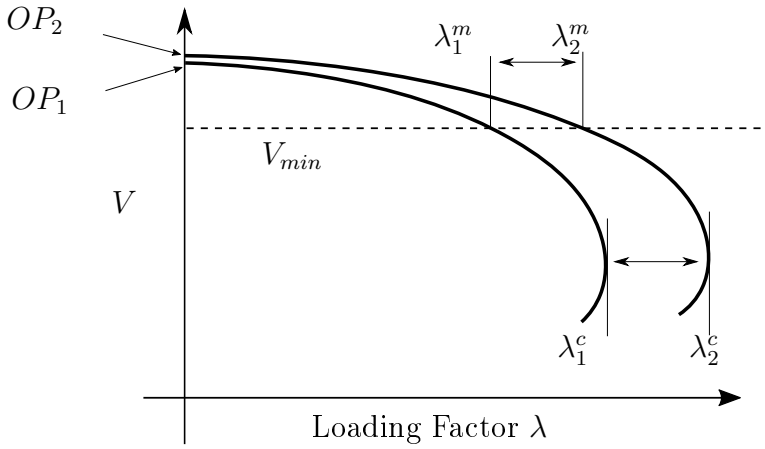

Figure 4.1: PV curves associated with two operating points OP_1 and OP_2. The points λ_1^m , λ_2^m and λ_1^c, λ_2^c represent infeasible boundary (V_{min}) and voltage collapse respectively.

$\left[Re\{v^m\}^T Im\{v^m\}^T\right]$ represents the maximum loading point, where $v = \{v_1, v_2, ..., v_n\}$ and $v^m = \{v_1^m, v_2^m, ..., v_n^m\}$. These voltages must satisfy all the constraints of the system including the power flow equations and equipment limits. Thus, the scalar λ and the variable λ^m are incorporated inside the optimization formulation to represent the current loading factor and maximum loading level, respectively. The system loading is considered to increase at constant power factor for all load buses. The system demand, therefore, can be written as

$$P_{D_i} = \lambda.P_{Do_i} \ , \ Q_{D_i} = \lambda.Q_{Do_i} \tag{4.5}$$

$$P_{D_i}^m = \lambda^m.P_{Do_i}, \quad Q_{D_i}^m = \lambda^m.Q_{Do_i} \tag{4.6}$$

Where P_{Do_i} and Q_{Do_i} are the system base active and reactive load at bus i.

The solution of VSC-OPF is to find the dispatch point that contains maximum stability margin by creating maximum distance to maximum loading point. The maximum loading is obtained by finding the feasible boundary of operational constraints. The critical loading is given by the voltage collapse point.

Table 4.2: Notations of Variables and Parameters

P, Q, S	Active, Reactive and Apparent power.
v_i	Voltage of bus i.
$\|v_i\|$	Voltage magnitude of bus i.
δ_i	Voltage angle of bus i.
λ	Current loading factor.
λ^m	Maximum loading factor.
λ^c W,W^m	Critical loading factor. $(2n \times 2n)$ PSD matrix variables.
$W_{i,j}$	(i,j) entry of matrix W
$e_1, e_2, \ldots, e_n$	Standard basis vectors of R^n
c_i, C_{i_k}	Cost function and cost coefficient at bus i
P_{D_i},Q_{D_i}	Active and reactive demand at bus i
Y	Admittance matrix
$y_{lm}, \bar{y}_{lm}$ $h(.), g(.)$	Line lm series and shunt admittance Equality & inequality functions of OPF
$f(.)$	Function of λ,λ^m
$H(.), G(.)$	Convex OPF equality & inequality functions
$F(.)$	Convex function of λ and λ^m
$\succeq$	Positive semidefinite
X^{min}, X^{max}	Minimum and maximum of X
$\underline{b}, \bar{b}$	Lower and upper bound of function b
X^m	X value at loading level of λ^m

Fig 4.1 depicts the voltage versus power (PV) curve corresponding to two operating points OP_1 and OP_2. The loading points λ_1^m and λ_2^m demonstrate the loading levels at which minimum voltage requirement is violated. The violation is not necessarily limited to voltage but can also include other constraints such as line flow and generation capacity. The critical points λ_1^c and λ_2^c represent the loading levels beyond which demand increase will result in voltage collapse.

The first step in convexification of VSC-OPF is to extend the objective function and constraints as a linear function of a quadratic matrix VV^T and V^mV^{mT}. The matrices VV^T and V^mV^{mT} are then replaced by matrices W and W^m respectively, yielding a linear problem in $S^{2n\times 2n}$. The relation between feasible boundary and variables

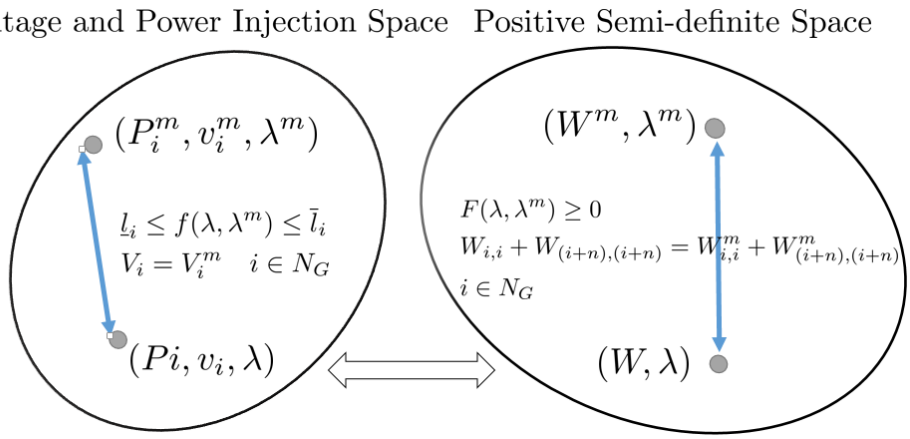

Figure 4.2: Feasible space and variables associated with (a) VSC-OPF and (b) convex VSC-OPF. (P_i, v_i), $(P_i, v_i)^m$ and λ^m are variables in conventional VSC-OPF and PSD matrices W, W^m and scalar λ^m are the corresponding ones in convex VSC-OPF.

of conventional and convex VSC-OPF is shown in Fig. 4.2; The red colored (P_i, v_i), $(P_i, v_i)^m$, λ^m are variables in conventional VSC-OPF, and parameter λ defines the current loading level; The positive semi-definite matrices W, W^m beside the variable λ^m are corresponding variables of VSC-OPF in convex space.

In the next step defined as the rank relaxation, the rank-1 constraints for W and W^m are eliminated from the constraints. These relaxations convert the nonlinear VSC-OPF problem to a convex optimization problem.

The quadratic objective function can also be replaced by equivalent linear matrix inequality constraints. The general convex VSC-OPF thus obtained is shown in (4.7)-(4.14). Notations are given in Tables 4.1 and 4.2. The function $H(.)$ is the power flow equality constraint in convex space. The system operational constraints is demonstrated by function $G(.)$. The last constraint $F(.)$ defines the relation between λ and variable λ^m. Please note that $i \in N_G$.

$$\underset{(W,W^m,\lambda^m)}{Min} \sum_i C_i\left(x, W, W^m, \lambda, \lambda^m\right) \tag{4.7}$$

$$s.t. \quad H(x, W, \lambda) = 0 \tag{4.8}$$

$$H(x^m, W^m, \lambda^m) = 0 \tag{4.9}$$

$$G\left(x, W, \lambda\right) \geq 0 \tag{4.10}$$

$$G\left(x^m, W^m, \lambda^m\right) \geq 0 \tag{4.11}$$

$$F(\lambda, \lambda^m) \geq 0 \tag{4.12}$$

$$W_{i,i} + W_{(i+n),(i+n)} = W^m_{i,i} + W^m_{(i+n),(i+n)} \tag{4.13}$$

$$W \succeq 0, W^m \succeq 0 \tag{4.14}$$

Another assumption that maps control variables at current loading to maximum loading is associated with generator terminal voltages. The generators are assumed to have same terminal voltage as the loading level increases. This is represented in (4.13) which enforces this constraint by equating the magnitude squared of terminal voltages. The entry $W_{i,i}$ and $W_{(i+n),(i+n)}$ of matrix W are equal to the magnitude squared of voltage real part $Re\{v_i\}^2$ and imaginary part $Im\{v_i\}^2$ respectively. These substitutions yield $|v_i|^2 = W_{i,i} + W_{(i+n),(i+n)}$; similar substitution in $|v^m_i|^2$ results in $|v^m_i|^2 = W^m_{i,i} + W^m_{(i+n),(i+n)}$.

The convexification and solution recovery algorithm are summarized in Fig. 4.3. Let W^{opt} and $W^{m^{opt}}$ denotes the solution of relaxed VSC-OPF. If these matrices are rank-1, the solution to the VSC-OPF problem is constructed using $W^{opt} = VV^T$ and $W^{m^{opt}} = V^m V^{m^T}$. Whenever the solution matrices are rank-2, matrices $(\rho_1 + \rho_2)EE^T$ and $(\rho^m_1 + \rho^m_2)E^m E^{m^T}$ are the rank-1 solutions to the VSC-OPF, and voltage vectors can be constructed using these matrices. The scalars ρ_1 and ρ_2 are eigenvalues of W^{opt}, and vector E denotes unit eigenvector associated with ρ_1. Correspondingly,

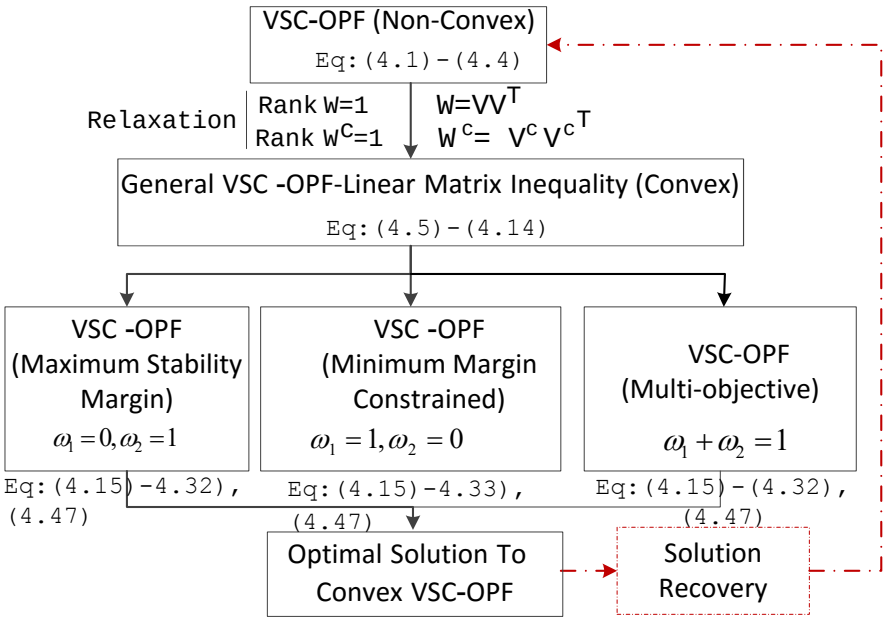

Figure 4.3: Convexification of VSC-OPF and solution recovery. VSC-OPF categories are: Maximum loading margin, Minimum margin constrained and Multi-objective VSC-OPFs.

the scalars ρ_1^m, ρ_2^m, and vector E^m demonstrate eigenvalues and eigenvector associated with $W^{m^{opt}}$. The convex VSC-OPF formulation ((4.7)-(4.14)) is extended to model three types of voltage stability constraint OPF illustrated in section 4.1. Objective function and constraints of convex VSC-OPF methods are detailed in following subsections.

4.2.0.1 Objective Function

The proposed objective function (4.15) takes into account two terms. The first term is weighted by scalar ω_1; it represents the total generation cost. The second term weighted by scalar ω_2 models the voltage stability margin $-(\lambda^m - \lambda)$.

This term demonstrates the distance to the maximum loading point, which is aimed to be maximized. The weighting factors are determined depending on VSC-OPF categories.

$$\underset{(W,W^m,\lambda^m)}{Min} \quad \omega_1 \sum_{i\in N_G} \{C_{i_2} \left(Tr\{Y_i W\} + \lambda P_{D_i}\right)^2 + C_{i_1} \left(Tr\{Y_i W\} + \lambda P_{D_i}\right) + C_{i_0}\} - \omega_2 \left(\lambda^m - \lambda\right) \tag{4.15}$$

4.2.0.2 Constraints

The first part of constraints demonstrates the convex power flow equations as shown in (4.16)-(4.19). These equality constraints model the active and reactive power generation at bus i associated with current loading point (P_i, Q_i) and maximum loading point (P_i^m, Q_i^m) respectively. Derivation of Y_i and $\bar{Y}_i$ from admittance matrix is presented in (4.34) where $i \in N$.

$$P_i = Tr\{Y_i W\} + \lambda P_{D_i} \tag{4.16}$$

$$P_i^m = Tr\{Y_i W^m\} + \lambda^m P_{D_i} \tag{4.17}$$

$$Q_i = Tr\{\bar{Y}_i W\} + \lambda Q_{D_i} \tag{4.18}$$

$$Q_i^m = Tr\{\bar{Y}_i W^m\} + \lambda^m Q_{D_i} \tag{4.19}$$

The next part denotes the inequality constraints imposing the maximum and minimum boundary of active power generation, reactive power generation, and bus voltages ((4.20)-(4.25));

$$P_i^{min} \leq P_i \leq P_i^{max} \tag{4.20}$$

$$P_i^{min} \leq P_i^m \leq P_i^{max} \tag{4.21}$$

$$Q_i^{min} \leq Q_i \leq Q_i^{max} \tag{4.22}$$

$$Q_i^{min} \leq Q_i^m \leq Q_i^{max} \tag{4.23}$$

$$\left(V_i^{min}\right)^2 \leq Tr\{M_i W\} \leq (V_i^{max})^2 \tag{4.24}$$

$$\left(V_i^{min}\right)^2 \leq Tr\{M_i W^m\} \leq (V_i^{max})^2 \tag{4.25}$$

Where $Tr\{M_i W\}$ and $Tr\{M_i W^m\}$ are equal to the magnitude squared of bus

voltages $|V_i|^2$ and $|V_i^m|^2$ respectively; matrix M_i is defined in (4.36).The admittance and coefficient matrices are derived in section 4.3.

The transmission line constraints are formulated in (4.26)-(4.31) with Y_{lm} and $\bar{Y}_{lm}$ as shown in (35) and $lm \in N_L$. The constraints (4.26) and (4.27) enforce the maximum power flow corresponding to λ and λ^m. The voltage drop limitation on transmission line $'lm'$ is demonstrated in (4.28) and (4.29), and matrix M_{lm} is defined in (4.37).

The last constraint on transmission lines is the limitation of voltage angle drop over the line ((4.30)-(4.31)). The derivation is detailed in Appendix 4.4 through (4.38)-(4.43)). The coefficient matrices B_{lm} and D_{lm} are shown in (4.42)-(4.43).

$$Tr\{Y_{lm}W\} \leq P_{lm}^{max} \tag{4.26}$$

$$Tr\{Y_{lm}W^m\} \leq P_{lm}^{max} \tag{4.27}$$

$$Tr\{M_{lm}W\} \leq \triangle \left(V_{lm}\right)^2 \tag{4.28}$$

$$Tr\{M_{lm}W^m\} \leq \triangle \left(V_{lm}\right)^2 \tag{4.29}$$

$$tan\left(\delta_{max}\right) \times Tr\{D_{lm}W\} - Tr\{B_{lm}W\} \geq 0 \tag{4.30}$$

$$tan\left(\delta_{max}\right) \times Tr\{D_{lm}W^m\} - Tr\{B_{lm}W^m\} \geq 0 \tag{4.31}$$

Equation (4.32) connects the weighting factors which determine the value priority of the terms in the objective function (minimizing cost versus maximizing stability margin). The minimum voltage stability margin which is required or acceptable by system operator is imposed using (4.33).

$$\omega_1 + \omega_2 = 1 \tag{4.32}$$

$$(\lambda^m - \lambda) \geq \triangle\lambda_{min} \tag{4.33}$$

4.3 Admittance and Coefficient Matrices

Y_i and $\bar{Y}_i$ are admittance matrices associated with bus i, which are derived from admittance matrix Y as shown in (4.34).

$$
\begin{aligned}
&Y_{e_i} = e_i e_i^T Y;\ Y_{1_i} = Y_{e_i} + Y_{e_i}^T;\ Y_{2_i} = Y_{e_i} - Y_{e_i}^T \\
&Y_i = \frac{1}{2}\begin{bmatrix} Re\left(Y_{1_i}\right) & -Im\left(Y_{2_i}\right) \\ -Im\left(Y_{2_i}\right) & Re\left(Y_{1_i}\right) \end{bmatrix} \\
&\bar{Y}_i = -\frac{1}{2}\begin{bmatrix} Im\left(Y_{1_i}\right) & Re\left(Y_{2_i}\right) \\ -Re\left(Y_{2_i}\right) & Im\left(Y_{1_i}\right) \end{bmatrix}
\end{aligned}
\tag{4.34}
$$

Y_{lm} and $\bar{Y}_{lm}$, derived from admittance matrix (Y) based on transmission line connection, are admittance matrices corresponding to transmission line lm as shown in (4.35).

$$
\begin{aligned}
&Y_{e_{lm}} = \left(\bar{y}_{lm} + y_{lm}\right) e_l e_l^T - \left(y_{lm}\right) e_l e_m^T \\
&Y_{1_{lm}} = Y_{e_{lm}} + Y_{e_{lm}}^T; \quad Y_{2_{lm}} = Y_{e_{lm}} - Y_{e_{lm}}^T \\
&Y_{lm} = \frac{1}{2}\begin{bmatrix} Re\left(Y_{1_{lm}}\right) & -Im\left(Y_{2_{lm}}\right) \\ -Im\left(Y_{2_{lm}}\right) & Re\left(Y_{1_{lm}}\right) \end{bmatrix} \\
&\bar{Y}_{lm} = -\frac{1}{2}\begin{bmatrix} Im\left(Y_{1_{lm}}\right) & Re\left(Y_{2_{lm}}\right) \\ -Re\left(Y_{2_{lm}}\right) & Im\left(Y_{1_{lm}}\right) \end{bmatrix}
\end{aligned}
\tag{4.35}
$$

Coefficient matrices M_i and M_{lm} defined in (4.36)-(4.37) are associated with bus i and transmission line lm respectively.

$$
M_i = \frac{1}{2}\begin{bmatrix} e_i e_i^T & 0 \\ 0 & e_i e_i^T \end{bmatrix} \tag{4.36}
$$

$$M_{lm} = \frac{1}{2}\begin{bmatrix} (e_l - e_m)(e_l - e_m)^T & 0 \\ 0 & (e_l - e_m)(e_l - e_m)^T \end{bmatrix} \tag{4.37}$$

4.4 Angle drop equation

To impose limitation on voltage angle drop over transmission lines, a convex formulation is developed using SDP relaxation. Considering (4.39) is same as (4.38), we can derive the angles in terms of V_m and V_l.

$$\delta_l - \delta_m \leq \delta_{max} \quad \forall (l,m) \in N_L \tag{4.38}$$

$$tan(\delta_l - \delta_m) \leq tan(\delta_{max}) \quad \forall (l,m) \in N_L \tag{4.39}$$

$$tan(\delta_l - \delta_m) = \frac{Re\{V_m\}Im\{V_l\} - Re\{V_l\}Im\{V_m\}}{Re\{V_l\}Re\{V_m\} + Im\{V_l\}Im\{V_m\}} \tag{4.40}$$

Further, substituting $Re\{V\}$ and $Im\{V\}$ by entries of matrix W results in a linear matrix inequality constraint (4.41) with B_{lm} and D_{lm} as shown in (4.42)-(4.43).

$$tan(\delta_{max}) \times Tr\{D_{lm}W\} - Tr\{B_{lm}W\} \geq 0 \tag{4.41}$$

$$B_{lm} = \frac{1}{2}\begin{bmatrix} 0 & e_l e_m^T - e_m e_l^T \\ e_l e_m^T - e_m e_l^T & 0 \end{bmatrix} \tag{4.42}$$

$$D_{lm} = \frac{1}{2}\begin{bmatrix} e_l e_m^T + e_m e_l^T & 0 \\ 0 & e_l e_m^T + e_m e_l^T \end{bmatrix} \tag{4.43}$$

Using 4.34-4.43 in 4.15-4.33, the convex OPF and all three VSC-OPF methods can be constructed.

4.4.1 Minimum Operating Cost Convex OPF

In this variation, the generation cost is considered as the objective function to be minimized. The weighting factor ω_1 in (15) is considered 1 to emphasize on cost minimization, and $\omega_2 = 0$ to eliminate the stability margin from objective function. Also, the constraint (4.33) modeling the margin requirement is removed. The objective function and constraints are summarized in (4.44)-(4.45).

$$\begin{aligned} \underset{(W)}{Min} \quad & \sum_{i \in N_G} \{C_{i_2} \left(Tr\{Y_i W\} + \lambda P_{D_i}\right)^2 \\ & + C_{i_1} \left(Tr\{Y_i W\} + \lambda P_{D_i}\right) + C_{i_0}\} \end{aligned} \tag{4.44}$$

$$\begin{cases} P_i = Tr\{Y_i W\} + \lambda P_{D_i} \\ Q_i = Tr\{\bar{Y}_i W\} + \lambda Q_{D_i} \\ P_i^{min} \leq P_i \leq P_i^{max} \\ Q_i^{min} \leq Q_i \leq Q_i^{max} \\ \left(V_i^{min}\right)^2 \leq Tr\{M_i W\} \leq \left(V_i^{max}\right)^2 \\ Tr\{Y_{lm} W\} \leq P_{lm}^{max} \\ Tr\{M_{lm} W\} \leq \triangle \left(V_{lm}\right)^2 \\ tan\left(\delta_{max}\right) \times Tr\{D_{lm} W\} - Tr\{B_{lm} W\} \geq 0 \end{cases} \tag{4.45}$$

4.4.2 Maximum Stability Margin Convex VSC-OPF

In this variation, the objective function defined as negative of distance to maximum loading point $(-(\lambda^m - \lambda))$ and is minimized. The equation (4.46) shows the objective function. The set of equations modeling the convex "maximum stability margin VSC-OPF" is obtained by having $\omega_2 = 1$ $(\omega_1 = 0)$. These equations impose the power flow

and equipment constraints for the optimal and maximum loading points as shown in (4.16)-(4.31).

$$\underset{(W,W^m,\lambda^m)}{Min} \quad -(\lambda^m - \lambda) \tag{4.46}$$

In this problem, the control variables are λ^m and PSD matrices W and W^m. The equation (4.47) enforces the equal terminal voltage at each generator as formulated in section 4.2.

$$W_{i,i} + W_{(i+n),(i+n)} = W^m_{i,i} + W^m_{(i+n),(i+n)} \quad i \in N_G \tag{4.47}$$

4.4.3 Minimum Margin Constrained Convex VSC-OPF

In this variation, the goal is to minimize the operating cost as shown in (4.48); however, a minimum stability margin is imposed as constraint which requires a minimum distance from the maximum loading point. This method is implemented by keeping $\omega_2 = 1$ and enforcing the constraint (4.33), which results in the elimination of stability margin from the objective function and activating a minimum stability margin constraint as shown in (4.48)-(4.49).

$$\begin{aligned} \underset{(W,W^b,\lambda^b)}{Min} \quad & \sum_{i \in N_G} \{C_{i_2} \left(Tr\{Y_i W\} + \lambda P_{D_i}\right)^2 \\ & + C_{i_1} \left(Tr\{Y_i W\} + \lambda P_{D_i}\right) + C_{i_0}\} \end{aligned} \tag{4.48}$$

In this VSC-OPF formulation, λ^b does not represent maximum loading point since the objective function is to minimize the cost; however, it represents a loading level (less or equal to maximum point) to which the system loading can be increased without violating constraints. The control variables are λ^b and PSD matrices W and W^b. The rest of the constraints are similar to (4.16)-(4.31) and (4.47), in which the control variables λ^m and W^m are replaced with λ^b and W^b.

4.4.4 Multi-Objective Convex VSC-OPF

This variation considers the trade-off between minimizing operating cost and maximizing stability margin. Two weighting factors ω_1 and ω_2 balance the importance of each goal in the objective function. The objective function is shown in equation (4.50). As ω_1 approaches to zero the optimization problem approaches to the maximum stability margin VSC-OPF. Multi-objective VSC-OPF tends to the minimum operating cost as the weighting factor ω_1 moves toward 1.

$$\begin{aligned} \underset{(W,W^b,\lambda^b)}{Min} \quad & \omega_1 \sum_{i \in N_G} \{C_{i_2} \left(Tr\{Y_i W\} + \lambda P_{D_i}\right)^2 \\ & + C_{i_1} \left(Tr\{Y_i W\} + \lambda P_{D_i}\right) + C_{i_0}\} - \omega_2 \left(\lambda^b - \lambda\right) \end{aligned} \tag{4.50}$$

The ω_1 and ω_2 values can be set based on relative importance of voltage stability and operation cost. The rest of the constraints are similar to (4.16)-(4.31) and (4.47), in which the control variables λ^m and W^m are replaced with λ^b and W^b. The control variables are λ^b and PSD matrices W and W^b. Here λ^b does not represent maximum loading point since the objective function is linear combination of two terms; however, it represents maximum loading point when the weighting factor ω_2 is high enough to make stability margin $(\lambda^b - \lambda)$ as the dominant term in the objective function.

4.5 Case Studies and Simulation Results

4.5.1 Proof Of Concept

To examine the proposed VSC-OPF methods, a small test system ,IEEE 14-bus, is considered. The 14-bus system consists of 5 generators, 17 lines and 11 loads; The details of these systems are given in [83]. The optimization package GAMS with MOSEK solver is used to implement the formulation. The results of proposed convex methods are evaluated in following sections.

- Maximum Stability Margin VSC-OPF.
- Minimum Margin Constrained VSC-OPF.

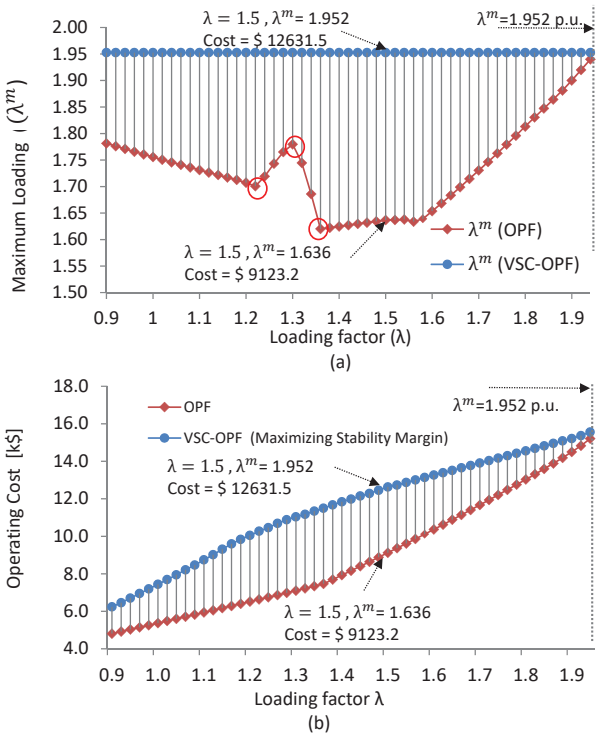

Figure 4.4: 14-bus test system (a) Maximum loading (λ^m) obtained from VSC-OPF and OPF. (b) System operating cost from VSC-OPF and OPF.

- Multi-Objective VSC-OPF.

4.5.1.1 Maximum Stability Margin VSC-OPF

Fig. 4.4a demonstrates the maximum loading λ^m obtained from VSC-OPF. The λ^m is equal to 1.952 as the system loading increases from 0.9 to 1.95. The maximum loading associated with OPF method is also shown in Fig. 4.4a.

The voltage dispatch for of generation buses are presented in Table 4.3. These voltages obtained from VSC-OPF are equal at different loading factors and represent a branch of feasible space which contains the operating point with the maximum loading margin. However, voltage dispatch obtained from OPF varies at different loading factors. This voltage dispatch of generator buses is then deployed in (4.47) to evaluate the corresponding λ^m at each loading level for OPF method. i.e. the generator voltages obtained from OPF are used to enforce the equal generator ter-

Table 4.3: Voltage of Generation Buses [p.u.] from OPF and VSC-OPF; IEEE 14-bus

λ	*Method*	V_{G1}	V_{G2}	V_{G3}	V_{G6}	V_{G8}
1.22	OPF	1.0600	1.0444	1.0045	1.0600	1.0600
1.22	VSC-OPF	1.0600	1.0484	1.0047	1.0332	1.0401
1.30	OPF	1.0600	1.0434	0.9958	1.0498	1.0600
1.30	VSC-OPF	1.0600	1.0484	1.0047	1.0332	1.0401
1.36	OPF	1.0600	1.0379	0.9847	1.0383	1.0600
1.36	VSC-OPF	1.0600	1.0484	1.0047	1.0332	1.0401
1.50	OPF	1.0600	1.0390	0.9886	1.0372	1.0600
1.50	VSC-OPF	1.0600	1.0484	1.0047	1.0332	1.0401

minal voltage at all loading factors. VSC-OPF converges to higher λ^m than OPF. Fig. 4.4b demonstrates the operating cost variation as a function of loading factor. It is noticeable that the operating cost associated with VSC-OPF is also higher than OPF. This high cost is the result of dispatching costly generators by VSC-OPF as shown in Table 4.4. Voltage dispatch and generation dispatch for four loading levels $\lambda = (1.22, 1.30, 1.36, 1.50)$ are presented in 4.3 and 4.4. The voltage dispatch for generator buses are equal in VSC-OPF while OPF provides different voltage dispatch for generators at each loading level. The difference between the operating cost of VSC-OPF and OPF is the result of dispatching costly generators as shown in Table 4.4. Cost of improving voltage security margin is defined as the difference between these operating cost. In 14-bus test system, the voltage security cost is increasing as the loading factor increases, and it declines as λ passes 1.36 p.u.. This reduction in cost is due to the tight feasible region after 1.36 p.u., which limits the variation of optimal dispatch point.

4.5.1.2 Minimum Margin Constrained VSC-OPF

Optimum operating point obtained from this method provides minimum generation cost among feasible points which meet the stability margin requirement ($\lambda^m - \lambda \geq \Delta\lambda_{min}$). Fig. 4.5a demonstrates the generation cost of solution point for 14-bus

Table 4.4: Generation Dispatch [p.u.] from OPF and VSC-OPF at $\lambda = 1.5$; IEEE 14-bus

λ	*Method*	P_{G1}	P_{G2}	P_{G3}	P_{G6}	P_{G8}
1.22	OPF	1.9168	1.4000	0.0000	0.0000	0.0000
1.22	VSC-OPF	0.8761	0.3911	0.8764	0.7740	0.2838
1.30	OPF	2.1516	1.4000	0.0000	0.0000	0.0000
1.30	VSC-OPF	0.8913	0.4020	0.9959	0.8089	0.3126
1.36	OPF	2.3309	1.4000	0.0000	0.0000	0.0000
1.36	VSC-OPF	0.9021	0.4800	0.9956	0.8608	0.3319
1.50	OPF	2.1933	1.4000	0.2664	0.2177	0.0000
1.50	VSC-OPF	0.9221	0.6499	0.9981	0.9885	0.3849

Table 4.5: Impact of $\Delta\lambda_{min}$ on VSC-OPF solution (14-bus)

λ	λ^b	$VSC-OPF$ [k\$] ($\triangle\lambda_{min} = 0.5$)	OPF [k\$]
1.00	1.5001	5371.50	5371.50
1.10	1.6001	5940.43	5940.42
1.20	1.7001	6517.30	6517.29
1.30	1.8000	7103.69	7103.22
1.40	1.9000	8212.11	7930.04
1.50	-	-	9123.24

system, which includes different $\Delta\lambda_{min}$ values. For each $\Delta\lambda_{min}$, the operating cost increases by loading factor (λ). It is noticeable that $\Delta\lambda_{min}$ shows more impact on optimum operating point at higher loading level λ; for instance, the difference between operating cost obtained from $\Delta\lambda_{min} = 0.1$ and $\Delta\lambda_{min} = 0.5$ is negligible until $\lambda = 1.30$. This difference is increased faster at loading level beyond 1.35 p.u.. This gap is explainable with the fact that the loading margin becomes a dominant constraint as λ approaches the critical point. In Fig. 4.5b, two cross sections at $\lambda = 1.4$ and $\lambda = 1.5$ show the generation cost variation by $\Delta\lambda_{min}$ augmentation. Table 4.5 provides the generation cost associated with this method for $\Delta\lambda_{min} = 0.5$. Rightly, VSC-OPF does not converge at 1.5 p.u. loading factor and the minimum margin 0.5 since the maximum loading point is located at 1.952 p.u. which is less than 2 p.u. (=1.5+0.5).

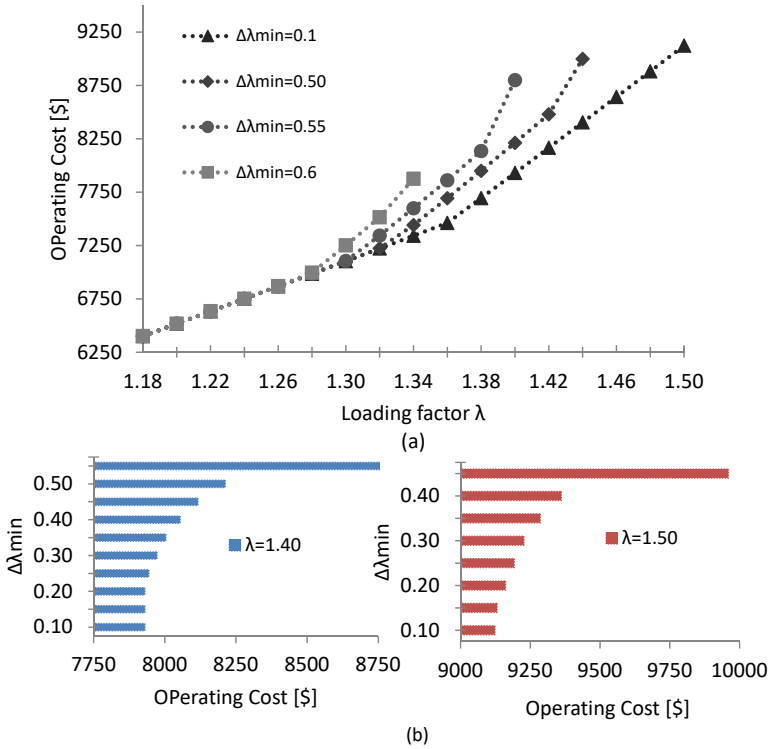

Figure 4.5: Operating cost versus λ using Minimum Margin Constrained VSC-OPF for 14-bus system. (a) Impact of increasing $\Delta\lambda_{min}$ on solution cost. (b) Two cross sections of operating cost at $\lambda = 1.4$ and $\lambda = 1.5$.

4.5.1.3 Multi-Objective VSC-OPF

This method provides a trade-off between minimizing cost and maximizing stability margin. Fig. 4.6 demonstrates the variation of optimum operating point for 14-bus test system; the loadability factor (λ^b) is presented as ω_1 changes from 0 to 0.0001 and λ increases from 1 to 1.4. It can be seen when the weighting factor ω_1 is low then the objective function tends to maximize stability. The λ^b is, therefore, getting close to maximum loading point. On the other hand, increasing the value of ω_1 pushes the objective function toward the minimum operating cost function. The value of λ^b is then getting close to current loading point (λ). Fig. 4.6 defines three operating area based on the ω_1. The first one refers to low ω_1; it is denoted as "maximum loading margin" area. Second area is a trade-off between stability and operating cost. Third area refers to high ω_1, and defines OPF, which provides minimum operation cost.

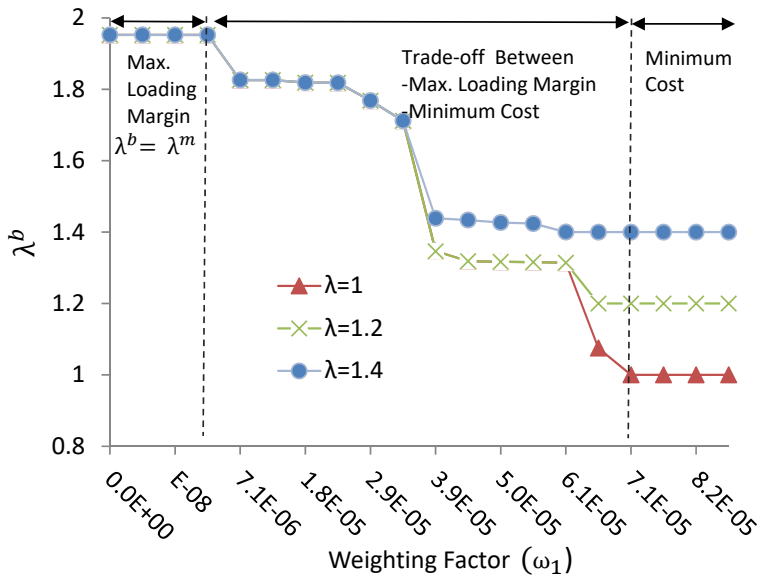

Figure 4.6: Three operating area defined based on weighting factor w_1: maximum stability area, trade-off area, minimum operating cost area; IEEE 14-bus.

4.5.2 Scalability

To examine the scalability of proposed methods, IEEE 57-bus and 118-bus test systems are considered. IEEE 57-bus test system contains 7 generators, 65 lines and 42 load buses; IEEE 118-bus system contains 19 generators, 177 lines and 91 loads. The details of these systems are given in [83].

Fig. 4.7 and Fig. 4.8 demonstrate the maximum loading λ^m obtained from VSC-OPF for 57-bus and 118-bus test systems respectively. The maximum loading point for 57-bus and 118-bus are equal to 1.08 and 2.036 respectively. Please note that λ^m represents the loading level to which the system demands can be increased universally by increasing power generation but keeping the voltage at PV buses constant. VSC-OPF converges to the same λ^m as the system loading increases. At all loading factors, VSC-OPF converges to higher λ^m than OPF. This stability margin brings higher operating cost. For instance, in 57-bus test system (Fig. 4.7), the cost of maximizing voltage security margin is equal to \$4365 at $\lambda = 1.03$. For a larger system (118-bus) as shown in Fig. 4.8, this security cost is equal to \$14368 at $\lambda = 1.50$.

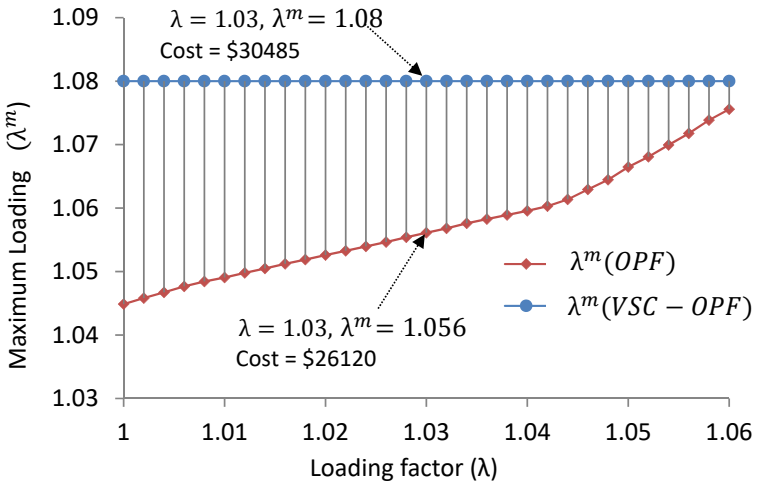

Figure 4.7: Maximum loading (λ^m) obtained from VSC-OPF and OPF; IEEE 57-bus.

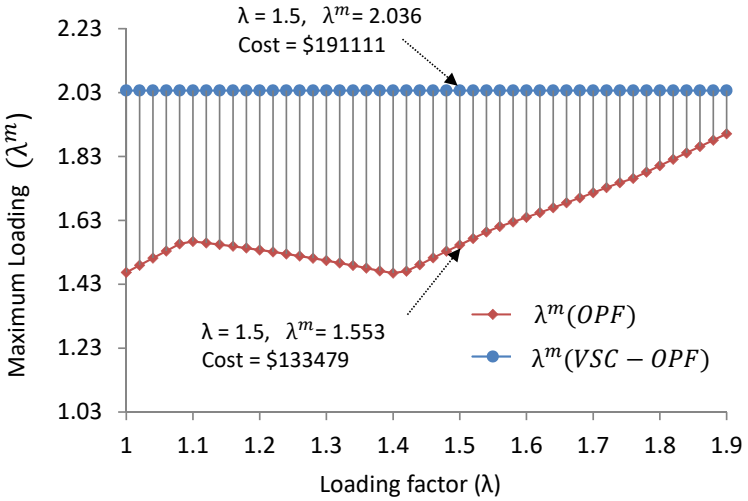

Figure 4.8: Maximum loading (λ^m) obtained from VSC-OPF and OPF; IEEE 118-bus.

Table 4.6 provides the generation cost associated with minimum margin constrained VSC-OPF for $\Delta\lambda_{min} = (0.3, 0.4, 0.5)$. This method does not converge beyond 1.54 p.u. $\Delta\lambda_{min} = 0.5$ since the maximum loading point is located at 2.036 p.u. which is less than 2.04 p.u. (=1.54+0.5). The system cost is also increases when $\Delta\lambda_{min}$ is increased.

Fig. 4.9 demonstrates the variation of optimum operating point for 118-bus test system using multi-objective VSC-OPF; (λ^m) is presented as ω_1 changes and λ increases from 1 to 1.5. The objective function tends to maximize stability when the

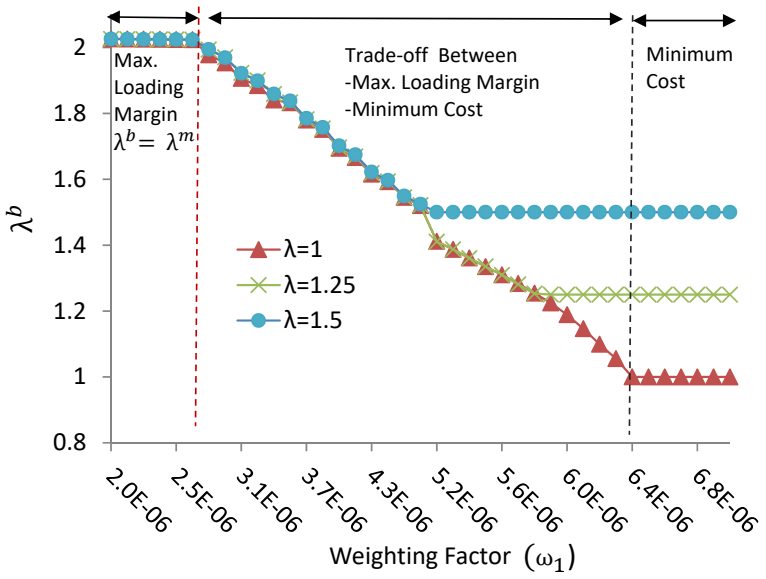

Figure 4.9: Three operating area defined based on weighting factor w_1: maximum stability area, trade-off area, minimum operating cost area; IEEE 118-bus.

Table 4.6: Impact of $\Delta\lambda_{min}$ on VSC-OPF solution (118-bus)

λ	$VSC-OPF$ [k$] ($\triangle\lambda_{min}=0.3$)	$VSC-OPF$ [k$] ($\triangle\lambda_{min}=0.4$)	$VSC-OPF$ [k$] ($\triangle\lambda_{min}=0.5$)
1	86299	86299	86299
1.4	122328	122330	122335
1.42	124184	124188	124192
1.44	126053	126057	126062
1.46	127967	127972	127977
1.48	130359	130366	130375
1.5	133486	133494	133504
1.52	136686	136694	136710
1.54	139917	139929	-
1.56	143167	143180	-
1.58	146428	146443	-
1.6	149699	149715	-
1.62	152980	152996	-
1.64	156269	-	-

weighting factor ω_1 is low, and it moves toward the minimum operating cost function as ω_1 increases. Fig. 4.9 defines three operating area based on the ω_1. The middle area is a trade-off between voltage stability and operating cost.

4.5.3 PV Curve Generation

It is important to note that one can develop PV curve using VSC-OPF method presented in 4.4.2. For analysis, here the voltage lower bound at load buses and the maximum power at slack bus are relaxed to obtain the PV curve. The load increment is kept uniform for all spot loads in the test system. Fig. 4.10 shows the PV curve for bus 14 (in 14-bus test system) .

The PV curves obtained from the proposed methods are also compared with continuation power flow (CPF). Fig. 4.10 compares the PV curve from CPF (using PSAT) with the curve from VSC-OPF for bus 14; the Q_{lim} of generators are relaxed. In both methods the voltage at PV buses are considered to be constant as system loading increases. It is noticeable that CPF curve shows less load-ability for the system, and loading level at which the voltage collapses is considerably lower than the collapse point obtained from optimization ($\Delta\lambda = 1.51$). This is resulted from the fact that CPF method does not have the mechanism to dispatch the generation over the whole feasible area. Fig. 4.11 compares the PV curve obtained from CPF and optimization by incorporating the Q_{lim} of generators. CPF results shows less load-ability for the system compared to convex VSC-OPF, and the difference between collapse points is 0.93 p.u. ($\Delta\lambda = 0.93$).

4.6 Conclusion

A new convex VSC-OPF architecture taking into account different types of VSC-OPF methods including maximum stability margin, minimum margin constrained, and multi-objective VSC-OPF is proposed. The proposed methods address the major issue of non-convex VSC-OPF, referred as the local optimum solution. The convex VSC-OPF methods are examined using IEEE 14-bus, 57-bus and 118-bus test systems. Results show the effectiveness of proposed methods to find the maximum and critical loading point and evaluate the voltage security cost. The proposed convex

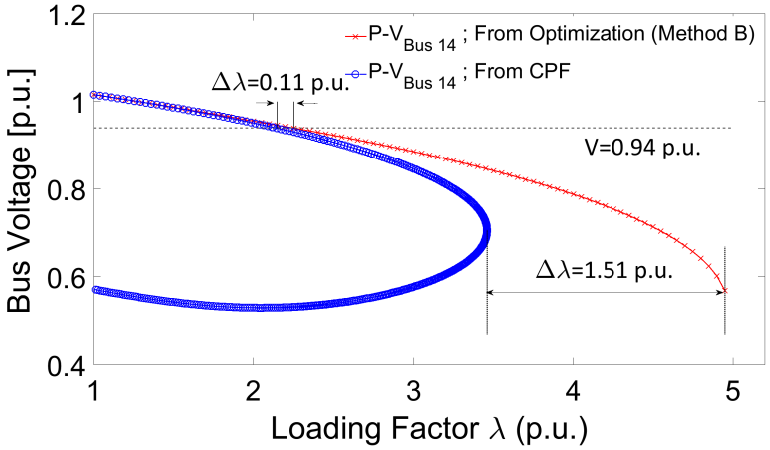

Figure 4.10: PV curve of bus 14 obtained from optimization (method B) compared to PV curve from CPF.

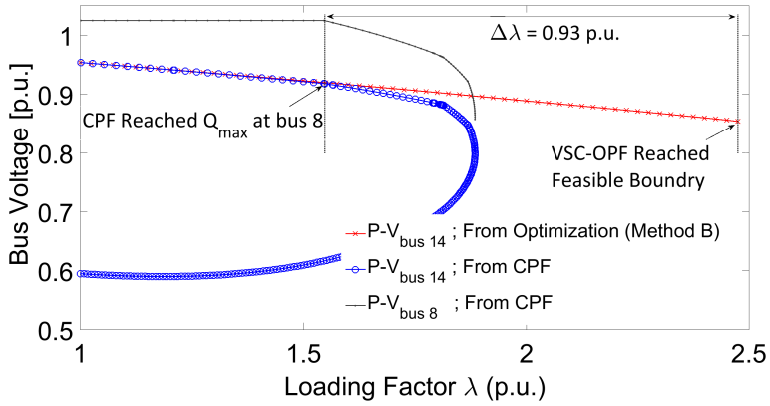

Figure 4.11: PV curves of bus 14; comparison method B with CPF; V_{lim} and Q_{lim} of generators are enforced.

VSC-OPF is also implemented to derive system PV curve and the results are compared with CPF. The comparison shows the superiority of VSC-OPF to dispatch the generators effectively with larger stability margin.

CHAPTER 5: VOLTAGE STABILITY CONSTRAINED CONVEX OPTIMAL POWER FLOW FOR INTEGRATED AC-DC SYSTEMS

5.1 Introduction

The congestion on power transmission systems is one of the main causes of voltage stability issues in power systems. This situation in turn challenges independent system operators (ISOs) for providing fair access for market participants. Coupled by demand growth, such conditions results in higher electricity price and pushes the system closer to its stability limit [70]. Voltage source converter (VSC) based DC transmission systems can alleviate this burden by providing DC corridors for active power and managing reactive power at converter terminals. The DC network can incorporate multi-terminal high voltage direct current (HVDC) systems with mesh configuration and form a robust AC-DC system [84].

Considerable research has been devoted to study the control and transient behavior of the AC-DC networks [84–86]. However, there have been less studies conducted investigating efficient methods for comprehensive scheduling of AC-DC systems. Generally OPF objective focus on achieving a minimum cost operating point. However, this is not the only objective in this OPF. The modern power grid utilities are also concerned about the loading margin to alleviate voltage stability issues [87,88]. Recently voltage instability scenarios has caused several blackouts. Incorporating voltage stability limits inside optimal power flow (OPF) is, therefore, becoming an essential part for new energy management systems. The voltage stability limits is modeled as the margin that defines the distance to maximum loading points [71]. This margin can be included either in the objective or in the constraints of OPF problem. This forms voltage stability constrained OPF (VSC-OPF) [72]. The VSC-OPF aims to find the

optimal scheduling of AC and DC grids together while considering this voltage limits. Integration of HVDC to AC transmission system extends the degree of freedom in OPF problem by including the converter set points at AC and DC sides [89]. If one considers separate scheduling of AC and DC networks this leads to a local optimum solution. The combined AC-DC solution is, therefore, needed to provide better optimal schedule for all sources, loads and converters in both AC and DC networks.

Earlier researches have discussed OPF algorithms for AC-DC transmission systems based on non-convex power flow equations. Ref. [26] presents the OPF model of VSC-based HVDC integrated in AC transmission system using Newton-Raphson (NR) technique and solved using augmented Lagrange method. A security-constrained unit commitment (SCUC) incorporating the DC grid has been presented in [90] using NR and linearization technique. Ref. [89] presents an algorithm for combined AC-DC OPF which is solved using interior point method. These algorithms contain the limitations referred to as the non-exact relaxation and finding only locally optimum solution mainly resulting from non-convexity of OPF equations [29]. Power flow equations placed in the constraints of OPF problems are nonlinear quadratic functions. This problem is a non-convex and NP-hard optimization problem. In recent years, considerable contributions are being reported for convexification and relaxation of OPF [30] to find the optimal solution. The first semidefinite programming (SDP) relaxation for meshed networks was proposed in [34]. The detailed analysis on SDP relaxation is then presented in [29] where the sufficient condition for zero duality gap for OPF problem is derived.

Convex AC-DC formulation considers convexifying combined AC-DC OPF. Ref. [91] formulates such AC-DC OPF in transmission network using second order conic programming (SOCP). However, SOCP solutions cannot provide exact relaxation for mesh networks and leads to a local or infeasible solution. Ref. [92] demonstrates a convex formulation for AC-DC network with multi objective of converter loss and gen-

eration cost. This chapter presents the formulation for voltage stability constrained OPF using semidefinite programming, which includes both AC and DC side equations together [93]. The proposed methods provide the solution for reaching the minimum cost or maximum stability margin in an integrated AC-DC system using convex OPF that is suitable for solving active mesh networks. It also investigates the impact of separate scheduling and converter ratings on the optimal schedule of integrated AC-DC system incorporating radial and meshed systems with DC resources. The voltage stability assessment in this chapter is focused on steady-state conditions.

Rest of the chapter is organized in the following order. The OPF and VSC-OPF formulations for AC-DC system are presented in Section 5.2. The equivalent converter model for is derived in 5.3. Section 5.4 discusses the convexification of AC-DC OPF. This optimization provides the optimum operating point (minimum cost) for both AC and DC system. Section 5.5 extends this formulation to convex VSC-OPF of integrated AC-DC systems. Implementation results of these methods on the IEEE 14-bus, IEEE 57-bus, and 118-bus test systems incorporating radial and meshed DC networks are presented in section 5.6. Finally, conclusions in 5.7 summarizes the main results and contribution.

5.2 AC-DC VSC-OPF

Voltage stability constrained OPF problem aims to provide the optimal dispatch which ensures that solution maintains the maximum distance to the maximum loading point or remains within the boundary of proper distance as opposed to solving only for the minimum cost as in the case of conventional AC-DC OPF problems. To solve these problems, one approach is to schedule DC system and then deploy its set points in scheduling of AC system. The separate scheduling, however, leads to a local solution. The reason is that DC problem only contains the local variables of DC system, and it lacks both the AC cost function and the AC constraints. Unlike separate scheduling of AC and DC systems which leads to a local solution, integrated approach incorporates

Table 5.1: Notations of Indexes and Short Usages

i, j, k	Bus indexes
lm	Line index from bus l to bus m
N	Set of buses
N_G	Set of generation buses $N_G \subseteq N$
N_C	Set of AC/DC converter buses $N_C \subseteq N$
N_L	Set of lines $N_L \subseteq N \times N$
S^n	$n \times n$ positive semidefinite (PSD) space
$Re\{.\}, Im\{.\}$	Real and imaginary part
$Tr\{.\}, rank\{.\}$	Trace and rank of given matrix
SDP	Semidefinite programming
VSC-OPF	Voltage stability constrained OPF
AC-DC	Integrated AC and DC systems
MTDC	Multi-terminal DC
HVDC	High voltage direct current
VSC-HVDC	Voltage source converter based HVDC

power flow and physical constraints of both sides in one optimization problem. The other difficulty in this approach is defining of the objective when solving the OPF problem over the DC space. In this section, first ,the non-convex AC-DC OPF is discussed. Then the formulation of AC-DC VSC-OPF is presented.

5.2.0.1 AC-DC OPF

Minimum cost AC-DC OPF aims to provide an operating point which minimizes the total operation cost of AC and DC system. Equation (5.1) demonstrates the formulation for AC-DC OPF with the generation cost as the objective function. The notations are given in Table 5.1 and Table 5.2.

$$\underset{(P_i,P_{DC_i},v_i,v_{DC_i})}{Min} \sum_i c_i\left(x, x_{DC}, P_i, P_{DC_i}, v_i, v_{DC_i}, Q_{conv}\right) \tag{5.1}$$

$$s.t. \begin{cases} h(x, Pi, v_i, \lambda) = 0 \\ h(x_{DC}, P_{DC_i}, v_{DC_i}, \lambda) = 0 \\ \underline{b}_i \leq g\left(x, Pi, v_i, \lambda\right) \leq \overline{b}_i \\ \underline{b}_{DC_i} \leq g\left(x_{DC}, P_{DC_i}, v_{DC_i}, \lambda\right) \leq \overline{b}_{DC_i} \\ \underline{d}_i \leq L(P_i, P_{DC_i}, \gamma_c) \leq \overline{d}_i \end{cases}$$

The control variables are the power and voltage associated with AC and DC buses. (P_i, v_i) , (P_{DC_i}, v_{DC_i}) and Q_{conv} are control variables. The objective function is total operation cost of AC and DC system. The loading factor λ determines the current loading level of power grid.

5.2.0.2 VSC-OPF (Maximum Stability Margin)

The optimization approaches contributed to VSC-OPF problem can be classified into three major categories [72]. In this chapter, the maximum stability margin VSC-OPF for AC-DC systems is modeled and then convexified using semidefinite programming.

A VSC-OPF formulation for AC-DC systems is represented in (5.2). In this formulation, the system loading point and the maximum loading point are represented by λ and λ^m respectively. The functions $g(.)$ and $h(.)$ define the equality constraints and inequality constraints associated with current and maximum loading points respectively. The function $f(.)$ provides the connection between λ and λ^m. The equation $V_i = V_i^m$ ensures the generator buses keep the same terminal voltage as the loading increases from λ and λ^m.

$$Min \ -(\lambda^m - \lambda) \tag{5.2}$$

$$s.t. \begin{cases} h(x, Pi, v_i, \lambda) = 0 \\ h(x_{DC}, P_{DC_i}, v_{DC_i}, \lambda) = 0 \\ h(x^m, P_i^m, v_i^m, \lambda^m) = 0 \\ h(x_{DC}^m, P_{DC_i}^m, v_{DC_i}^m, \lambda^m) = 0 \\ \underline{b}_i \leq g\left(x, Pi, v_i, \lambda\right) \leq \overline{b}_i \\ \underline{b}_{DC_i} \leq g\left(x_{DC}, P_{DC_i}, v_{DC_i}, \lambda\right) \leq \overline{b}_{DC_i} \\ \underline{b}_i^m \leq g\left(x^m, P_i^m, v_i^m, \lambda^m\right) \leq \overline{b}_i^m \\ \underline{b}_{DC_i}^m \leq g\left(x_{DC}^m, P_{DC_i}^m, v_{DC_i}^m, \lambda^m\right) \leq \overline{b}_{DC_i}^m \\ \underline{l}_i \leq f(\lambda, \lambda^m) \leq \overline{l}_i \\ V_i = V_i^m \quad (i \in N_G) \\ \underline{d}_i \leq L(P_i, P_{DC_i}, \gamma_c) \leq \overline{d}_i \\ \underline{d}_i^m \leq L(P_i^m, P_{DC_i}^m, \lambda^m, \gamma_c) \leq \overline{d}_i^m \end{cases}$$

The $L(.)$ provides the links between AC system and DC sides of converter. This constraint is enforced over the buses which contains AC/DC converters. In this method the optimization output is an operating point that creates the maximum distance to the maximum loading point.

5.3 Converter Model and DC Resources

In AC-DC system, the voltage source converter (VSC) is the point of connection between AC and DC network. Fig. 5.1 shows a converter station which synthesizes the voltage waveform on AC side using either the multilevel modular converter (MMC) or pulse width modulation technique (PWM). The converter station contains series

Table 5.2: Notations of Variables and Parameters

v_i	Voltage of bus i
$\|v_i\|$	Voltage magnitude of bus i
δ_i	Voltage angle of bus i
λ	Current loading factor
λ^m	Maximum loading factor
λ^c	Critical loading factor
W,W^m	$(2n \times 2n)$ PSD matrix variables
$W_{i,j}$	(i,j) entry of matrix W
$e_1, e_2, \ldots, e_n$	Standard basis vectors of R^n
$h(.), g(.)$	Equality & inequality functions of OPF
$f(.)$	Function of λ,λ^m
$H(.), G(.)$	Convex OPF equality & inequality functions
$F(.)$	Convex function of λ and λ^m
$\succeq$	Positive semidefinite
X^{min}, X^{max}	Minimum and maximum of X
$\underline{b}, \bar{b}$	Lower and upper bound of function b
X^m	X value at loading level of λ^m
P, Q, S	Active, Reactive and Apparent power
P_{D_i},Q_{D_i}	Active and reactive demand at bus i
Y	Admittance matrix
$y_{lm}, \bar{y}_{lm}$	Line lm series and shunt admittance
Y_i, Y_{lm}	Bus and line oriented admittance matrices
M_i	Configuration coefficient matrix for bus i
M_{lm}	Configuration coefficient matrix for line lm
W_{DC},W^m_{DC}	DC system $(n \times n)$ PSD matrix variables
P_{DC_i}	DC system active demand at bus i
Y_{DC_i}	DC system bus oriented admittance matrix
$Y_{DC_{lm}}$	DC system line oriented admittance matrix
γ_c, Q_{cmax}	Converter loss and reactive capacity

transformer, phase filter and reactor, VSC and DC capacitors. The station has the capability to control the voltage at ac and dc terminals independently. Given the voltage magnitude of one side, the modulation parameter m varies to set the other side voltage with respect to their range as shown in (5.3).

$$v_i = m.v_{DC_i} \quad i \in N_C \tag{5.3}$$

For modeling purpose, the converter stations are replaced by two power sources and two loads. This model is shown in Fig. 5.2. The ac side model contains a power source (v_i, p_{g_i}, q_{g_i}), a load (p_{l_i}) and a series impedance z_c. The dc side is represented by a dc power source (v_{dc_i}, p_{dcg_i}) and a dc load p_{dcl_i}. The equivalent ac and dc loads are considered to avoid the negative values of p_{g_i} and p_{dcg_i}. The power source located in AC side is capable of supplying active and reactive power up to the converter rating capacity (p_{cmax}). The power source in DC side only provide the active power. The equivalent generation and load value is determined by the amount of active power absorbed/injected from/to the other side and the converter loss γ_c as shown in (5.4)-(5.5) . The equations modeling the connection between AC and DC variables and the converter loss are presented in (5.4)-(5.8).

$$p_{l_i} = (1 + \gamma_c) p_{dcg_i} \tag{5.4}$$

$$p_{dcl_i} = (1 + \gamma_c) p_{g_i} \tag{5.5}$$

$$p_{g_i} + p_{l_i} \leq p_{cmax} \tag{5.6}$$

$$p_{dcl_i} + p_{dcg_i} \leq p_{cmax} \tag{5.7}$$

$$(p_{l_i}, p_{g_i}, p_{dcl_i}, p_{dcg_i}) \geq 0, \quad i \in N_C \tag{5.8}$$

The sum of equivalent generation and load in each side is bounded by converter capacity since only one of these variables takes the positive value and the other one is equal to zero, which is determined in optimization as illustrated in (5.6)-(5.7). The positive p_{g_i}, for instance, means the equivalent ac generator is producing active power, and the power flows from dc to ac system. This amount of active power plus the converter loss is absorbed from dc system as shown in (5.5).

DC Resources (DCRs) injecting active power into DC network. DCR includes the

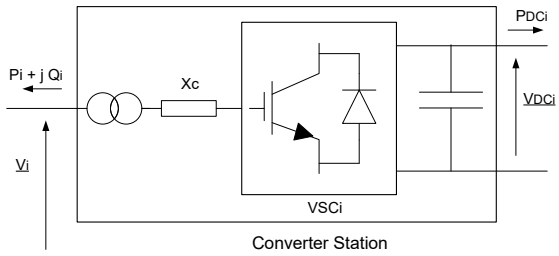

Figure 5.1: Converter Model in AC-DC OPF Formulation

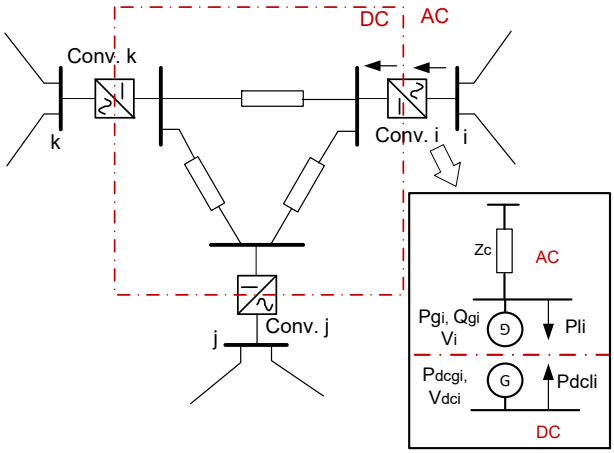

Figure 5.2: Converter Model in AC-DC OPF Formulation

recourses which produce DC voltage output and the AC generators, in which the output is converted to DC before connecting to the network. The off-shore wind turbines are the example of latter DCRs. VSC converters are used to convert the off-shore generation to DC voltage, which is then transferred to the shore using the HVDC lines.

5.4 AC-DC Convex OPF (Minimum Cost)

The minimum cost OPF is commonly formulated using bus injection model (BIM) and aims to minimize the operating cost. The convex relaxation is derived by imposing convex supersets over the non-convex feasible set of OPF problem and minimizing cost function over these sets. An equivalent rank-1 matrix is introduced to transform the constraints to linear space. SDP relaxation of OPF is then obtained by dropping

the rank-1 constraint. This relaxation does not affect the optimal solution if the solution matrix is either rank-1 or rank-2. This yields a quadratic convex optimization problem.

In the next step defined as the rank relaxation, the rank-1 constraints for W and W^m are eliminated from the constraints. These relaxations convert the nonlinear AC-DC OPF problem to a convex optimization problem. The general convex AC-DC OPF thus obtained is shown in (5.9)-(5.13).

$$\underset{S^{+}_{AC-DC}}{Min} \sum_{i} C_i\left(x, W, x_{DC}, W_{DC}, \lambda\right) \tag{5.9}$$

$$s.t. \quad H(x, W, x_{DC}, W_{DC}, \lambda) = 0 \tag{5.10}$$

$$G\left(x, W, x_{DC}, W_{DC}, \lambda\right) \geq 0 \tag{5.11}$$

$$L(W, W_{DC}, \gamma_c) = 0 \tag{5.12}$$

$$W \succeq 0, W_{DC} \succeq 0 \tag{5.13}$$

The voltages V_{AC} referred as $V = \left[Re\{v\}^T Im\{v\}^T\right]$ and $V_{DC} = \left[Re\{v_{DC}\}^T\right]$ contains the bus voltage real and imaginary parts. The objective function and constraints are extended as a linear function of two quadratic matrix VV^T and $V_{DC}{V_{DC}}^T$.

The matrices VV^T and $V_{DC}{V_{DC}}^T$ are replaced by matrix variables W and W_{DC} respectively, yielding a linear matrix inequality problem over the joint space, which is S^{2n} on AC system and S^m on DC side, in which m and n represent the number of buses in AC and DC systems. The extended formulation for AC-DC OPF is shown in (5.14)-(5.16) and (5.4)-(5.8) modeling the converter.

$$\begin{aligned} Min \quad & \sum_{i \in N_G} \{C_{i_2} \left(Tr\{Y_i W\} + P_{D_i}\right)^2 \\ & + C_{i_1} \left(Tr\{Y_i W\} + P_{D_i}\right) + C_{i_0}\} \end{aligned} \tag{5.14}$$

$$\begin{cases} P_i = Tr\{Y_i W\} + P_{D_i}, \quad Q_i = Tr\{\bar{Y}_i W\} + Q_{D_i} \\ P_i^{min} \leq Tr\{Y_i W\} + P_{D_i} \leq P_i^{max} \\ Q_i^{min} \leq Tr\{\bar{Y}_i W\} + Q_{D_i} \leq Q_i^{max} \\ \left(V_i^{min}\right)^2 \leq Tr\{M_i W\} \leq \left(V_i^{max}\right)^2 \\ Tr\{Y_{lm} W\} \leq P_{lm}^{max} \\ Tr\{M_{lm} W\} \leq (\triangle V_{lm})^2 \\ W = V V^T \end{cases} \tag{5.15}$$

$$\begin{cases} P_{DC_i} = Tr\{Y_{DC_i} W_{DC}\} + P_{DC_{D_i}} \\ P_{DC_i}^{min} \leq Tr\{Y_{DC_i} W_{DC}\} + P_{DC_{D_i}} \leq P_{DC_i}^{max} \\ \left(V_{DC_i}^{min}\right)^2 \leq Tr\{M_i W_{DC}\} \leq \left(V_{DC_i}^{max}\right)^2 \\ Tr\{Y_{DC_{lm}} W_{DC}\} \leq P_{DC_{lm}}^{max} \\ W_{DC} = V_{DC} V_{DC}^T \end{cases} \tag{5.16}$$

The admittance and coefficient matrices needs to be derived for a tractable solution. These derivations are shown in Appendix A. The matrices $Y_{DC_i}, Y_{DC_{lm}}$ are derived from the admittance matrix of the DC network. The formulas are similar to Y_i, Y_{lm} derived from the admittance matrix of AC network. Due to the coefficient matrix

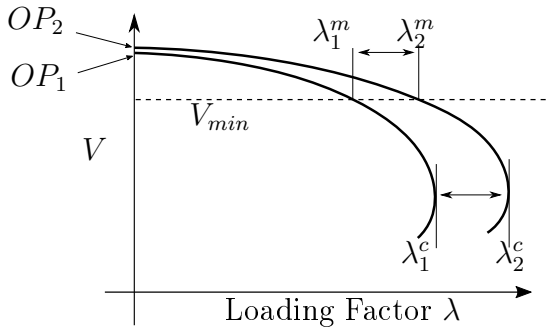

Figure 5.3: PV curves associated with two operating points OP_1 and OP_2. The points λ_1^m , λ_2^m and λ_1^c, λ_2^c represent infeasible boundary (V_{min}) and voltage collapse respectively.

in DC network has a size reduction since its variables only contain real parts. For instance, the size of coefficient matrix M_i is $(2n \times 2n)$, while M_{DC_i} is a $(m \times m)$ matrix, where n and m are the size of AC and DC systems respectively. The convex AC-DC OPF formulations consists of four major sections. The first section (5.14) defines the objective function which is the operating cost. The quadratic objective function can also be replaced by equivalent linear matrix inequality constraints. The second part (5.15) demonstrates the AC power flow and physical constraints which are convexified using SDP. The next equation (5.16) models DC power flow equations and constraints using SDP variables to form a unified SDP optimization problem. The final part (5.4)-(5.8) models the connection between AC and DC sides and the converter loss γ_c.

5.5 AC-DC Convex VSC-OPF (Maximum Stability Margin)

In this section, we extend the AC-DC convex OPF formulation from section 5.4 to develop voltage stability constrained OPF (VSC-OPF). In this formulation, the maximum loading of a bus is obtained from violating the feasible boundary of operational constraints and the critical loading is derived based on the voltage collapse point. Fig 5.3 depicts the voltage versus power (PV) curve corresponding to two operating points OP_1 and OP_2.

The critical points λ_1^c and λ_2^c represent the maximum loading levels beyond which

any increase in the demand will result in voltage collapse. The loading points λ_1^m and λ_2^m demonstrate the loading levels at which minimum voltage requirement is violated. It is worth noting that, the constraints are not just limited to voltage violations; it also includes other constraints such as line flow and generation capacity. The general convex formulation for AC-DC VSC-OPF is demonstrated in (5.17)-(5.27), which are detailed in this section.

$$\underset{S^+_{AC-DC}}{Min} \quad -(\lambda^m - \lambda) \tag{5.17}$$

$$s.t. \quad H(x, W, x_{DC}, W_{DC}, \lambda) = 0 \tag{5.18}$$

$$H(x^m, W^m, x^m_{DC}, W^m_{DC}, \lambda^m) = 0 \tag{5.19}$$

$$G\left(x, W, x_{DC}, W_{DC}, \lambda\right) \geq 0 \tag{5.20}$$

$$G\left(x^m, W^m, x^m_{DC}, W^m_{DC}, \lambda^m\right) \geq 0 \tag{5.21}$$

$$F(\lambda, \lambda^m) \geq 0 \tag{5.22}$$

$$L(W, W_{DC}, \gamma_c) = 0 \tag{5.23}$$

$$W_{i,i} + W_{(i+n),(i+n)} = W^m_{i,i} + W^m_{(i+n),(i+n)} \tag{5.24}$$

$$W_{DC_{i,i}} = W_{DC^m_{i,i}} \tag{5.25}$$

$$W \succeq 0, W^m \succeq 0 \tag{5.26}$$

$$W_{DC} \succeq 0, W^m_{DC} \succeq 0 \tag{5.27}$$

In VSC-OPF four sets of vector variables are defined to model the optimal and maximum points of AC and DC systems. Therefore, two more sets of variables in addition to $V = \left[Re\{v\}^T Im\{v\}^T\right]$ and $V_{DC} = \left[Re\{v_{DC}\}^T\right]$ are defined to model maximum loading points. The variables $V^m = \left[Re\{v^m\}^T Im\{v^m\}^T\right]$ is associated with the maximum loading point at the AC network and $V^m_{DC} = \left[Re\{v^m_{DC}\}^T\right]$ represents the corresponding maximum point in DC system. These voltages must satisfy all the

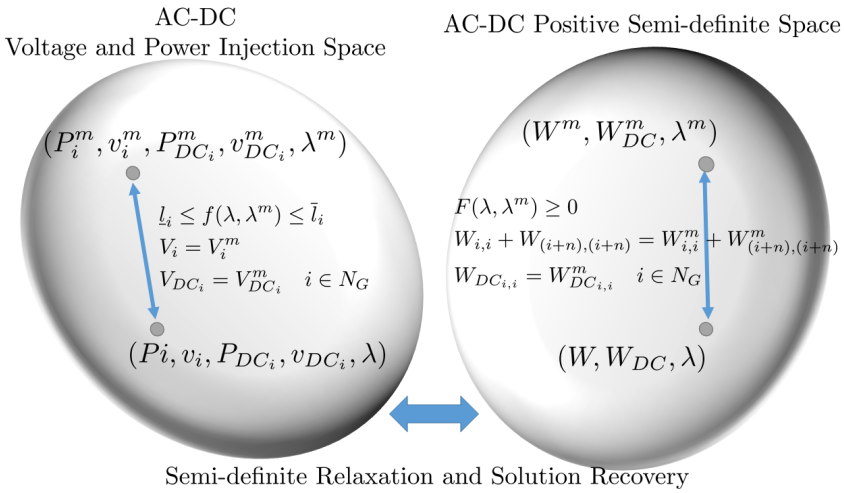

Figure 5.4: Feasible space and variables associated with AC-DC VSC-OPF. (P_i, v_i), $(P_i, v_i)^m$ and λ^m are variables in conventional VSC-OPF and PSD matrices W, W^m and λ^m are the corresponding variables in convex VSC-OPF.

constraints of the system including the power flow equations and equipment limits. The relation between variables in conventional and convex VSC-OPF is shown in Fig. 5.4. The system demand equations including the corresponding loading factors is shown in (5.28).

$$P_D = \lambda.P_{Do}\ ,\ Q_D = \lambda.Q_{Do} \tag{5.28}$$
$$P_D^m = \lambda^m.P_{Do},\quad Q_D^m = \lambda^m.Q_{Do}$$

The convexification and solution recovery algorithm are summarized in Fig. 5.5. Let W^{opt} and $W^{m^{opt}}$ denotes the solution of relaxed VSC-OPF. If these matrices are rank-1, the solution to the VSC-OPF problem is constructed using $W^{opt} = VV^T$ and $W^{m^{opt}} = V^m V^{m^T}$. Whenever the solution matrices are rank-2, matrices $(\rho_1 + \rho_2)EE^T$ and $(\rho_1^m + \rho_2^m)E^m E^{m^T}$ are the rank-1 solutions to the VSC-OPF, and voltage vectors can be constructed using these matrices. The scalars ρ_1 and ρ_2 are eigenvalues of W^{opt}, and vector E denotes unit eigenvector associated with ρ_1. Correspondingly, the scalars ρ_1^m, ρ_2^m, and vector E^m demonstrate eigenvalues and eigenvector associated with $W^{m^{opt}}$. Similarly, the DC voltage are recovered through $W_{DC}^{opt} = V_{DC}V_{DC}^T$ and

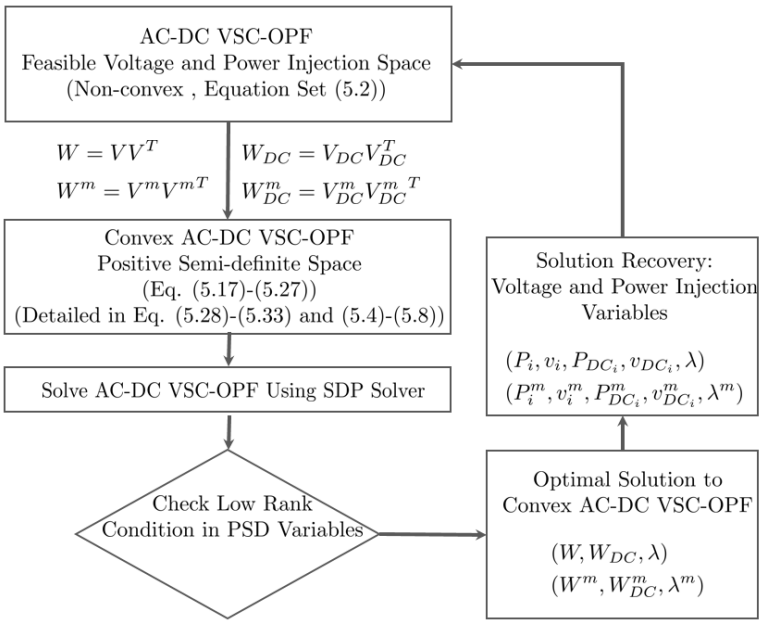

Figure 5.5: Convexification of VSC-OPF and Solution Recovery for AC-DC systems.

$W_{DC}^{m^{opt}} = V_{DC}^m V_{DC}^{m^T}$.

The set of equations modeling the relaxation process of convex VSC-OPF for the AC-DC system is shown in (5.29)-(5.33). First, the rank-1 constraints for W,W^m, W_{DC} and W_{DC}^m are eliminated from the constraints. This relaxation converts the non-linear AC-DC VSC-OPF problem to a convex optimization problem without affecting the optimal solution.

The objective function (5.29) is defined as the distance to the maximum loading point which should be maximized while in (5.14) the goal is to find minimum cost operating point. AC power flow and constraints at optimal and maximum loading points is demonstrated in (5.30), while (5.31) demonstrate similar constraints for DC system. Another assumption that maps control variables at current loading to maximum loading is associated with generator terminal voltages. The generators are assumed to have same terminal voltage as the loading level increases. Equation (5.33) enforces this constraint by equating the magnitude squares of the terminal voltages. The entry $W_{i,i}$ and $W_{(i+n),(i+n)}$ of matrix W are equal to the magnitude squared of voltage real part $Re\{v_i\}^2$ and imaginary part $Im\{v_i\}^2$ respectively. These

substitutions yield $|v_i|^2 = W_{i,i} + W_{(i+n),(i+n)}$; similar substitution in $|v_i^m|^2$ results in $|v_i^m|^2 = W_{i,i}^m + W_{(i+n),(i+n)}^m$. For the DC system, the voltages contain the real component, and therefore, $|v_{DC_i}|^2 = W_{DC_{i,i}}$ and $|v_{DC_i}^m|^2 = W_{DC(i,i)}^m$.

The equations modeling the connection between AC and DC variables at current loading level are same as (5.4)-(5.8). In addition, a new set of equations is added to model the DC and AC connection at maximum loading points. This set of equations is obtained by substituting $(p_{l_i}, p_{g_i}, p_{dcl_i}, p_{dcg_i})$ with $(p_{l_i}^m, p_{g_i}^m, p_{dcl_i}^m, p_{dcg_i}^m)$ at (5.4)-(5.8). Each equivalent generator and load is included in the equations as a actual generator and load, and must satisfy the corresponding constraints.

$$Min \quad -(\lambda^m - \lambda) \tag{5.29}$$

$$\begin{cases} P_i = Tr\{Y_i W\} + \lambda P_{D_i}, \quad Q_i = Tr\{\bar{Y}_i W\} + \lambda Q_{D_i} \\ P_i^m = Tr\{Y_i W^m\} + \lambda^m P_{D_i}, \quad Q_i^m = Tr\{\bar{Y}_i W^m\} + \lambda^m Q_{D_i} \\ P_i^{min} \le Tr\{Y_i W\} + \lambda P_{D_i} \le P_i^{max}, \\ P_i^{min} \le Tr\{Y_i W^m\} + \lambda^m P_{D_i} \le P_i^{max} \\ Q_i^{min} \le Tr\{\bar{Y}_i W\} + \lambda Q_{D_i} \le Q_i^{max} \\ Q_i^{min} \le Tr\{\bar{Y}_i W^m\} + \lambda^m Q_{D_i} \le Q_i^{max} \\ (V_i^{min})^2 \le Tr\{M_i W\} \le (V_i^{max})^2 \\ (V_i^{min})^2 \le Tr\{M_i W^m\} \le (V_i^{max})^2 \\ Tr\{Y_{lm} W\} \le P_{lm}^{max}, \quad Tr\{Y_{lm} W^m\} \le P_{lm}^{max} \\ Tr\{M_{lm} W\} \le (\triangle V_{lm})^2, Tr\{M_{lm} W^m\} \le (\triangle V_{lm})^2 \\ W = V V^T, \quad W^m = V^m V^{mT} \end{cases} \tag{5.30}$$

$$\begin{cases} P_{DC_i} = Tr\{Y_{DC_i} W_{DC}\} + \lambda P_{DC_{D_i}} \\ P^m_{DC_i} = Tr\{Y_{DC_i} W^m_{DC}\} + \lambda^m P_{DC_{D_i}} \\ P^{min}_{DC_i} \leq Tr\{Y_{DC_i} W_{DC}\} + \lambda P_{DC_{D_i}} \leq P^{max}_{DC_i} \\ P^{min}_{DC_i} \leq Tr\{Y_{DC_i} W^m_{DC}\} + \lambda^m P_{DC_{D_i}} \leq P^{max}_{DC_i} \\ \left(V^{min}_{DC_i}\right)^2 \leq Tr\{M_i W_{DC}\} \leq \left(V^{max}_{DC_i}\right)^2 \\ \left(V^{min}_{DC_i}\right)^2 \leq Tr\{M_i W^m_{DC}\} \leq \left(V^{max}_{DC_i}\right)^2 \\ Tr\{Y_{DC_{lm}} W_{DC}\} \leq P^{max}_{DC_{lm}},\ Tr\{Y_{DC_{lm}} W^m_{DC}\} \leq P^{max}_{DC_{lm}} \\ W_{DC} = V_{DC} V^T_{DC},\ W^m_{DC} = V^m_{DC} {V^m_{DC}}^T \end{cases} \tag{5.31}$$

$$W_{i,i} + W_{(i+n),(i+n)} = W^m_{i,i} + W^m_{(i+n),(i+n)} i \in N_G \tag{5.32}$$

$$W_{DC_{i,i}} = W^m_{DC_{i,i}} \tag{5.33}$$

5.6 Case Studies and Simulation Results

5.6.1 Proof Of Concept

To examine the proposed VSC-OPF methods, first IEEE 14 bus test system incorporating a DC line is examined (Fig. 5.6). The 14-bus system consists of 5 generators, 17 lines and 11 loads; An HVDC is considered between bus 5 and bus 14. This is considered as a proof of concept system. The active and reactive power capacity of converters are 1.0 p.u and 0.66 p.u. respectively unless specified in case studies. Other test system data and diagram are given in [83] and [94]. The optimization package GAMS with MOSEK solver is used to implement the formulation.

The results for 14-bus test system are presented in Fig. 5.7a and Fig. 5.7b for the loading factor increase from 0.9 to 2.7 p.u.. In both test cases (with and without HVDC) the VSC-OPF method exhibits higher operating cost since its objective is to

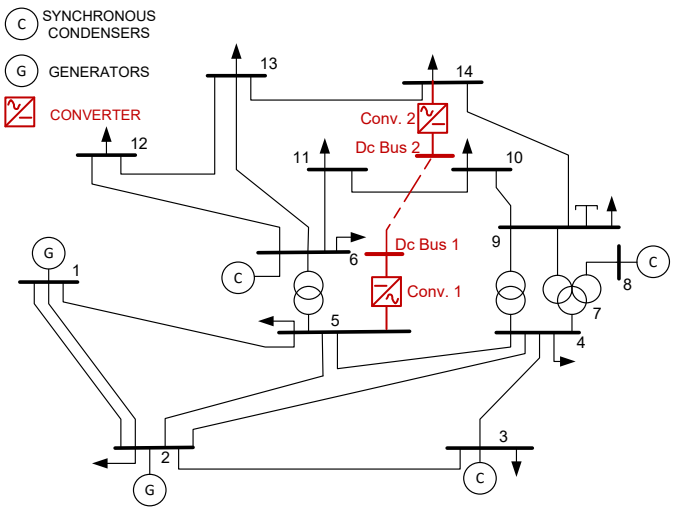

Figure 5.6: Modified IEEE 14-bus test system incorporating HVDC transmission system.

find the operating point which has longer distance to maximum loading point. The cost of improving voltage security margin is defined as the difference of operating cost associated with VSC-OPF and OPF. It can be seen from Fig. 5.7a that voltage security cost increases by λ increase, and it then decreases when the loading factor is beyond a) 1.35 p.u.(No HVDC) and b) 1.70 p.u. (with HVDC). Both methods converge to the same operating cost at the end. This convergence is due to the fact that OPF is approaching a smaller feasible solution area which limits the variation in optimal point. Fig. 5.7b depicts the loading margin versus λ for the system with and without HVDC. It is noticeable that DC link improve system loading margin, and maximum loading is increased from 1.952 to 2.62; The system without HVDC has no feasible solution for the loading factors beyond 1.952 p.u..

The impact of converter reactive power capacity Q_{cmax} on the optimal operating point of AC-DC system is also examined using AC-DC convex OPF (Method A). Fig. 5.8a demonstrates operating cost at four level of Q_{cmax}. It can be seen that increment of reactive power capacity provides the system a larger feasible area so that the OPF can converge at higher loading factors λ. The operating cost of optimal point is reduced as the Q_{cmax} is increased. Fig. 5.8b depicts four cross sections of

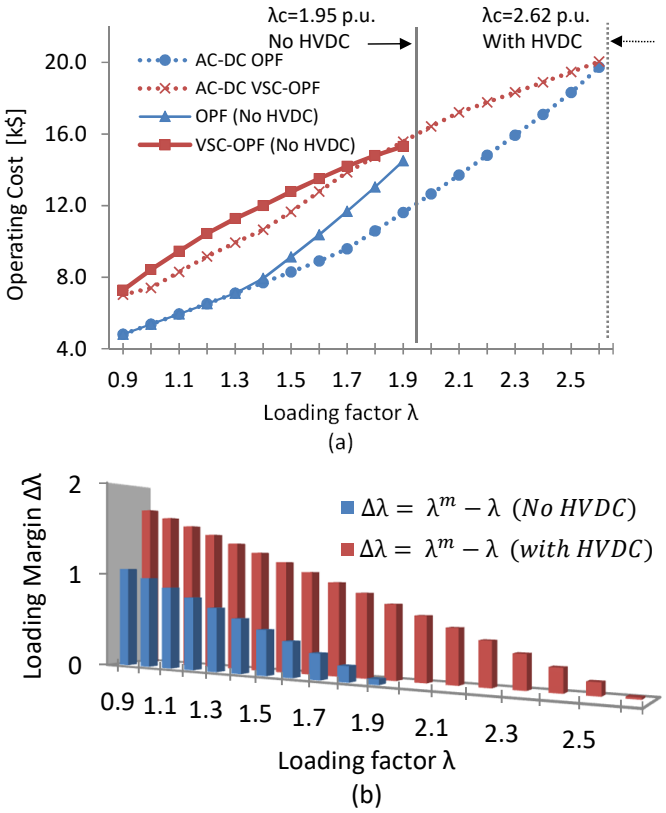

Figure 5.7: 14-bus system with and without HVDC using VSC-OPF and OPF (a): system operating cost V; (b): system loading margin

Fig. 5.8a at loading levels of $\lambda = 1.4, 1.5, 1.6, 1.7$ respectively. Although the increase of Q_{cmax} results in the reduction of optimal cost, this improvement will be saturated beyond some points of Q_{cmax} as identified by vertical lines in Fig. 5.8b.

5.6.2 Scalability

The IEEE 57-bus (Fig. 5.9) incorporating HVDC line is considered to test the effectiveness of proposed method on a larger system with a tight feasible space. IEEE 57-bus test system contains 7 generators, 65 lines and 42 load buses; The system includes a HVDC line between bus 31 and 46.

The 57-bus test system has a very tight feasible area with $\lambda^m = 1.08$. The results for IEEE 57-bus using AC-DC OPF and VSC-OPF are presented in Fig. 5.10a and Fig. 5.10b. It can be seen that the maximum loading point is improved from 1.08 p.u. to 1.525 by incorporating HVDC system, and system loading margin is increased

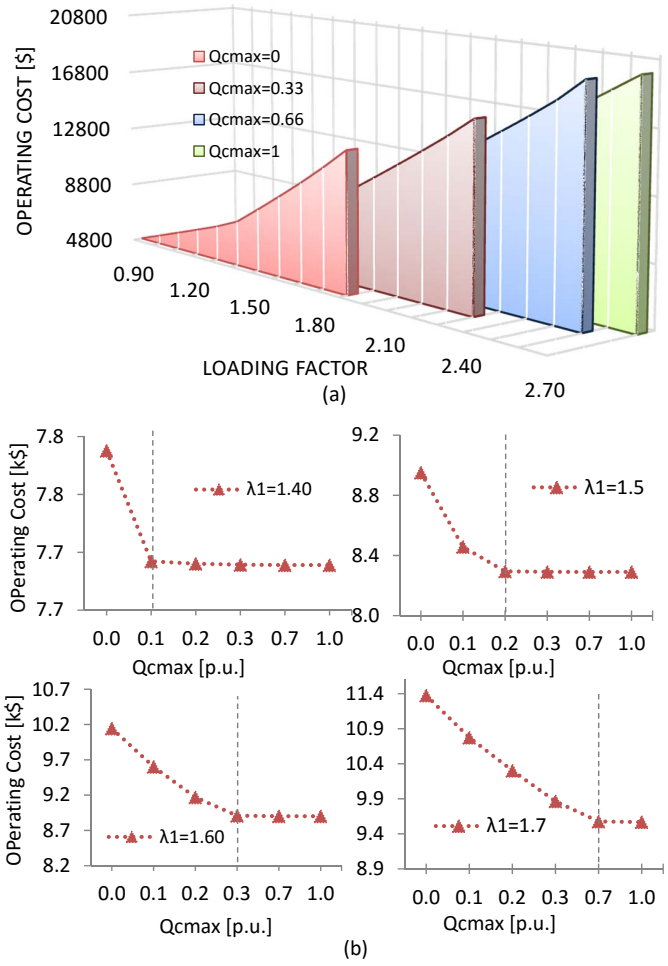

Figure 5.8: 14-bus test system; (a): The Impact of increasing Q_{cmax} on optimal operating cost; (b): Four cross Sections of Fig. 5.8a at $\lambda = 1.4, 1.5, 1.6, 1.7$ p.u.

at different loading factors as shown in Fig. 5.10b.

The impact of converter reactive power capacity Q_{cmax} on maximum loading point λ^m is evaluated using proposed VSC-OPF. Table 5.3 presents the λ^m value as Q_{cmax} varies from 0.01 to 1.00 p.u. for 14-bus and 57-bus test systems.

In 14-bus system, the increment of Q_{cmax} from 0.01 to 1 p.u. yields in the improvement of maximum loading point, while in 57-bus test system, the increase of Q_{cmax} beyond 0.1 p.u. does not provide better loading margin as shown in Table 5.3.

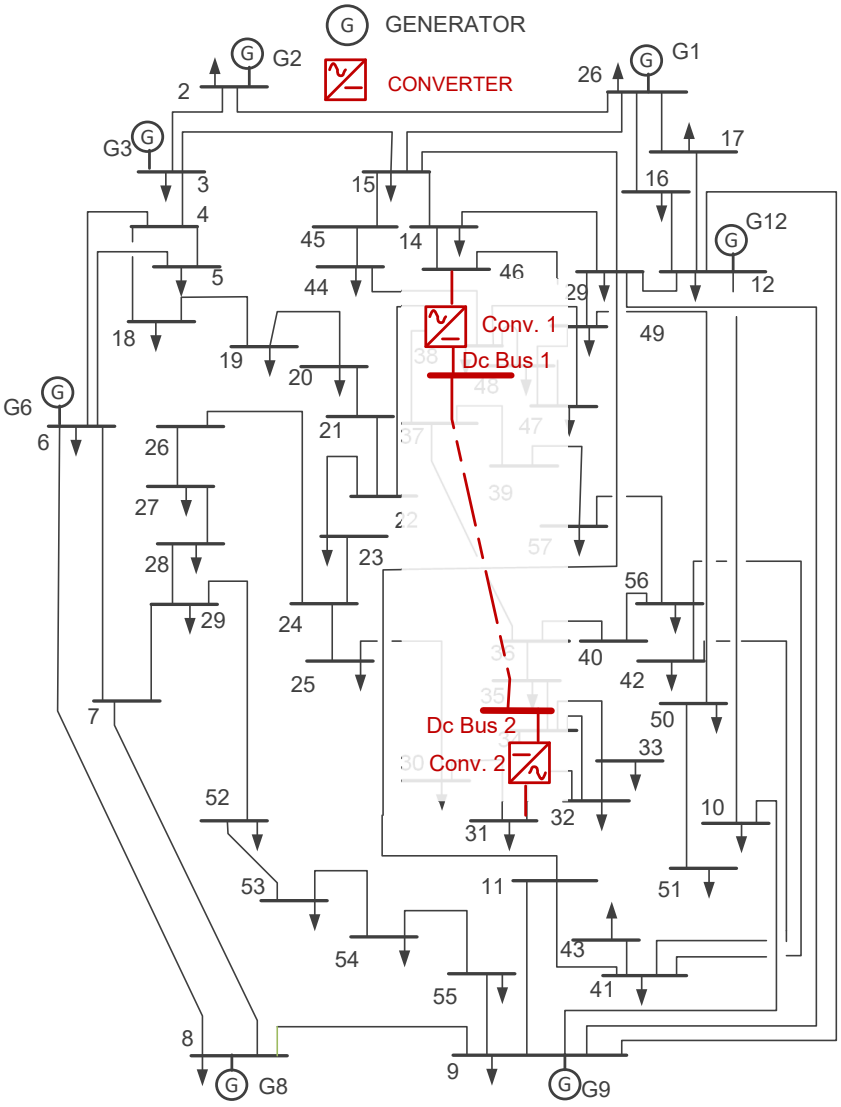

Figure 5.9: Modified IEEE 57-bus test system incorporating HVDC transmission system.

5.6.3 AC - Active Meshed DC Network

A larger test system with active meshed DC network, the modified 118-bus (Fig. 5.11), is considered to examine the proposed AC-DC OPF method. In this test system, a DC network composing of DC lines, converters and DC resources are connecting to AC transmission system through bus 9, bus 75 and bus 118. The DC system also includes 9 buses and 4 DC resources (DCRs). The DCRs are at DC buses 2, 3, 5, and 6. The active power capacity of DCRs at DC bus 1 and 6 is 1.5

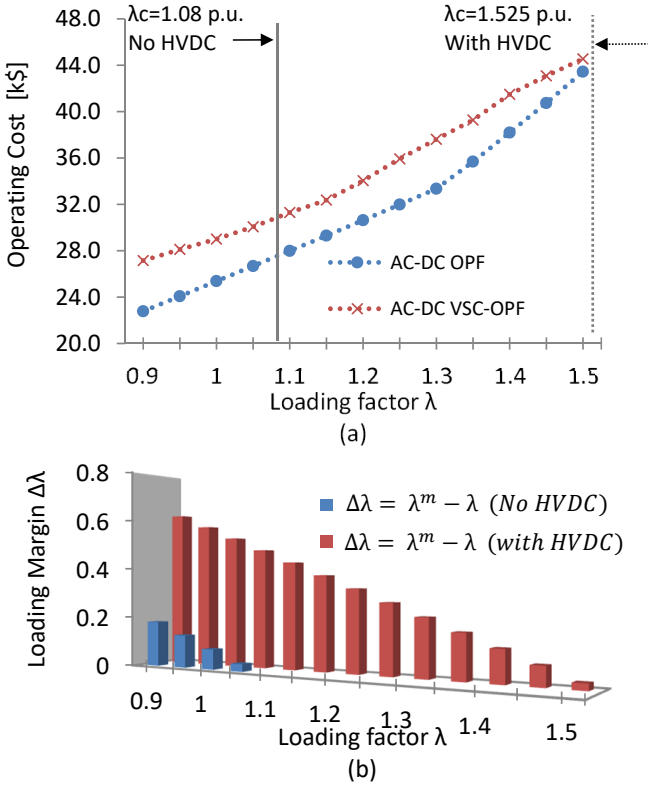

Figure 5.10: 57-bus system with and without HVDC using AC-DC VSC-OPF and OPF (a): system operating cost V; (b): system loading margin

Table 5.3: Impact of Converter Reactive Capacity on Maximum Loading Point λ^m for IEEE 14-bus and IEEE 57-bus Using AC-DC VSC-OPF

Q_{cmax} [p.u.]	λ^m (14-Bus)	λ^m (57-Bus)
(No HVDC)	1.952	1.080
0.00 (With HVDC)	1.988	1.146
0.01	2.002	1.449
0.05	2.057	1.507
0.10	2.122	1.525
0.33	2.380	1.525
0.66	2.617	1.525
1.00	2.767	1.525

p.u., and the size of DCRs at bus 3 and 5 is 1 p.u.. Converters are considered to have the active power rating of 2 p.u. and reactive power capacity of 1.0 p.u.. The DCRs generation cost is considered \$1000/p.u.. This is considered as test Case I.

To examine the impact of proposed AC-DC OPF versus separate scheduling of AC

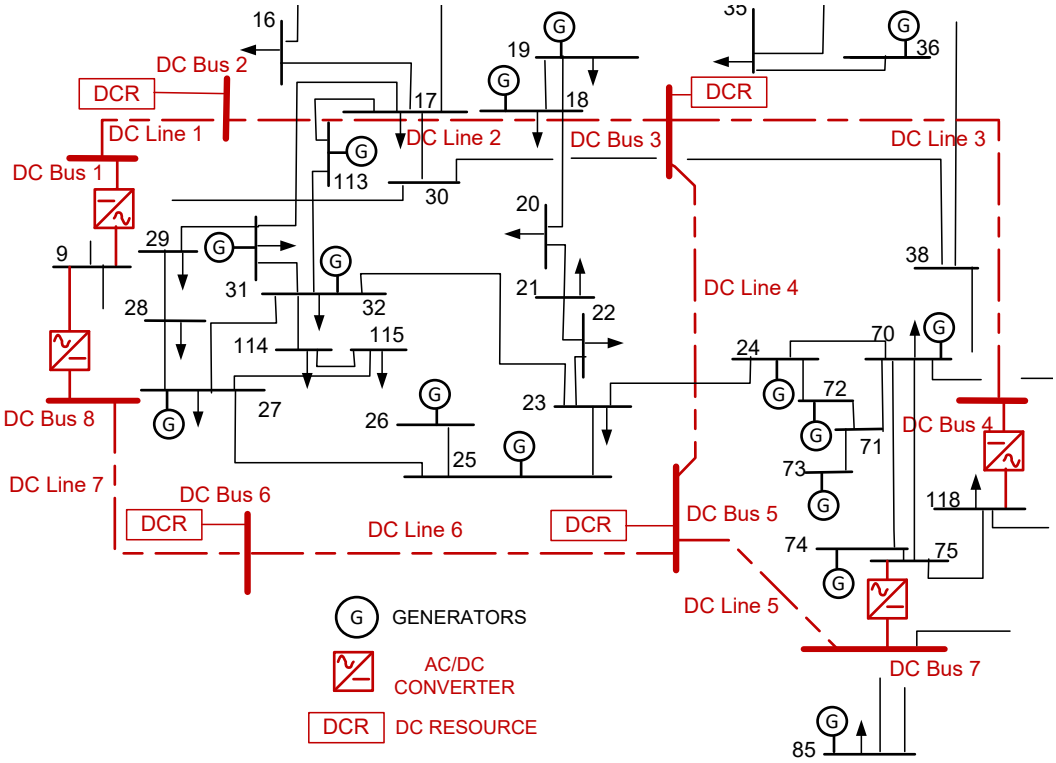

Figure 5.11: Modified IEEE 118-bus test system incorporating MTDC transmission system.

and DC system, the results of proposed OPF is compared with the case in which some converters are pre-scheduled. This situation happens when the system is operated between different entities, and it is not scheduled under one unified OPF. In separate scheduling, all converters are assumed to generated 0.5 p.u. reactive power injection, and the converters at DC bus 1 and DC bus 8 are set to transfer 0.5 p.u. from AC system to DC network. The test system is examined using AC-DC OPF and the results are compared with the system without any pre-scheduling. Fig 5.12 presents the difference of operating cost obtained from the separate scheduling and proposed AC-DC OPF. The saving in operating cost varies from \$4100 to \$10500 per hour as loading factor varies from 0.9 to 1.60 p.u.. These results show the loss due to pre-scheduling which will lead to a non optimal solution.

The optimal schedule of converter reactive power compensation are illustrated in Fig. 5.13. The converters connected to bus 9, bus 75, and bus 118. Results are shown

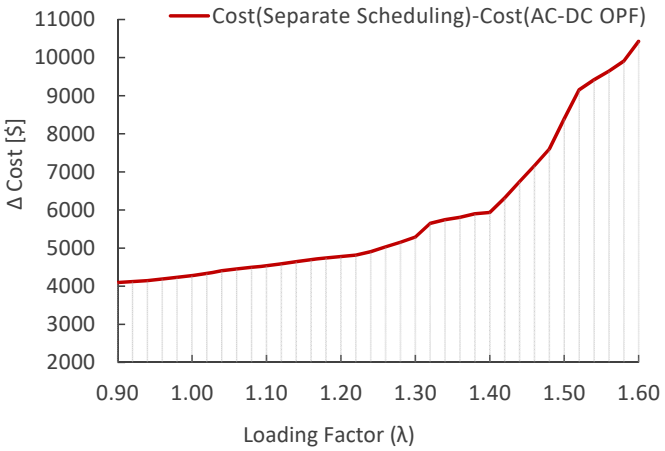

Figure 5.12: Saving in operating cost comparing separate scheduling with AC-DC OPF; 118-bus system.

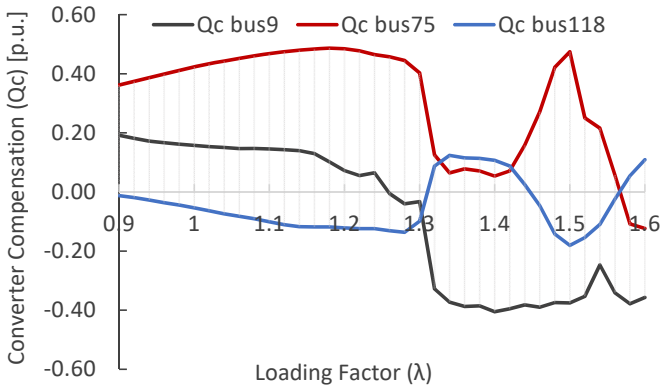

Figure 5.13: Optimal schedule of converter reactive compensation (Qc) using AC-DC OPF; 118-bus system.

for Case I, which all DCRs have equal generation cost. The converter optimal operating points varies at different loading factors. It is notable that the converters switch from reactive compensation to reactive generation as the loading factor changes.

The test case II includes DCRs with different generation cost. In Case II, the DCRs at buses 3 and 6 have the generation cost of \$1900/p.u. and DCRs at buses 1 and 5 have the cost of \$1000/p.u. while in Case I, the all DCRs have equal generation cost of \$1000/p.u.

To examine the impact of DC generation cost on the optimal solution of AC-DC system, the AC-DC system with two set of DCR cost is evaluated using AC-DC OPF.

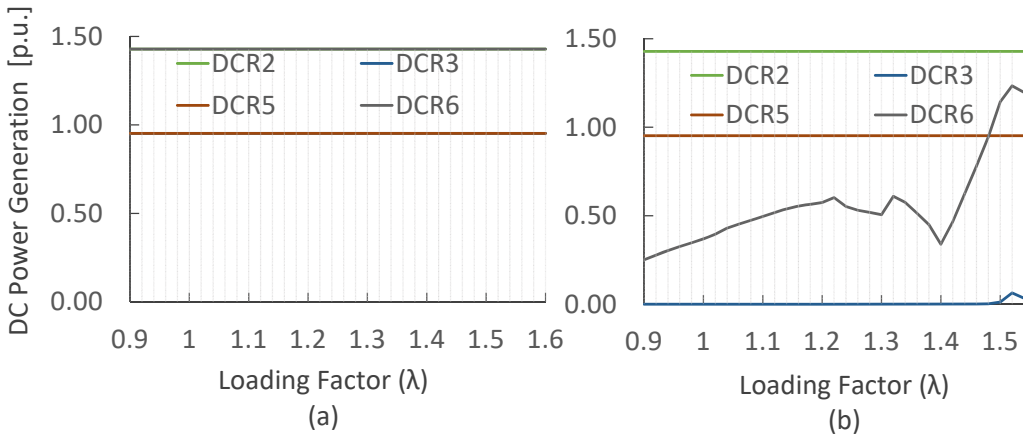

Figure 5.14: Impact of DCRs generation cost on optimal schedule of DC resources; (a): Case I (b): Case II; 118-bus test system.

The AC-DC OPF dispatches all resources including DCRs. . Fig. 5.14 depicts the optimal operating point for all DCRs connected to DC network. In Case I, all DGs are dispatched at their maximum capacity due to less production cost. In case II, the higher price of DCR3 and DCR6 with respect to other DCRs, dictates the partial dispatching of DCR6 and DCR3.

Fig. 5.15 compares the power flowing through DC lines comparing Case I and Case II. It is noticeable that the flow direction is reversed in DC line 2 from Case I to Case II because of DCR generation cost. The voltage profile of DC bus 7 and DC bus 8 are depicted in Fig. 5.16. The OPF provides higher voltage at DC buses in Case I. The higher DC generation at DCR3 and DCR6 improves the voltage at DC buses.

To evaluate the economic value of DC network, the optimal schedule of 118-bus with and without DC is calculated. Fig 5.17 shows the saving in operating cost due to DC network as the loading factor increases from 0.9 to 1.6 p.u.. It is noticeable that DC network provides more value as the system loading factor increases.

The DC network can alleviate the active power congestion on AC transmission lines by providing the DC corridors. DC resources can provide a cost effective generation for AC-DC system, which changes the power flow on AC lines. To evaluate the impact of DC network on the line flows, the active power flowing through each line (P_{lm}) is

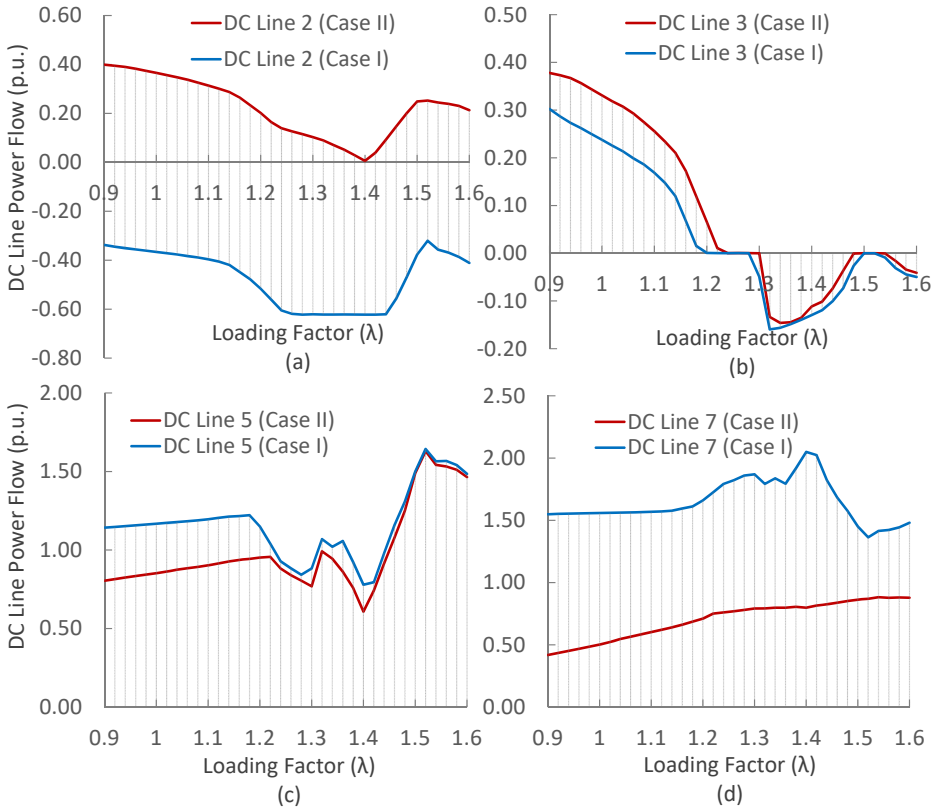

Figure 5.15: Optimal schedule of DC lines comparing the system Case I and Case II (a) DC Line 2, (b) DC Line 3, (c) DC Line 5 and (d) DC Line 7.

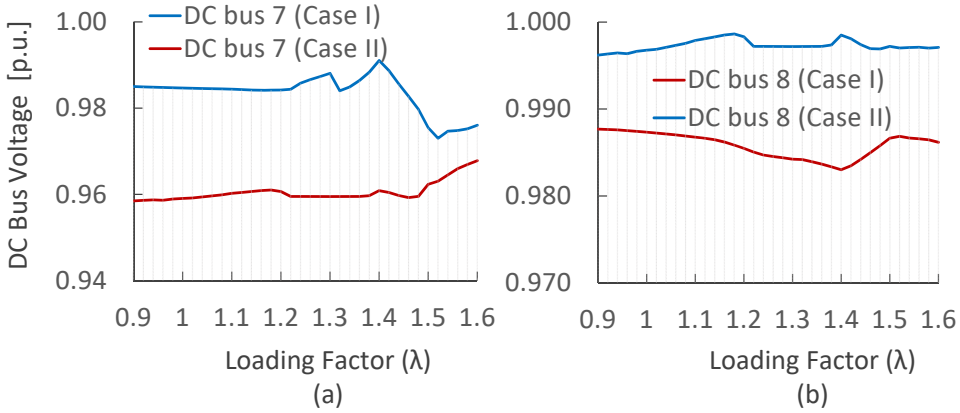

Figure 5.16: Optimal DC bus voltage Case I versus Case II; (a): DC Bus 7; (b): DC Bus 8; 118-bus test system.

calculated using AC-DC OPF. The changes in line flow (ΔP_{lm}) is then obtained by comparing (P_{lm}) in 118-bus and Case II (118-bus incorporating DC network) at $\lambda = 1.5$. Table 5.4 demonstrates the transmission lines with the highest relief in

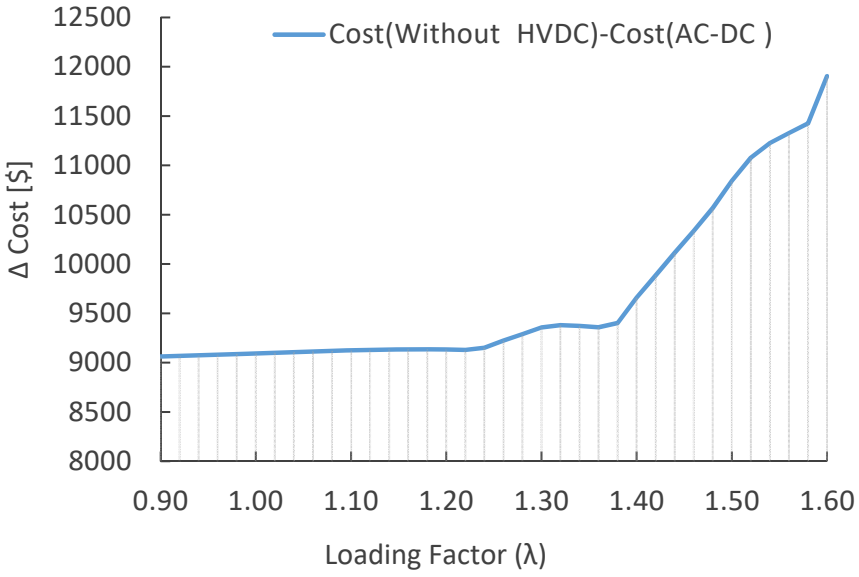

Figure 5.17: Saving in operating cost comparing the system with and without DC system; 118-bus system.

Table 5.4: Impact of DC Network on Line Power Flow (ΔP_{lm}); Lines with the Highest Relief in Active Power Flow(118-bus)

Line	*From Bus*	*To Bus*	$P_{lm}[p.u.]$	$P_{lm_{AC-DC}}[p.u.]$	$\Delta P_{lm}[p.u.]$
9	9	10	-5.42935	-4.13886	-1.290486
107	68	69	-2.14299	-1.28282	-0.8601679
97	64	65	-2.14412	-1.32505	-0.8190709
116	69	75	1.74907	0.989053	-0.7600165
96	38	65	-2.39385	-1.65041	-0.7434492
98	49	66	-1.41604	-0.74325	-0.6727885
99	49	66	-1.41604	-0.74325	-0.6727885
141	89	92	2.290735	1.663369	-0.6273665
78	54	56	0.653814	0.036451	-0.6173629
94	63	64	-1.90127	-1.30573	-0.5955393

active power congestion. For example, the highest decline is related to line 9 between bus 9 and 10. This congestion relief is due to the decrease in power generation on the AC generator connected to bus 10.

Table 5.5 presents the transmission lines with the highest increase in active power flow. These increases are mostly related to dispatching the DC resources in DC network. The extra power generated through DCRs are injected to AC system through

Table 5.5: Impact of DC Network on Line Power Flow (ΔP_{lm})
Lines with the Highest Increase in Active Power Flow(118-bus)

Line	*From Bus*	*To Bus*	$P_{lm}[p.u.]$	$P_{lm_{AC-DC}}[p.u.]$	$\Delta P_{lm}[p.u.]$
104	65	68	0.568095	1.609647	1.041552
37	8	30	0.562046	1.273986	0.711941
7	8	9	-5.36524	-5.98036	0.615121
54	30	38	0.630136	1.212649	0.582513
102	65	66	-0.2614	0.292448	0.553852
128	77	82	-0.01822	0.343109	0.361331
155	94	100	-0.49044	-0.80092	0.310473
82	56	58	-0.01906	0.19081	0.20987
30	23	24	0.205045	0.411385	0.206339
160	100	101	0.010547	0.211486	0.200939

VSC converters. This injected power changes the power flow pattern in AC side and increase the power flowing through the lines around the VSC converters which exchange the active power. For example, (P_{lm}) increase in line 7 is directly caused by injecting the active power from DC network to AC through bus 9. It should be noticed that the objective in this optimization is the decrease of total operation cost.

5.7 Conclusion

The convex VSC-OPF and OPF formulations taking into account maximum stability margin and minimum operating cost objectives for optimal scheduling of integrated AC-DC system are presented in this chapter. The proposed methods address some limitations of AC-DC OPF methods due to non-convexity, separate scheduling of AC and DC networks or using equivalent of DC network. Also, a new voltage stability constrained optimal power flow (VSC-OPF) formulation for integrated AC-DC transmission systems are developed. The effectiveness of the methods are examined on the IEEE 14-bus, 57-bus, and 118-bus incorporating meshed DC network and DC resources. The results demonstrate the capability of proposed convex methods to find the optimal operating points and assess the voltage security cost for AC-DC systems.

CHAPTER 6: Conclusion and Future Work

Non-convexity of Optimal Power Flow (OPF) problem poses difficulties in reaching optimal solutions which can adversely affect the overall solution efficiency, convergence and appropriate scheduling of generators. Power flow equations placed as constraints in OPF problems are nonlinear quadratic functions. Given a quadratic cost function, OPF problem is defined as quadratically constrained quadratic programming (QCQP) problem. This problem is a nonconvex NP-hard optimization problem. Numerous studies have investigated the solution to OPF problem and proposed the optimization algorithms to solve OPF problem including linear programming, nonlinear programming, and evolutionary programming. Despite the particular edge which each method may hold for a specific optimization problem, the main disadvantages of these methods are non-exact relaxation of nonlinear OPF, heavy computational burden and locally optimum solution. These limitations are mainly resulting from non-convexity of OPF equations. This dissertation focuses on the convex optimal power flow approaches in modern power grid, which mitigate some limitations of existing methods in radial and mesh networks.

Chapter 1 of the dissertation discusses the challenges associated with conventional OPF methods and summarizes the recent advances in convex relaxation of OPF problem classified into second order conic programming (SOCP), semi definite programming (SDP) and chordal relaxation based on power flow models. Convex relaxation of OPF is generally classified into two types: Relaxation of bus injection model (BIM) OPF, and Relaxation of branch flow model (BFM) OPF. Despite using different equations and set of variables, these models yields equivalent model of power system. Also Receding Horizon Control (RHC) and its capability in dynamic optimization and han-

dling uncertainties is discussed. RHC output is a set of consecutive control actions, derived by minimizing the objective function over a horizon window. The process has the capability of dealing with the constrained dynamic optimization problems, which includes uncertain inputs or parameters.

Fast optimal scheduling of power grid is now an important requirement for economic operation and integration of electric network with high degree of stochastic components such as renewable sources, plug-in electric vehicles (PEVs), price responding demands, and electricity markets. Distribution systems are gradually transforming from passive networks to an active system. The studies presented so far focus on separately considering OPF convexification or RHC method integrated in conventional OPF. To overcome these challenges, Chapter 2 of this dissertation proposes a dynamic optimization framework by incorporating a convex conic OPF within the RHC (RHC-SOCP-OPF) for radial networks. The main advantages of the proposed method are a) optimum scheduling b) including the dynamic of storages c) integration of uncertain resources. Dynamic optimal power flow (OPF) aims to provide generation schedule and determine control action across operational time frames for different components of active distribution systems. The effectiveness of this method is evaluated on an active distribution system connected to upstream network and neighboring distribution system. The proposed method includes system constraints, market price variation, energy storage dynamics and source uncertainties.

An architecture for the real-time implementation of dynamic convex OPF is proposed in chapter 3, and the scalability of proposed method is examined on a larger radial system. The real-time implementation consists of 1) energy management incorporating convex OPF; 2) control interface; and 3) real-time digital simulator. This real-time framework is useful especially for implementation on the grids with small scheduling time steps. The scalability of proposed method is also tested in this chapter. The results show the improvements in operation cost and computational time in

comparison with the current methods.

In transmission systems, incorporating voltage stability limits inside OPF problem is becoming an essential part for economic power dispatch in new energy management systems. Voltage instability scenarios have recently caused several blackouts. Moving towards the competitive environment in power grid besides demand growth and rise of stochastic players such as renewable sources push the system closer to its stability limits. The voltage stability limits are modeled as the margin that defines the distance to maximum or critical loading points. This margin can be included either in the objective or constraints of OPF problem, which forms voltage stability constrained OPF (VSC-OPF). In Chapter 4, A new convex VSC-OPF architecture taking into account different types of VSC-OPF methods including maximum stability margin, minimum margin constrained, and multi-objective VSC-OPF is proposed. This method is also implemented to derive system PV curve, and the results are compared with CPF method. The voltage stability assessment in these chapters is focused on steady-state conditions.

In chapter 5, convex VSC-OPF and OPF formulations are presented to find maximum loading point margin and minimum operating cost of integrated AC-DC system. Voltage source converter (VSC) based DC transmission systems can alleviate the congestion by providing DC corridors for active power and managing reactive power at converter terminals. The DC network can incorporate multi-terminal DC systems with meshed configuration and form a robust AC-DC system. The proposed methods include both AC and DC side equations together. It provides the solution for reaching the minimum cost or maximum stability margin in AC-DC systems using convex OPF, that is suitable for solving active mesh networks. It also investigates the impact of separate scheduling and converter ratings on the optimal schedule of integrated AC-DC system incorporating radial and meshed systems with DC resources. The proposed methods address some limitations of AC-DC OPF methods due to

non-convexity, separate scheduling of AC and DC networks or using equivalent of DC network.

There are a number of different ways that could help to extend the work in this dissertation. The dynamic convex OPF presented in this dissertation has the capability to provide the optimal scheduling including the dynamics of energy storage and uncertain resources with the advantage of computational efficiency. This method is implemented on the symmetrical radial network. Additional study may be conducted to extended the method to 3-phase asymmetrical radial systems. As discussed earlier there are global optimization methods which may be integrated within proposed method and solve the problem in asymmetrical grid.

The convex VSC-OPF approaches, which are examined on IEEE test systems, reaches to the rank-1 or rank-2 solution. The low rank solution are sufficient conditions that guaranty the optimal schedule for the system. Some additional studies may be required to provide and prove the necessary conditions for the optimality.

Finally, the proposed AC-DC OPF and VSC-OPF includes the equations on both AC and DC side together. The voltage source converter model (VSC) based DC system are usually deployed in different modes which may impose some limitations on operational constraints of the converter. These limitations enforce new constraints on the converter model in OPF problem. Further works may be required to include a detailed converter model and its operational modes.

REFERENCES

[1] Jacob Mattingley, Yang Wang, and Stephen Boyd. Code generation for receding horizon control. In *Computer-Aided Control System Design (CACSD), 2010 IEEE International Symposium on*, pages 985–992. IEEE, 2010.

[2] Paul J Werbos. Computational intelligence for the smart grid-history, challenges, and opportunities. *Computational Intelligence Magazine, IEEE*, 6(3):14–21, 2011.

[3] J Carpentier. Contribution to the economic dispatch problem. *Bulletin de la Societe Francoise des Electriciens*, 3(8):431–447, 1962.

[4] George R Davison. Dividing load between units. *Electrical World*, pages 1385–1387, 1922.

[5] A Wilston. Dividing load economically among power plants. *AIEE Journal*, 1928.

[6] Edward CM Stahl. Load division in interconnections. *Electrical World*, 1930.

[7] Gabriel Kron. Tensorial analysis of integrated transmission systems part i. the six basic reference frames. *American Institute of Electrical Engineers, Transactions of the*, 70(2):1239–1248, 1951.

[8] LK Kirchmayer and GW Stagg. Evaluation of methods of coordinating incremental fuel costs and incremental transmission losses. *AIEE Trans*, 71(Part III):513–520, 1952.

[9] JB Ward. Economy loading simplified. *Electrical Engineering*, 73(1):38–38, 1954.

[10] Gabriel Kron. Tensorial analysis of integrated transmission systems, part iii-the primitive division. *AIEE Transactions*, 71(Pt 3):814–821, 1952.

[11] AF Glimn, LK Kirchmayer, and GW Stagg. Analysis of losses in interconnected systems. *Power Apparatus Systems*, 2, 1952.

[12] HH Happ. Optimal power dispatch: A comprehensive survey. *Power Apparatus and Systems, IEEE Transactions on*, 96(3):841–854, 1977.

[13] HH Happ, JF Aldrich, PT Chan, ME El-Hawary, CR Gagnon, T Kennedy, EF Koncel, JW Lamont, HD Limmer, S Riddington, et al. Description and bibliography of major economy-security functions part ii and part iii. *Power Apparatus and Systems, IEEE Transactions on*, (1):215–223, 1981.

[14] Badrul H Chowdhury and Saifur Rahman. A review of recent advances in economic dispatch. Institute of Electrical and Electronics Engineers, 1990.

[15] M. Huneault and F.D. Galiana. A survey of the optimal power flow literature. *Power Systems, IEEE Transactions on*, 6(2):762–770, May 1991.

[16] James A Momoh, ME El-Hawary, and Ramababu Adapa. A review of selected optimal power flow literature to 1993. part i: Nonlinear and quadratic programming approaches. *IEEE transactions on power systems*, 14(1):96–104, 1999.

[17] James A Momoh, ME El-Hawary, and Ramababu Adapa. A review of selected optimal power flow literature to 1993. part ii: Newton, linear programming and interior point methods. *IEEE Transactions on Power Systems*, 14(1):105–111, 1999.

[18] KS Pandya and SK Joshi. A survey of optimal power flow methods. *Journal of Theoretical & Applied Information Technology*, 4(5), 2008.

[19] Zhifeng Qiu, Geert Deconinck, and Ronnie Belmans. A literature survey of optimal power flow problems in the electricity market context. In *Power Systems Conference and Exposition, 2009. PSCE'09. IEEE/PES*, pages 1–6. IEEE, 2009.

[20] TS Chung and Ge Shaoyun. A recursive lp-based approach for optimal capacitor allocation with cost-benefit consideration. *Electric power systems research*, 39(2):129–136, 1996.

[21] J David Fuller, Raynier Ramasra, and Amanda Cha. Fast heuristics for transmission-line switching. *Power Systems, IEEE Transactions on*, 27(3):1377–1386, 2012.

[22] Saikat Chakrabarti, Elias Kyriakides, and Demetrios G Eliades. Placement of synchronized measurements for power system observability. *Power Delivery, IEEE Transactions on*, 24(1):12–19, 2009.

[23] Alberto Borghetti, Mauro Bosetti, Samuele Grillo, Stefano Massucco, Carlo Alberto Nucci, Mario Paolone, and Federico Silvestro. Short-term scheduling and control of active distribution systems with high penetration of renewable resources. *Systems Journal, IEEE*, 4(3):313–322, 2010.

[24] Frederick S Hillier. *Introduction to operations research*. Tata McGraw-Hill Education, 1995.

[25] Narayana Prasad Padhy. Congestion management under deregulated fuzzy environment. In *Electric Utility Deregulation, Restructuring and Power Technologies, 2004.(DRPT 2004). Proceedings of the 2004 IEEE International Conference on*, volume 1, pages 133–139. IEEE, 2004.

[26] Alejandro Pizano-Martinez, Claudio R Fuerte-Esquivel, H Ambriz-Perez, and Enrique Acha. Modeling of vsc-based hvdc systems for a newton-raphson opf algorithm. *Power Systems, IEEE Transactions on*, 22(4):1794–1803, 2007.

[27] S Sivasubramani and KS Swarup. Sequential quadratic programming based differential evolution algorithm for optimal power flow problem. *IET generation, transmission & distribution*, 5(11):1149–1154, 2011.

[28] DP Kothari. Power system optimization. In *Computational Intelligence and Signal Processing (CISP), 2012 2nd National Conference on*, pages 18–21. IEEE, 2012.

[29] Javad Lavaei and Steven H Low. Zero duality gap in optimal power flow problem. *Power Systems, IEEE Transactions on*, 27(1):92–107, 2012.

[30] Steven H Low. Convex relaxation of optimal power flow, part i: Formulations and equivalence. *arXiv preprint arXiv:1405.0766*, 2014.

[31] Brian Stott, Jorge Jardim, and Ongun Alsaç. Dc power flow revisited. *Power Systems, IEEE Transactions on*, 24(3):1290–1300, 2009.

[32] Carleton Coffrin and Pascal Van Hentenryck. A linear-programming approximation of ac power flows. *arXiv preprint arXiv:1206.3614*, 2012.

[33] Bose Subhonmesh, Steven H Low, and K Mani Chandy. Equivalence of branch flow and bus injection models. In *Communication, Control, and Computing (Allerton), 2012 50th Annual Allerton Conference on*, pages 1893–1899. IEEE, 2012.

[34] Xiaoqing Bai, Hua Wei, Katsuki Fujisawa, and Yong Wang. Semidefinite programming for optimal power flow problems. *International Journal of Electrical Power & Energy Systems*, 30(6):383–392, 2008.

[35] Javad Lavaei, David Tse, and Baosen Zhang. Geometry of power flows and optimization in distribution networks. 2012.

[36] Xiaoqing Bai and Hua Wei. A semidefinite programming method with graph partitioning technique for optimal power flow problems. *International Journal of Electrical Power & Energy Systems*, 33(7):1309–1314, 2011.

[37] RA Jabr. Exploiting sparsity in sdp relaxations of the opf problem. *Power Systems, IEEE Transactions on*, 27(2):1138–1139, 2012.

[38] Rabih A Jabr. Radial distribution load flow using conic programming. *Power Systems, IEEE Transactions on*, 21(3):1458–1459, 2006.

[39] Mesut E Baran and Felix F Wu. Optimal capacitor placement on radial distribution systems. *Power Delivery, IEEE Transactions on*, 4(1):725–734, 1989.

[40] Mesut E Baran and Felix F Wu. Optimal sizing of capacitors placed on a radial distribution system. *Power Delivery, IEEE Transactions on*, 4(1):735–743, 1989.

[41] Joshua Adam Taylor. *Conic optimization of electric power systems*. PhD thesis, Massachusetts Institute of Technology, 2011.

[42] Joshua A Taylor and Franz S Hover. Convex models of distribution system reconfiguration. *Power Systems, IEEE Transactions on*, 27(3):1407–1413, 2012.

[43] Masoud Farivar, Christopher R Clarke, Steven H Low, and K Mani Chandy. Inverter var control for distribution systems with renewables. In *Smart Grid Communications (SmartGridComm), 2011 IEEE International Conference on*, pages 457–462. IEEE, 2011.

[44] Masoud Farivar, Russell Neal, Christopher Clarke, and Steven Low. Optimal inverter var control in distribution systems with high pv penetration. In *Power and Energy Society General Meeting, 2012 IEEE*, pages 1–7. IEEE, 2012.

[45] Masoud Farivar and H Steven. Low. branch flow model: relaxations and convexification (part i). *IEEE Trans. on Power Systems*, 2013.

[46] Subhonmesh Bose, Dennice F Gayme, K Mani Chandy, and Steven H Low. Quadratically constrained quadratic programs on acyclic graphs with application to power flow. *arXiv preprint arXiv:1203.5599*, 2012.

[47] Subhonmesh Bose, Dennice F Gayme, K Mani Chandy, and Steven H Low. Quadratically constrained quadratic programs on acyclic graphs with application to power flow. *IEEE Transactions on Control of Network Systems*, 2(3):278–287, 2015.

[48] Na Li, Lijun Chen, and Steven H Low. Exact convex relaxation of opf for radial networks using branch flow model. In *Smart Grid Communications (SmartGridComm), 2012 IEEE Third International Conference on*, pages 7–12. IEEE, 2012.

[49] Ajit Gopalakrishnan, Arvind U Raghunathan, Daniel Nikovski, and Lorenz T Biegler. Global optimization of optimal power flow using a branch & bound algorithm. In *Communication, Control, and Computing (Allerton), 2012 50th Annual Allerton Conference on*, pages 609–616. IEEE, 2012.

[50] I. Stoyanova, M. Biglarbegian, and A. Monti. Cooperative energy management approach for short-term compensation of demand and generation variations. In *2014 IEEE International Systems Conference Proceedings*, pages 559–566, March 2014.

[51] M. Davoudi, V. Cecchi, and J. R. AgÃŒero. Increasing penetration of distributed generation with meshed operation of distribution systems. In *2014 North American Power Symposium (NAPS)*, pages 1–6, Sept 2014.

[52] I. Mazhari, M. Chamana, B. H. Chowdhury, and B. Parkhideh. Distributed pv-battery architectures with reconfigurable power conversion units. In *2014 IEEE Applied Power Electronics Conference and Exposition - APEC 2014*, pages 691–698, March 2014.

[53] Saeed Mohajeryami, Iman N Moghaddam, Milad Doostan, Behdad Vatani, and Peter Schwarz. A novel economic model for price-based demand response. *Electric Power Systems Research*, 135:1–9, 2016.

[54] James A Momoh. Smart grid design for efficient and flexible power networks operation and control. In *Power Systems Conference and Exposition, 2009. PSCE'09. IEEE/PES*, pages 1–8. IEEE, 2009.

[55] James A Momoh. Smart grid design for efficient and flexible power networks operation and control. In *Power Systems Conference and Exposition, 2009. PSCE'09. IEEE/PES*, pages 1–8. IEEE, 2009.

[56] R. F. Arritt and R. C. Dugan. Distribution system analysis and the future smart grid. *IEEE Transactions on Industry Applications*, 47(6):2343–2350, Nov 2011.

[57] Mojtaba Khanabadi, Seyedmahdi Moghadasi, and Sukumar Kamalasadan. Real-time optimization of distribution system considering interaction between markets. In *Industry Applications Society Annual Meeting, 2013 IEEE*, pages 1–8. IEEE, 2013.

[58] Matt Kraning, Eric Chu, Javad Lavaei, and Stephen Boyd. Message passing for dynamic network energy management. *arXiv preprint arXiv:1204.1106*, 2012.

[59] James Robertson, Gareth P Harrison, and A Robin Wallace. A receding-horizon opf for active network management. In *Electricity Distribution (CIRED 2013), 22nd International Conference and Exhibition on*, pages 1–4. IET, 2013.

[60] Philipp Fortenbacher. *Power flow modeling and grid constraint handling in power grids with high RES in-feed, controllable loads, and storage devices*. PhD thesis, Master thesis PSL 1113, Power Systems Laboratory, ETH Zurich, Switzerland, 2011.

[61] A Subramanian, M Garcia, A Dominguez-Garcia, D Callaway, K Poolla, and P Varaiya. Real-time scheduling of deferrable electric loads. In *American Control Conference (ACC), 2012*, pages 3643–3650. IEEE, 2012.

[62] Panagiotis Patrinos, Sergio Trimboli, and Alberto Bemporad. Stochastic mpc for real-time market-based optimal power dispatch. In *Decision and Control and European Control Conference (CDC-ECC), 2011 50th IEEE Conference on*, pages 7111–7116. IEEE, 2011.

[63] S. Moghadasi and S. Kamalasadan. Optimal fast control and scheduling of power distribution system using integrated receding horizon control and convex conic programming. *IEEE Transactions on Industry Applications*, 52(3):2596–2606, 2016.

[64] S. Moghadasi and S. Kamalasadan. Real-time optimal scheduling of smart power distribution systems using integrated receding horizon control and convex conic

programming. In *2014 IEEE Industry Application Society Annual Meeting*, pages 1–7, 2014.

[65] Mesut E Baran and Felix F Wu. Network reconfiguration in distribution systems for loss reduction and load balancing. *Power Delivery, IEEE Transactions on*, 4(2):1401–1407, 1989.

[66] Meysam Doostizadeh and Hassan Ghasemi. Day-ahead scheduling of an active distribution network considering energy and reserve markets. *International Transactions on Electrical Energy Systems*, 23(7):930–945, 2013.

[67] Dong Zhang, Zhengcai Fu, and Liuchun Zhang. An improved ts algorithm for loss-minimum reconfiguration in large-scale distribution systems. *Electric Power Systems Research*, 77(5):685–694, 2007.

[68] Real-Time Digital Simulator (RTDS). *rtds.com/*.

[69] Anurag K. Srivastava, Sukumar Kamalasadan, Daxa Patel, Sandhya Sankar, and Khalid S. Al-Olimat. Electricity markets: an overview and comparative study. *International Journal of Energy Sector Management*, 5(2):169–200, 2011.

[70] Antonio J Conejo, Federico Milano, and Raquel García-Bertrand. Congestion management ensuring voltage stability. In *Power and Energy Society General Meeting-Conversion and Delivery of Electrical Energy in the 21st Century, 2008 IEEE*, pages 1–8. IEEE, 2008.

[71] JA Momoh, RJ Koessler, MS Bond, B Stott, D Sun, A Papalexopoulos, and P Ristanovic. Challenges to optimal power flow. *Power Systems, IEEE Transactions on*, 12(1):444–455, 1997.

[72] William D Rosehart, Claudio A Canizares, and Victor H Quintana. Multiobjective optimal power flows to evaluate voltage security costs in power networks. *Power Systems, IEEE Transactions on*, 18(2):578–587, 2003.

[73] KS Pandya and SK Joshi. A survey of optimal power flow methods. *Journal of Theoretical & Applied Information Technology*, 4(5), 2008.

[74] Thierry Van Cutsem. A method to compute reactive power margins with respect to voltage collapse. *Power Systems, IEEE Transactions on*, 6(1):145–156, 1991.

[75] Luonan Chen, Y Taka, Hiroshi Okamoto, Ryuya Tanabe, and Asako Ono. Optimal operation solutions of power systems with transient stability constraints. *Circuits and Systems I: Fundamental Theory and Applications, IEEE Transactions on*, 48(3):327–339, 2001.

[76] Jason Yuryevich and Kit Po Wong. Evolutionary programming based optimal power flow algorithm. *Power Systems, IEEE Transactions on*, 14(4):1245–1250, 1999.

[77] Deqiang Gan, Robert J Thomas, and Ray D Zimmerman. Stability-constrained optimal power flow. *Power Systems, IEEE Transactions on*, 15(2):535–540, 2000.

[78] William Rosehart, Claudio Cañizares, and VH Quintana. Optimal power flow incorporating voltage collapse constraints. In *Proc. 1999 IEEE-PES Summer Meeting, Edmonton, Alberta*. Citeseer, 1999.

[79] William Rosehart, Claudio Cañizares, and Victor Quintana. Costs of voltage security in electricity markets. In *Power Engineering Society Summer Meeting, 2000. IEEE*, volume 4, pages 2115–2120. IEEE, 2000.

[80] Andreas S Pedersen, Mogens Blanke, and Hjortur Johannsson. Convex relaxation of power dispatch for voltage stability improvement. In *Control Applications (CCA), 2015 IEEE Conference on*, pages 1528–1533. IEEE, 2015.

[81] Seyedmahdi Moghadasi and Sukumar Kamalasadan. An architecture for voltage stability constrained optimal power flow using convex semi-definite programming. In *North American Power Symposium (NAPS), 2015*, pages 1–6. IEEE, 2015.

[82] Bernard C Lesieutre, Daniel K Molzahn, Alex R Borden, and Christopher L DeMarco. Examining the limits of the application of semidefinite programming to power flow problems. In *Communication, Control, and Computing (Allerton), 2011 49th Annual Allerton Conference on*, pages 1492–1499. IEEE, 2011.

[83] Ray D Zimmerman, Carlos E Murillo-Sánchez, and Deqiang Gan. A matlab power system simulation package, 2005.

[84] Nikolas Flourentzou, Vassilios G Agelidis, and Georgios D Demetriades. Vsc-based hvdc power transmission systems: An overview. *Power Electronics, IEEE Transactions on*, 24(3):592–602, 2009.

[85] Jef Beerten and Ronnie Belmans. Modeling and control of multi-terminal vsc hvdc systems. *Energy Procedia*, 24:123–130, 2012.

[86] Stefan G Johansson, Gunnar Asplund, Erik Jansson, and Roberto Rudervall. Power system stability benefits with vsc dc-transmission systems. In *CIGRE Conference, Paris, France*, 2004.

[87] Arthit Sode-Yome, Nadarajah Mithulananthan, and Kwang Y Lee. A maximum loading margin method for static voltage stability in power systems. *Power Systems, IEEE Transactions on*, 21(2):799–808, 2006.

[88] S Moghadasi and S Kamalasadan. An architecture for voltage stability constrained optimal power flow using convex semi-definite programming. In *North American Power Symposium, Charlotte, USA*, 2015.

[89] Johan Rimez and Ronnie Belmans. A combined ac/dc optimal power flow algorithm for meshed ac and dc networks linked by vsc converters. *International Transactions on Electrical Energy Systems*, 2014.

[90] Azim Lotfjou, Mohammad Shahidehpour, and Yong Fu. Hourly scheduling of dc transmission lines in scuc with voltage source converters. *Power Delivery, IEEE Transactions on*, 26(2):650–660, 2011.

[91] Mohamadreza Baradar, Mohammad R Hesamzadeh, and Mehrdad Ghandhari. Second-order cone programming for optimal power flow in vsc-type ac-dc grids. *Power Systems, IEEE Transactions on*, 28(4):4282–4291, 2013.

[92] Shahab Bahrami, Vincent WS Wong, and Juri Jatskevich. Optimal power flow for ac-dc networks. In *Smart Grid Communications (SmartGridComm), 2014 IEEE International Conference on*, pages 49–54. IEEE, 2014.

[93] S. Moghadasi and S. Kamalasadan. Voltage security cost assessment of integrated ac-dc systems using semidefinite programming. In *2016 IEEE Power Energy Society Innovative Smart Grid Technologies Conference (ISGT)*, pages 1–5, Sept 2016.

[94] Brahim Gasbaoui and Boumediene Allaoua. Ant colony optimization applied on combinatorial problem for optimal power flow solution. *Leonardo Journal of Sciences*, 14:1–17, 2009.

[95] Electric Reliability Council of Texas (ERCOT). *ercot.com/mktinfo/index.html/*.

APPENDIX A: System Information

In Chapter 2, 32-bus radial distribution system is considered to examine the convex RHC method. The system is 12.66 kV and contains 33 buses (bus 0 is the contact point to upstream network) and 32 lines. The system is modified to incorporate the market transaction, wind generation, and storage (see Fig. A.1). This radial network is connected to the upstream network and neighboring DISCO through tie lines from bus 0 and bus 30 respectively. Two wind farms are located at bus 13 and 16. One storage station is connected to bus 20. Contracted loads are considered at bus 7, 13, 24, and 31. The electrical parameters are given in [65].

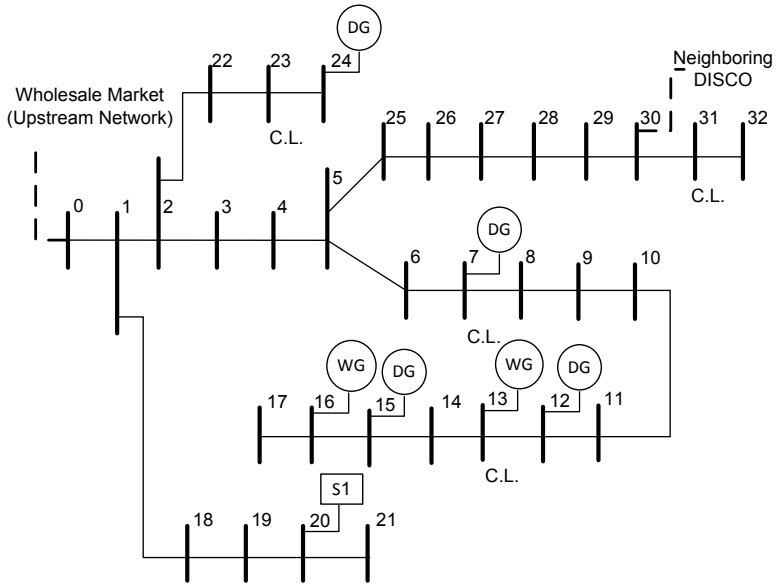

Figure A.1: Modified 32-bus Distribution Test System

In Chapter3, a modified 119-bus distribution system is examined to test the effectiveness of proposed method as shown in Fig. A.2. The system operates at 11 kV and contains 22709.7kW and 17041.1 kVar of demand. The system is modified to incorporate the market and neighboring DISCOs transaction, wind generation, contracted loads and storage. This radial network is connected to the upstream network from bus 1 and exchanges power with neighboring DISCOs through tie lines from the buses 48 and 80. The DGs are connected to the feeders at the buses

35, 44, 52, 56, 60, 64, 69, 84, 85 , 89, 96, 109, 116, 121. Seven wind generators are integrated to the system through buses 14, 20, 50, 74, 76, 101, 113. The contracted loads are connected to buses 24, 25, 42 , 43, 55, 59, 79, 82, 97, 112, 117 and up to 20% of these loads are contracted to be curtailed.

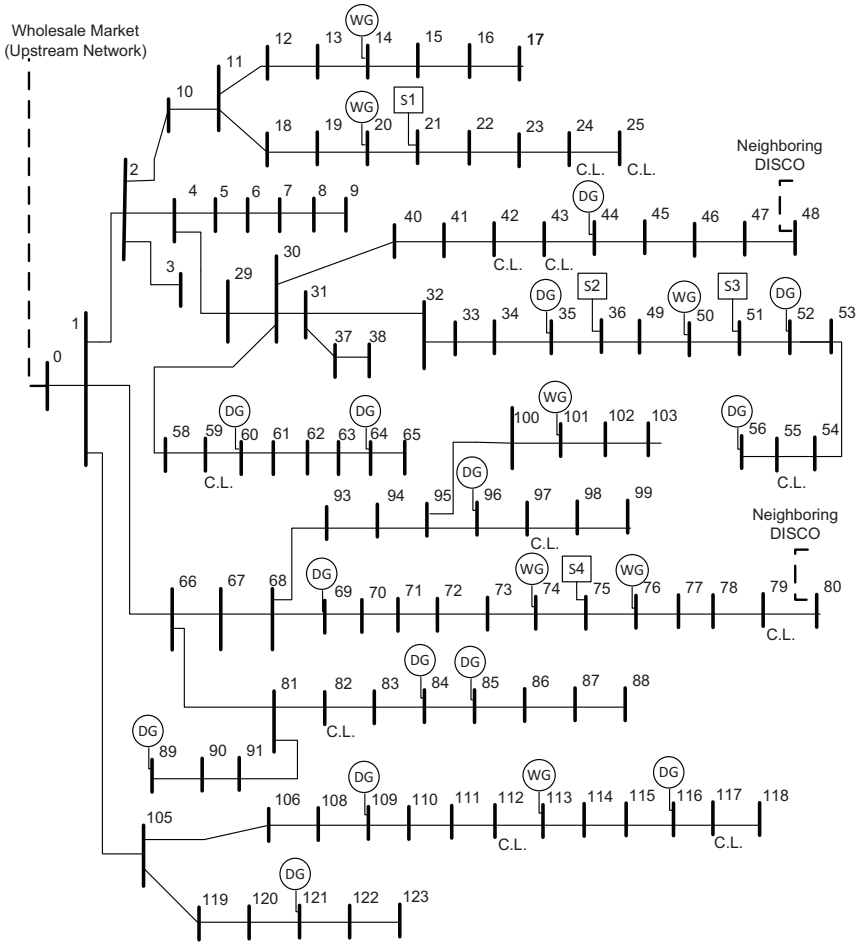

Figure A.2: Modified 119-bus Distribution Test System

In chapters 2 and 3, the market price is equal to market price variation coefficient times the base price. Similar procedure goes with the load demand variation. Neighboring DISCO and upstream networks exchange power based on the hourly energy price. The base market price, and neighboring price are considered \$0.09/kWh and \$0.0825/kWh respectively. The cost of contracted loads is \$0.1/kWh. The least operational cost is associated with wind generators \$0.05/kWh. The variation coefficient

Table A.1: Price Variation Coefficient At Different Time Steps For Upstream Network and Neighboring DISCO

Step (k)	Price Coe.	Load	Step (k)	Price Coe.	Load
1	0.7	0.88	13	1.31	1.38
2	0.64	0.83	14	1.46	1.41
3	0.62	0.80	15	1.66	1.44
4	0.59	0.78	16	1.43	1.45
5	0.62	0.80	17	1.80	1.43
6	0.63	0.85	18	1.43	1.39
7	0.65	0.92	19	1.18	1.39
8	0.65	1.02	20	1.14	1.34
9	0.77	1.11	21	1.07	1.28
10	0.84	1.20	22	0.92	1.15
11	0.95	1.28	23	0.85	1.02
12	1.09	1.34	24	0.80	0.94

Table A.2: DG, wind and energy storage capacity; 32-bus Test System

	Pgmax [p.u.]		Pgmax [p.u.]
bus7	3.5	bus16	3.0
bus12	3.0	bus24	4.1
bus13	3.2	bus20	4.0
bus15	3.0		

of energy price at upstream and neighboring DISCO with respect to base price are presented in Table A.1. The wind forecasts over the horizon window are obtained at each time step from ERCOT wind forecast data [95]. The detailed data of DGs and storage capacity for modified 32-bus and 119-bus test systems are given in Table A.2 and A.3 respectively. Power base for two systems is 100 kW. The DG's generation cost for the test systems are shown in Table A.4 and A.5.

Table A.3: DG, wind and energy storage capacities; 119-bus Test System

	Pgmax [p.u.]	Smax [p.u.]		Pgmax [p.u.]	Smax [p.u.]
bus14	2	-	bus74	10	-
bus20	7	-	bus75	0	6
bus21	0	8	bus76	10	-
bus35	5	-	bus80	10	-
bus36	0	8	bus84	3	-
bus44	7	-	bus85	3	-
bus48	10	-	bus89	2	-
bus50	10	-	bus96	2	-
bus51	0	6	bus101	7	-
bus52	10	-	bus109	7	-
bus56	5	-	bus113	10	-
bus60	2	-	bus116	10	-
bus64	2	-	bus121	3	-
bus69	5	-	-	-	-

Table A.4: DG Generation Cost: 32-bus Test System

DG	Cost Function [$/kW]	DG	Cost Function [$/kW]
bus7	0.079	bus15	0.092
bus12	0.087	bus24	0.081

Table A.5: DG Generation Cost: 119-bus Test System

DG	Cost Function [$/kW]	DG	Cost Function [$/kW]	DG	Cost Function [$/kW]
bus35	0.085	bus64	0.092	bus96	0.092
bus44	0.082	bus69	0.085	bus109	0.082
bus52	0.08	bus84	0.088	bus116	0.08
bus56	0.085	bus85	0.088	bus121	0.088
bus60	0.092	bus89	0.092		